NEGATIVELY BUOYANT SLOT JETS IN STAGNANT AND FLOWING ENVIRONMENTS

by

David M. Shahrabani

and

John D. Ditmars

Ocean Engineering Report No. 8

June 1976

Department of Civil Engineering
University of Delaware
Newark, Delaware

Acknowledgments

The authors wish to thank James Coverdale, Roland Essex, and John Mark of the Department of Civil Engineering for their contributions in the design and construction of much of the laboratory equipment. Karen Spry typed the report and Barbara Shelton assisted in its preparation. Professor Robert G. Dean suggested the particular numerical integration technique employed.

The material contained in this report is based on a thesis submitted by David M. Shahrabani to the Faculty of the University of Delaware in partial fulfillment of the requirements for the degree of Master of Civil Engineering. John D. Ditmars, Assistant Professor of Civil Engineering and Marine Studies, provided technical supervision of the study. D. M. Shahrabani was supported during the 1975-76 academic year by an Edward C. Davis Fellowship. Additional research funding was provided by the University of Delaware Research Foundation.

Abstract

Negatively buoyant discharges sink, impinge on the receiving water bottom, and, in some cases, pose a hazard to the relatively immobile benthic community. Design and evaluation of discharge structures for the discharge of negatively buoyant effluents require that the mixing and transport characteristics of negatively buoyant jets be determined.

The purpose of this study was an examination of the near-field characteristics of a negatively buoyant effluent discharged upward from a slot or line-source situated on the bottom of the receiving water body. The slot length has been extended fully across the flow to allow a two-dimensional analysis of the problem. The receiving water body was of uniform density and either stagnant or flowing.

Laboratory experiments with turbulent slot discharges were conducted to determine jet trajectories and downstream dilutions. In particular, centerline dilutions at the maximum height of rise and in the zone of bottom impingement were determined. Results are reported for jets discharged into stagnant environments at angles of 30°, 45°, 60°, and 90° from the horizontal for discharge densimetric Froude numbers which ranged from 10 to 50. Similar data are reported for jets discharged at 45° and 90° into uniformly flowing receiving waters with velocity ratios (jet discharge velocity to ambient current velocity) of 15 to 25.

Predictions of an integral-similarity model for a negatively buoyant slot jet in a stagnant environment were compared with experimental data. The model was found to be inadequate because it did not include the effect of the reattachment eddy generated in the presence of the bottom boundary.

Table of Contents

1. Introduction

The disposal of man-made wastes is a major problem for environmental engineers of today. Among coastal cities around the world, it has been common practice for many years to discharge waste products into the nearby marine environment. At times, indiscriminate discharges have resulted in serious contamination of the receiving body of water. If pollution levels of the aquatic environment are to be controlled, it is necessary to understand the phenomenon of the mixing of these waste discharges with the receiving waters.

Negatively buoyant effluents can be the result of various types of industrial discharges. In particular, some discharges may be composed of:

(1) heavy acids or dissolved solids,

(2) concentrated brine, such as from a desalination plant, or

(3) drastically cooled water such as heating water discharge from a liquid, natural gas receiving plant.

Any of these by-products, when in sufficiently high concentration result in a mixture with specific weight greater than that of fresh or even salt water.

If a given effluent is heavier than the ambient fluid, then it can create a negatively buoyant jet. Negatively buoyant characteristics create a much different problem than the one associated with positively buoyant jets. Assuming a non-stratified environment, positively buoyant fluids will rise and eventually reach the surface of the receiving body of water. At the surface, the fluids will undergo additional mixing due to the wind and wave actions.

Negatively buoyant fluid realizes no such additional mixing process. Insufficiently mixed dense fluid will eventually sink and inpinge on the bottom. Here, it may lay in depressions and be prevented from moving away from the area. This can create an undesirable bottom condition and destroy the benthic organisms. Consequently, it is imperative that systems handling negatively buoyant discharges allow adequate mixing before the jet fluid reaches the bottom of the receiving body of water, or, if feasible, prevent the fluid from reaching the bottom entirely.

Waste effluent is usually discharged into the environment through a submerged outfall system. This type of system consists of diffuser pipes laid along the bottom of the receiving water body. The diffuser pipes contain a row or rows of round ports from which the

wastes are expelled. The initial mixing of the effluent with the receiving water is due to the behavior of the jets created. Individual jets from a multi-port diffuser with closely spaced ports may merge near the diffuser to form a slot-like jet similar to that resulting from the slot discharge studied here. However, because the initial penetration of ambient water between the individual jets does not occur in the case of a slot discharge, the downstream behavior of these two cases may differ. Also, it should be emphasized that for the case studied here, the slot discharge is strictly two-dimensional, that is, it extends completely across the flow. For multi-port diffusers or slots of finite length, the end effects or three-dimensionality of the flow field may alter the jet characteristics significantly.

In this study, a submerged, negatively buoyant jet shall be defined as one in which the following conditions hold:

(1) The initial direction of momentum flux is opposed to the direction of gravity, and

(2) The jet is sufficiently far from the surface so that the surface effects are negligible.

2. Literature Review of Negatively Buoyant Jets

2.1 Round, Negatively Buoyant Jets in a Stagnant Environment

2.1.1 Morton's Analytical Model

The earliest work with negatively buoyant jet behavior was an analytical investigation conducted by Morton[1] in 1959. Morton's study was an extension of the integral-similarity technique of Morton, Taylor, and Turner[2], which was concerned with the mixing and spreading of round, positively buoyant jets issuing vertically upwards into a stagnant environment. Morton, Taylor, and Turner predicted jet behavior by using the conservation principles of mass, linear momentum and density deficiency and by assuming similarity of density and velocity profiles at any cross section in the jet plume. These conservation equations were applied to an incremental length of the jet plume and integrated radially to eliminate the cross-sectional variations of density and velocity. The lateral spreading rate was determined by integrating the equations along the centerline trajectory. This is a very powerful technique and has been used by most investigators since then. Hereafter, this method shall be referred to as the Morton, Taylor, and Turner integral-similarity technique.

Morton used this technique to investigate the behavior of a vertically directed, round, negatively buoyant jet in a stagnant environment. He assumed that the rate of entrainment was proportional to the jet's centerline velocity as suggested by Taylor:

$$\frac{dQ}{ds} = 2\pi b\alpha u \tag{2-1}$$

and that any cross section, normal to the jet's centerline, the profiles of velocity and density deficiency followed a Gaussion distrubution:

$$u(s,r) = u(s)e^{-r^2/b^2} \tag{2-2}$$

$$(\rho_a-\rho)(s,r) = (\rho_a-\rho)(s)e^{-r^2/\lambda^2 b^2} \tag{2-3}$$

where

Q = volume of fluid contained in an incremented length of the jet,

s = distance along centerline axis,

r = radial distance, normal to the centerline,

α = entrainment coefficient,

$u=u(s)$ = jet centerline velocity,

$u(s,r)$ = jet velocity at any point in plume,

b = characteristic jet half-width (=nominal width/$2\sqrt{2}$),

λ = spreading coefficient (accounts for the different spreading rate of mass and momentum) see Rouse, Yih, and Humphreys[3],

ρ_a = ambient fluid density,

ρ = jet fluid density.

By substituting these terms (2-2 and 2-3) into the conservation equations and applying the Bousinesq assumption, the following governing equations were obtained:

$$\frac{d}{ds}(b^2u) = 2\alpha bu \quad \text{(Conservation of Mass)} \tag{2-4}$$

$$\frac{d}{ds}(b^2u^2) = 2\lambda^2 b^2 \frac{(\rho_a-\rho)}{\rho_a}$$

(Conservation of Vertical Momentum) (2-5)

$$\frac{d}{ds}(b^2u(\rho_a-\rho)] = 0$$

(Conservation of Density Deficiency) (2-6)

Morton developed non-dimensional plots of the jet's characteristic half-width, velocity, and centerline dilution with respect to

the distance from a virtual source (at s=0, b=0). Due to the negative buoyancy effect, the jet is eventually arrested at some terminal point whereat the plume begins to fall back on itself. At this point, the similarity assumptions of velocity and density deficiency break down. As a result, Morton's analysis was only valid for the initial plume pulse up to the point of maximum rise.

2.1.2 Turner's Experiments

Turner[4] in 1966 studied the behavior of a heavy salt water jet injected vertically upwards into a freshwater environment and developed a dimensional analysis to predict its maximum rise. Experimental observations revealed that, after the initial pulse, a steady state height was quickly established which rose to a somewhat greater height than the subsequent equilibrium level. Through a dimensional argument, Turner assumed that two parameters would completely define the flow situation. The two parameters were M and F_2, the momentum and buoyancy fluxes, respectively. He claimed that the mean maximum rise of the jet, Zm, could be determined by the following equation:

$$Zm = C\, M^{3/4}\, F_2^{-1/2} \qquad (2\text{-}7)$$

where

C = experimental constant.

Assuming that the velocity distribution across the jet could be approximated by a "top hat" profile, the values of the momentum and

buoyancy fluxes were easily shown to be:

$$M = \pi r_o^2 u_o^2 \tag{2-8}$$

$$F_2 = \pi g\left(\frac{\rho_o - \rho_a}{\rho_a}\right) r_o^2 u_o \tag{2-9}$$

where $(\ )_o$ denotes the initial condition. Substituting Equations (2-8) and (2-9) into Equation (2-7) yields:

$$Z_m = C \pi^{1/4} r_o^{1/2} u_o \Big/ \left(g \frac{(\rho_o - \rho_a)}{\rho_a}\right)^{1/2} \tag{2-10}$$

Turner confirmed his equations with experimental tests. His findings showed:

$$C = 1.85 \tag{2-11}$$

Although various-sized jet orifices were used, no "virtual source" effects were found.

2.1.3 Abrahams Analytical Model

Abraham[5] also devised a model to predict the maximum height of rise of a round, negatively buoyant jet issuing vertically upwards into a quiescent environment. He considered the jet plume to be composed of two regions of different types of entrainment. The first region, near the jet nozzle, underwent positive entrainment and the total mass flux

increased with distance, as had been assumed by the previous investigators. But, at some distance from the origin, the jet goes through a transition zone and enters a region of negative entrainment. Here, the positive mass flux actually decreased as the edge of the plume began to fall back while the fluid at the centerline continued to drive upwards. The centerline density was assumed to remain constant from the transition zone up to the point of maximum rise. Abraham assumed that a Gaussian similarity of the velocity profile was still maintained in the region of negative entrainment.

Using the integral-similarity technique and approximating the constant coefficients, Abraham determined:

$$Zm/D_o = 1.94\ F_r \tag{2-12}$$

where

D_o = diameter of the jet orifice,

F_r = the densimetric jet Froude number

$$= \frac{u_o}{\sqrt{g\ D_o \frac{\rho_o - \rho_a}{\rho_a}}} \tag{2-13}$$

2.1.4 Zeitoun's Analytical Model and Experiments

In 1970, Zeitoun conducted studies on the behavior of round, heavy salt water jets for the purpose of designing discharge systems

for the disposal of brine blowdown. His goal was to develop a conceptual design of outfall systems for desalination plants. Dense jet phenomena were examined analytically as well as experimentally.

Zeitoun used a Morton, Taylor, and Turner integral-similarity approach to theoretically evaluate the flow characteristics. It was assumed that the mass and momentum spread at the same rate (i.e., $\lambda = 1$). No account was taken of the zone of flow establishment. Better correlation was obtained between experiments and the model predictions when the entrainment function proposed by Fox[7] was used. Fox's entrainment exhibits not only dependency on the centerline velocity but also on a local densimetric Froude number as well:

$$\frac{dQ}{ds} = \left(\alpha - \frac{\beta}{Fr_L^2}\right) ub \qquad (2\text{-}14)$$

where

α, β = experimental constants,

b = the local characteristic jet half-width,

Fr_L = the local densimetric Froude number.

It is worthwhile to note that if the density difference is very small, the local densimetric Froude number gets very large, and the second term in Equation (2-14) drops out, with the remaining term being the Taylor assumption of entrainment:

$$\frac{dQ}{ds} = \alpha \, ub \qquad (2\text{-}15)$$

Theoretical results were found by solving the governing equations by a finite difference technique. The best fit value of the entrainment coefficient was obtained by fitting the predicted curves with the experimental data. The best fit α and ρ values were 0.07 and -1.0, respectively. Comparison plots of the trajectories and dilutions of jets inclined at 30°, 45°, and 60° from the horizontal were presented. It was found that the 60° jet had the greatest arc length before falling back to the bottom.

Similar data for corresponding conditions were also obtained from experimental tests. Centerline dilutions at the maximum height of rise and centerline trajectories were recorded. Some work was also done with a 90° jet, but dilutions were found to be too small for practical use, so extensive study was abandoned.

The overall trajectory predictions of the analytical model for the experimental tests were very good. While the trajectory of the 60° case was slightly underpredicted, the 30° and 45° case predictions were excellent. Very limited comparison of the dilution ratios was presented. The predicted centerline dilution ratios at the maximum height of rise were compared with the experimental tests and found to be reasonable.

Zeitoun concluded from his study that the 60° jet was the most satisfactory for application to a diffuser outfall system, because the long trajectory of the 60° jet afforded the greatest dilution before the jet's fluid fell back to the ocean floor.

2.2 Round, Negatively Buoyant Jets in a Uniformly Flowing Environment

2.2.1 Holly and Grace Experiments

The first published study of the effects of a uniform ambient crosscurrent on a round, negatively buoyant jet was presented by Holly and Grace[8] in 1972. Their study was a continuation of Zeitoun's investigations. Physical model tests were conducted to determine what degree of mixing of a dense brine solution was attainable by a diffuser situated on the ocean floor subject to uniform currents. All tests involved circular jets issuing vertically upwards. Near and far field phenomena were examined.

Holly and Grace briefly studied the feasibility of linear superposition to calculate the effects of the merging of a series of round jets on downstream dilutions. They reported good agreement with experiments and stated that the superposition technique is a viable tool for synthesizing single port results to predict downstream mixing patterns for a multiple-port diffuser.

2.2.2 Pincince and List Experiments

In 1973, Pincince and List[9] studied a very specific problem involving a round dense jet of a densimetric Froude number equal to 50, inclined at an angle of 60° and subject to various crossflows. Their purpose was to design a diffuser for the discharge of concentrated brine. Water quality criteria demanded that a dilution of 50:1 be attained before the jet fluid impinged on the bottom. According to the results of Zeitoun[6], a 60° jet with a densimetric Froude number equal to 50 allowed these criteria to be met in a stagnant environment. It was assumed that the added crossflow effect would supply a factor of safety.

Experimental tests were then conducted to see in what manner different crossflows affected the preset conditions. Three different crossflows were examined. They corresponded to velocity ratios, k, equal to 37, 25, and 10, where the velocity ratio is defined:

$$k = u_o/u_a, \tag{2-16}$$

u_o = initial jet velocity,

u_a = ambient velocity.

Results indicated that the velocity ratio did not affect the dilution ratios very near the jet source, but became the dominating factor when the jet fluid reached 200 jet diameters downstream

(measured horizontally). It was found that the jet went through three distinct zones of different dilution rates as it got farther away from the source. In the first zone, 0-200 jet diameters downstream, it was obvious that the dilution rate was almost completely independent of the crossflow. In the second zone, 200-100 jet diameters downstream, interaction of the ambient turbulence became apparent, and in the third zone, ambient turbulence was the dominating influence. The downstream dilution results indicate that the effect of changing the velocity ratio is merely to shift the origin of ambient-influenced mixing.

The velocity ratio had a more pronounced effect on the jet trajectory. Results showed that the greater the velocity ratio (i.e., the slower the crosscurrent), the greater the rise in trajectory. It was found that for a relatively fast crosscurrent flow (i.e., low velocity ratio), the jet became sufficiently mixed so that it did not fall back to the bottom even at 200 jet diameters downstream.

2.2.3 Anderson's Analytical Model and Experiments

The most extensive research concerning round negatively buoyant jets was conducted by Anderson et al.[10] in 1973. This study investigated the mixing process and trajectories of round, dense jets, in uniform crossflows, inclined at the various angles of 45°, 60°, and 90° from the horizontal. The analytical models for buoyant jets by Fan[11]

and Abraham[12] were modified for application to the case of a negatively buoyant jet. The models were then compared with experimental results. Both Fan's and Abraham's models employed the Morton, Taylor, and Turner integral-similarity technique.

Velocity profiles were assumed similar and Gaussian above the component of the ambient velocity parallel to the jet trajectory, $u_a \cos \theta$:

$$u(s,r) = u_a \cos \theta + u(s)\, e^{-r^2/b^2} \tag{2-17}$$

The buoyance and tracer material concentration also followed a Gaussian profile:

$$[\rho_a - \rho(s,r)] = [\rho_a - \rho(s)]\, e^{-r^2/b^2} \tag{2-18}$$

$$c(s,r) = c(s)\, e^{-r^2/b^2} \tag{2-19}$$

respectively, where

c = concentration of any tracer material (salt dye, etc.),

and the other symbols are the same as defined earlier. It was assumed that mass and velocity spread at the same rate.

In the modified Fan model, entrainment was governed by the Taylor assumption. The entrainment equation was:

$$\frac{dQ}{ds} = 2\,\pi\alpha b\left|\bar{u}-\bar{u}_a\right| \qquad (2\text{-}20)$$

where

$\left|\bar{u}-\bar{u}_a\right|$ = the magnitude of the vector difference between the jet and ambient velocities.

The modified Abraham model assumed that there were two regions of different entrainment mechanisms with constant coefficients. These coefficients were assumed independent of any densimetric Froude number, injection angle, or velocity ratio effects. Very near the jet source, the entrainment was assumed governed by the initial momentum:

$$\frac{dQ}{ds} = \alpha_m\, 2\pi bu \qquad (2\text{-}21)$$

where

αm = the coefficient of entrainment for jets primarily influenced by initial momentum = 0.057 (according to Albertson et al.[13]).

Far from the jet, the modified Abraham model assumed that the jet fluid moved at a rate equal and parallel to the ambient flow. Entrainment in this region was governed by the relationship for a cylindrical thermal in a stagnant fluid as described by Richards[14]:

$$\frac{dQ}{ds} = \alpha th\ 2\pi b\ u_a \sin\theta \qquad (2\text{-}22)$$

where

$\alpha th = 0.5$ (according to Richards).

Thus, the total entrainment in the modified Abraham model was:

$$\frac{dQ}{ds} = 2\pi b\ (\alpha m\ u + \alpha th\ u \sin\theta \cos\theta) \qquad (2\text{-}23)$$

where the cosine function has been arbitrarily added to the second term to prevent it from contributing to entrainment close to the jet source.

The conservation equations of mass, momentum, and density deficiency were developed and cross-sectionally integrated for both models and put into normalized form to expedite calculation. Solutions were obtained through a fourth order Runge-Kutta technique. The coefficient of entrainment, α, for the modified Fan model was determined from the prediction curve that "best fit" experimental data.

Anderson presented a formula for determining a priori the correct entrainment coefficient to be used in the Fan model. It was found that α depended on the densimetric Froude number, the velocity ratio, and the inclination angle, in the following manner:

$$\alpha = -0.17 + 0.104 \log (F_r) - 0.553 \log (k) + 1.05 \sin (\theta_o)$$

Note: This equation is only valid for the range of parameters used in Anderson's study, which were θ=45°, 60°, 90°, k=5 to 20, and F_r=10 to 60.

Anderson found the best fit predictions for both models when jets of high densimetric Froude numbers and low velocity ratios ($F_r \rightarrow 40$, $k \rightarrow 5$) were compared. At high Froude numbers, the density difference between the jet and ambient fluids was relatively small, which resulted in a "less" negatively buoyant jet. For low velocity ratios, the effect of the ambient velocity was greater, which increased mixing and tended to minimize the negative buoyancy effect.

At low densimetric Froude numbers and high velocity ratios, a poorer prediction in the analytical results was found. It was noted that for these conditions there was a very pronounced curvature at the peak of the jet trajectory in the experimental tests. This violated the assumption of maintaining a large radius of curvature. More important, at this point, the jet had a tendency to fall back on itself and thus the similarity assumption was destroyed.

Anderson noted a particularly poor prediction for the low Froude number, high velocity ratio conditions in Abraham's model. This was due to Abraham's assumption that far from the source, the jet plume moves parallel to the ambient current, as would be the case of a well-mixed buoyant jet. But, for a negatively buoyant

jet of these conditions, the plume reached its peak and quickly plunged to the bottom. When this behavior was very pronounced, the assumption that the trajectory remains parallel to the ambient current became very weak. For this reason, Anderson suggested that the modified Abraham model not be used for these conditions.

In summary, Anderson's results showed that the closer a jet approached the characteristics of a buoyant jet, the better the analytical model predicted the experimental data.

2.3 Slot, Negatively Buoyant Jets in a Stagnant Environment

2.3.1 Jain and Peña Analytical Model

The only study investigating the phenomenon of negatively buoyant slot jets in a stagnant environment was presented in February, 1974, by Jain and Peña[15]. They conducted an analytical study of the very specific problem of heated effluents discharged from round and slot jets during the winter months in a cold climate. The ambient temperature of the receiving body of water was at or very near the freezing point. Due to the nonlinearity of the water density-temperature function and the reversal of the rate of the density change at 32.2°F (4.0°C), slightly warmer-than-ambient effluents are heavier than the receiving water and are thus another example of a negatively buoyant jet.

The governing equations developed by Fan and Brooks[16] for a positively buoyant jet were modified to account for the nonlinear variation of the water density. Modification was necessary because this is a somewhat different problem than the one studied by the previous investigators. Whereas Fan and Brooks were able to assume a Gaussian distribution of the density difference across the jet's cross section, this was impossible for the Iowa study because of the nonlinearity complication. In contrast, Jain and Peña assumed a Gaussian distribution of the temperature difference which they had proven to be a viable assumption through previous experiments. The conservation equations of heat was substituted for the density deficiency equation used in the Fan and Brooks model.

The governing equations were put into normalized form and solved by a modified Euler predictor-corrector method. Dimensionless plots were presented which illustrated how the normalized trajectories and dilutions varied with a momentum flux parameter. Situations involving different injection angles (0°, 15°, and 30°) and initial temperature differences were solved. No experimental verification of the results was presented.

There are two major differences which prevent close comparison of the Jain and Peña study with the present one. First, as already stated, their study dealt with a nonlinear phenomenon that prevents the conservation of the density deficiency flux. It would seem

reasonable to expect that this complication would create a jet with different behavior than one where the density deficiency flux is conserved. Second, the analytical solution of Jain and Peña ignores the effect of the bottom boundary and the reattachment eddy that is created by slot discharges. This phenomenon will be shown later in this study to be very significant (Appendix I is a discussion of the paper by Jain and Peña based on the results of the study).

2.4 Slot, Negatively Buoyant Jets in a Uniformly Flowing Environment

2.4.1 Present Study

At this time, no published literature on the behavior of a negatively buoyant slot jet in a flowing environment has been found. This phenomenon is investigated experimentally in the present study.

3. Experimental Methods

3.1 Introduction

The objective of the experimental portion of this study was to measure the centerline trajectories and downstream dilution ratios of negatively buoyant slot jets. Dilution ratios were determined at two positions along the centerline trajectory:

(1) the maximum height of rise, and

(2) the point of the plume's impingement on the bottom.

All experiments were conducted in the fluid mechanics laboratory of the Department of Civil Engineering at the University of Delaware. An overall view of the experimental facilities is shown in Figure 3-1.

Household table salt was used to make solutions to model the discharge fluid. The salt solution, being heavier than the fresh receiving water, created a negatively buoyant jet. An advantage in using a salt solution was that the concentrations of salt and hence dilution could be correlated with the conductivity measurements in the jet.

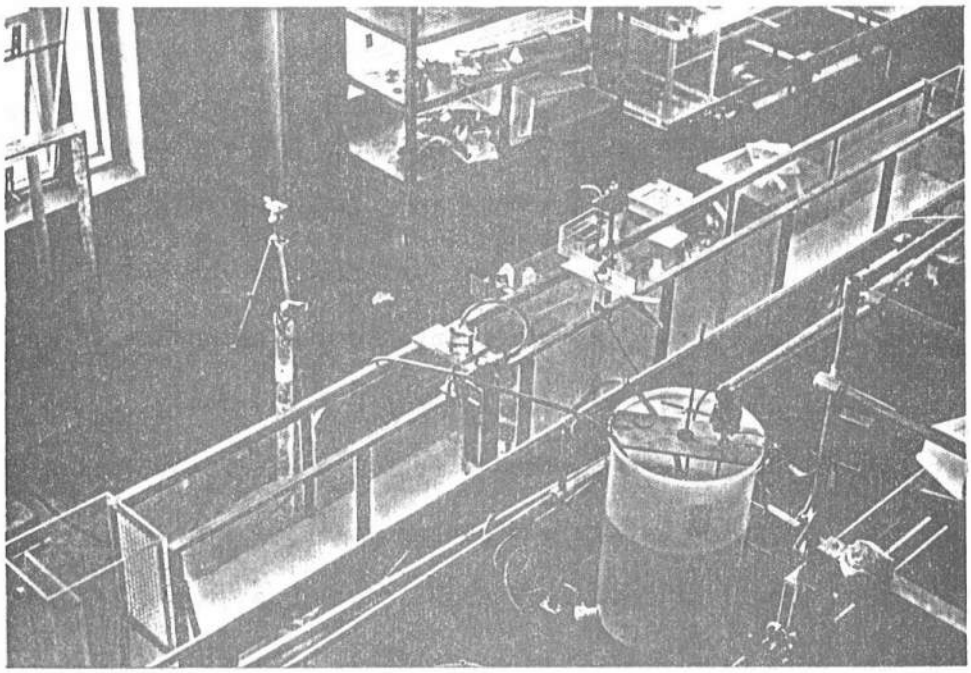

Figure 3-1 Plan View of Experimental Facilities

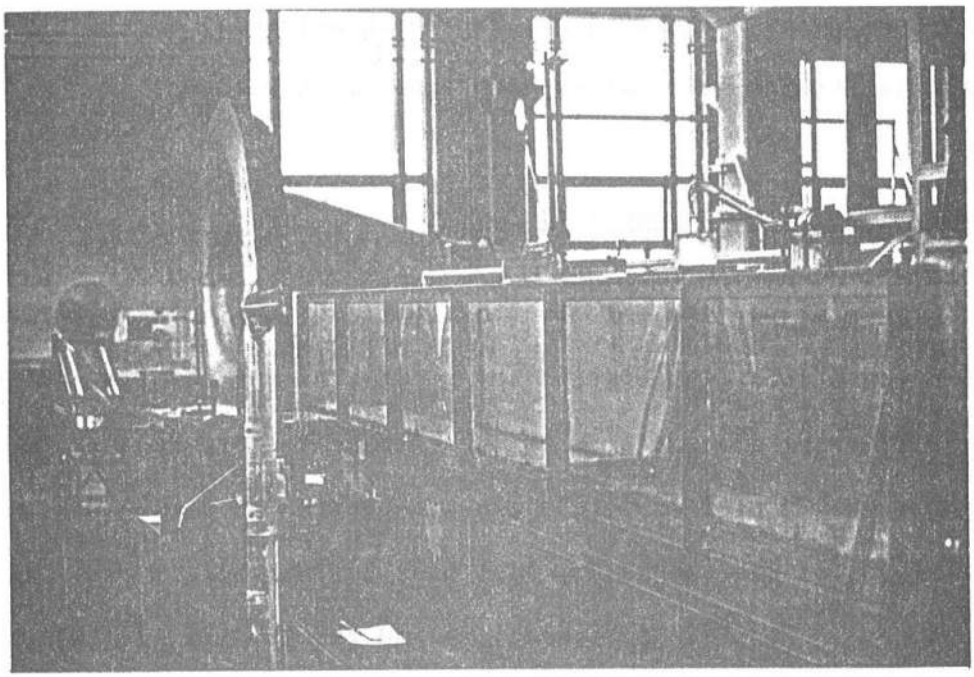

Figure 3-2 Side View of Flume

3.2 The Flume (receiving the water body)

All experiments were conducted in a plexiglass-walled plume. The flume measured 13"W x 18"D x 18'L (see Figure 3-2). Originally, this flume had been used for wave experiments and had closed ends. To facilitate a flowing environment, it was necessary to add drop and head boxes at either end (see Figures 3-3 and 3-4). A 350 GPM (22 liters/sec) pump was connected to the flume to produce the ambient current. The pump system was set up to allow diversion of the main flow from the flume into a recirculation loop. This provided an easy and effective method to control the ambient flow. Finally, posterboard, on which a two-inch grid system was printed, was affixed to the back side of the flume. All tests were recorded with photographs against this grid system, which allowed accurate plotting of the jet trajectories after each experiment was run.

3.3 The Jet Discharge Slot Design

It was necessary to construct a discharge structure which would not interfere significantly with the ambient flow and would lend itself easily to changing of the different slot sizes and injection angles. The slot structure was constructed of plexiglass. It was a shallow box that would lay flat on the flume bottom (see Figures 3-5, 3-6, and 3-7). Fluid entered one end through six 1/4" plastic tubes

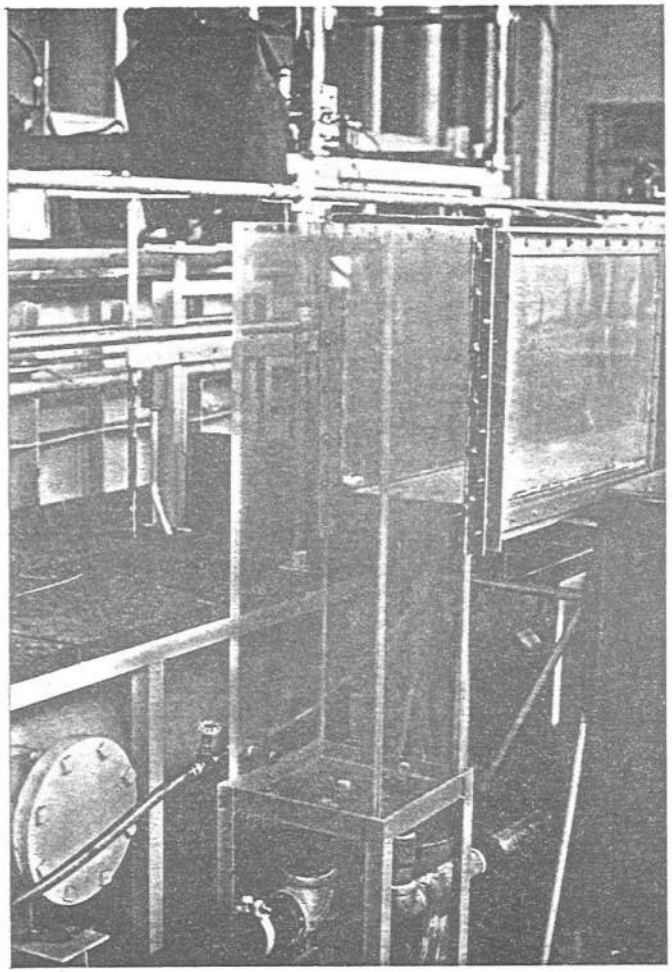

Figure 3-3 Drop Box at Downstream End of Flume

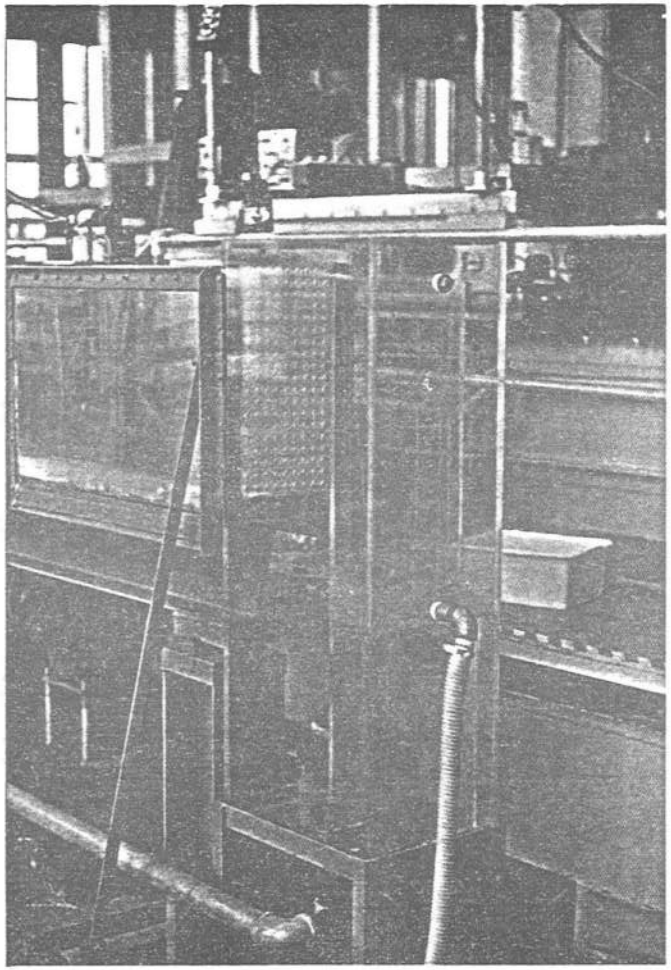

Figure 3-4 Head Box at Upstream End of Flume

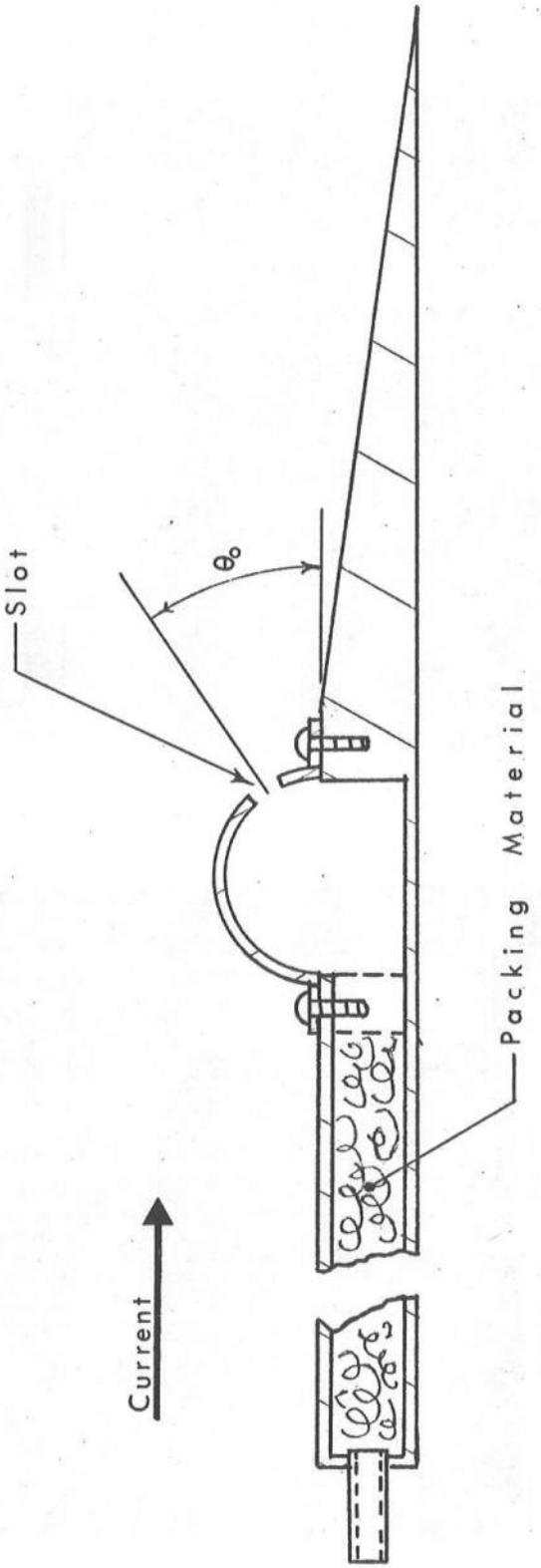

Figure 3-5 Schematic of the Slot Discharge Structure (Side View)

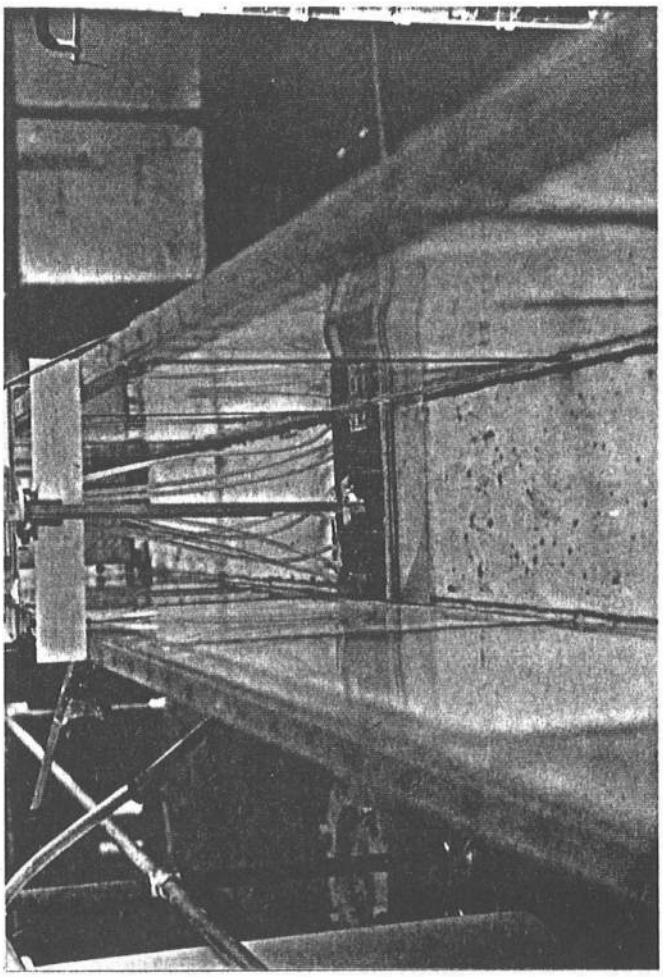

Figure 3-7 Front View of Discharge Structure (from downstream end)

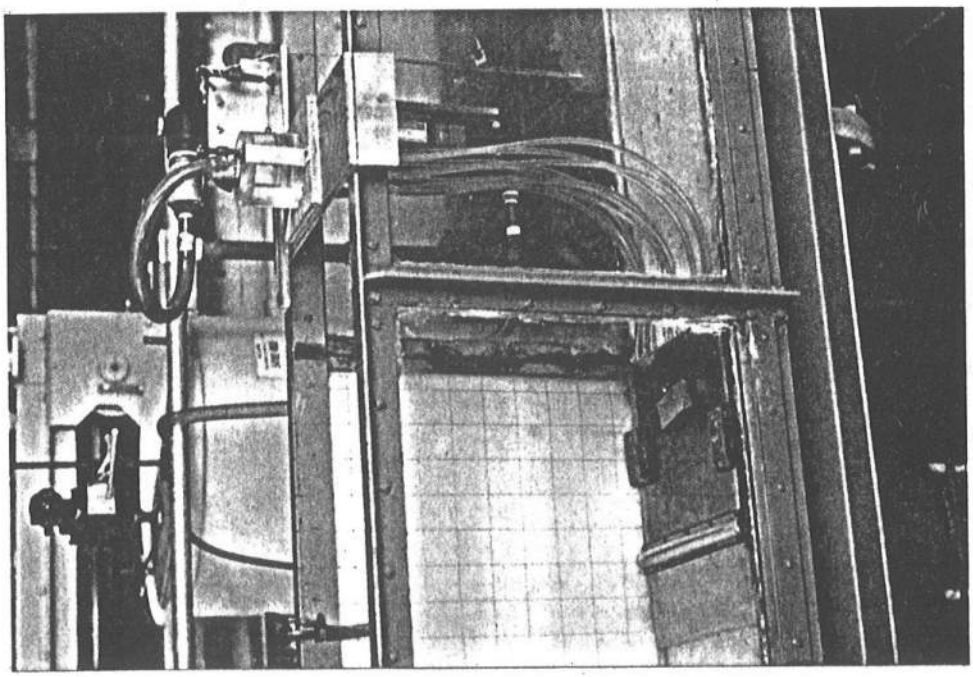

Figure 3-6 Side View of Manifold and Discharge Structure

and exited out the slot at the other end. The box was filled with coarse, sponge packing material to "smooth" out the fluid flow. Various slots were cut along interchangeable 1/2" radius half-round lengths which were attached to the slot box by eight screws. Two slot sizes, 1/8" and 1/4" were cut for each injection angle. The two sizes enable the modeling of densimetric Froude numbers in the range of 10 to 50. There was a shallow incline on the downstream side of the slot to minimize eddy effects from the ambient current. It was observed that there were no noticeable eddy effects due to the slot structure during the flowing environment cases.

3.4 Discharge Fluid Injection and Control

The discharge solution was mixed in a fifty-five gallon polyethelene barrel with a variable speed electric propellor-type mixer (see Figure 3-8). Methylene blue dye was added to aid in locating the jet's centerline and provided contrast for the photographic records. Immediately preceding each run, the densities and temperatures of the ambient and discharge fluids were recorded. A reservoir was used to store all water before the experimental runs. This allowed the water temperature to stabilize, so that there was very little temperature difference between the discharge and ambient fluids.

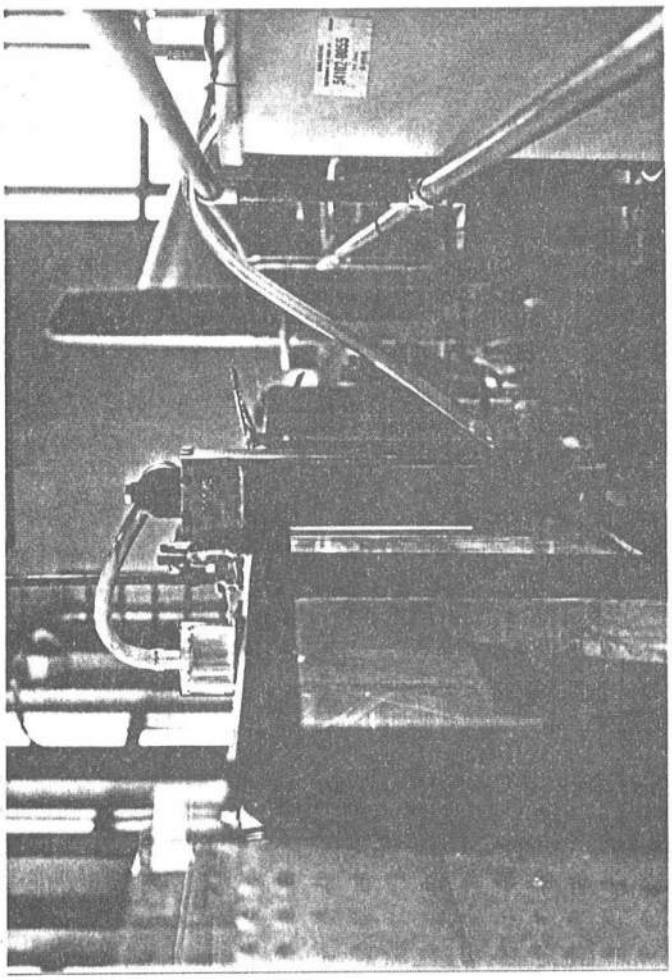

Figure 3-9 Brook's "Full-View" Rotometer

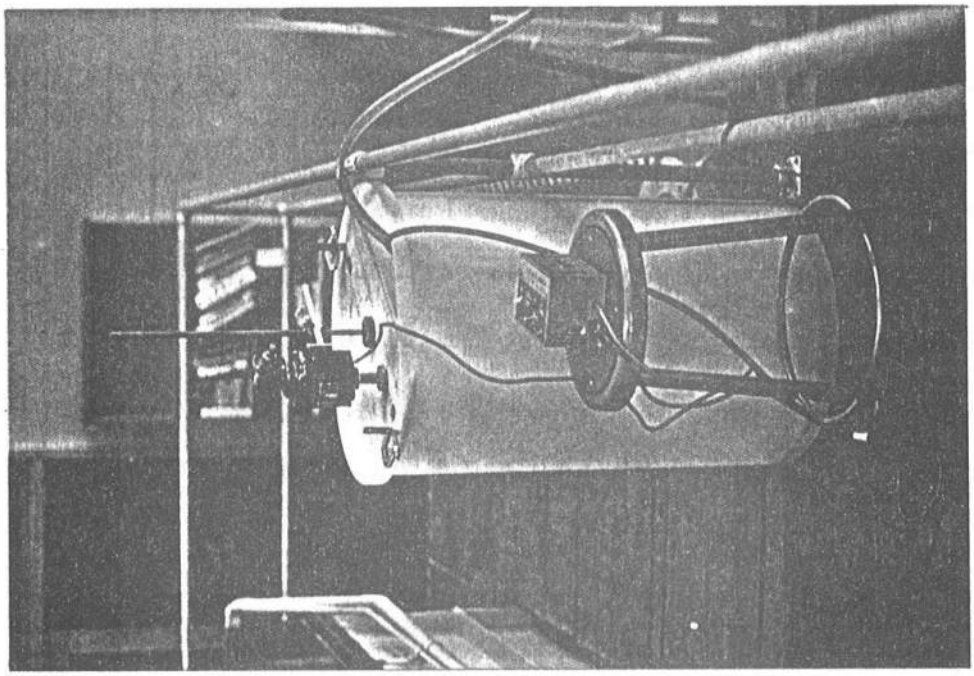

Figure 3-8 Barrell and Mixer

The jet fluid was delivered to the jet by means of a 15 GPM (.95 liters/sec) submersible pump located within the mixing barrel. Flow rate was controlled by a hand-operated gate valve and a Brook's "Full View" rotometer (see Figure 3-9). Flow rate was found to be very stable for the duration of each run.

The discharge fluid was pumped from the mixing barrel through 3/4" plastic tubing into a plexiglass manifold. The manifold split the main flow into six smaller tubes that led to the slot box (see Figure 3-6).

3.5 The Conductivity Probe

An electrical conductivity probe was used to measure the local solution conductivity and hence the salt concentration (see Figure 3-10). The probe consisted of a 20 gauge copper wire threaded through a 1/4" glass tube elbow. At one end, the probe tip, the wire was sealed within the glass tube with epoxy cement, while just the tip of the wire was left exposed. The other end of the wire was connected to a BNC female jack, type UC-1094-U. The sensitivity of the probe and electronics was a function of the wire diameter. It was found that 20 gauge wire provided the most desirable sensitivity in the range of salt solution concentrations used in the experiments. This range was from 2.9 g/liter of salt through 50.0 g/liter of salt.

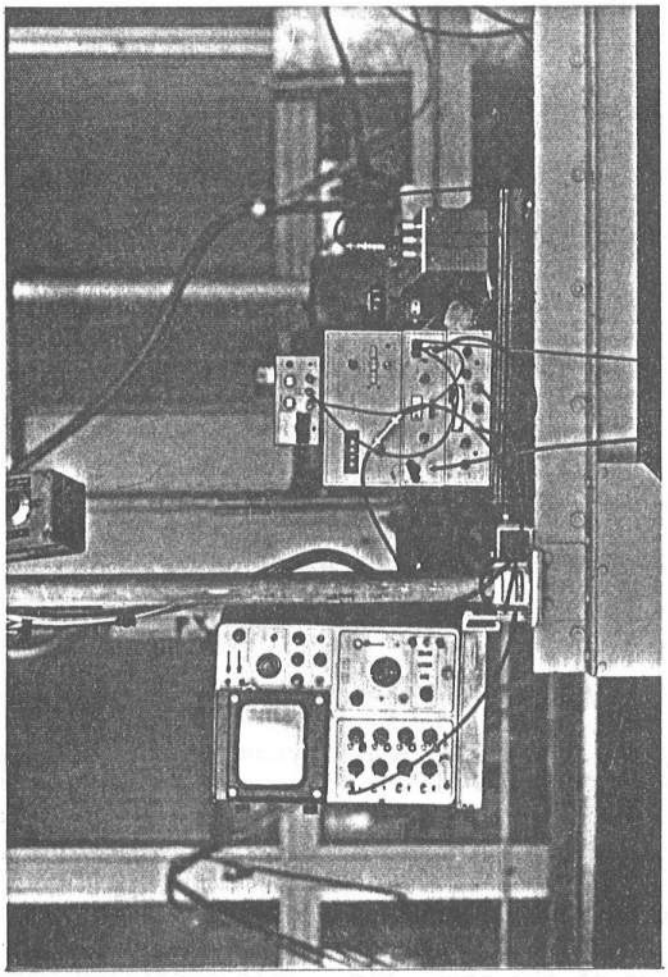

Figure 3-11 Hot-Film Probe Electronics

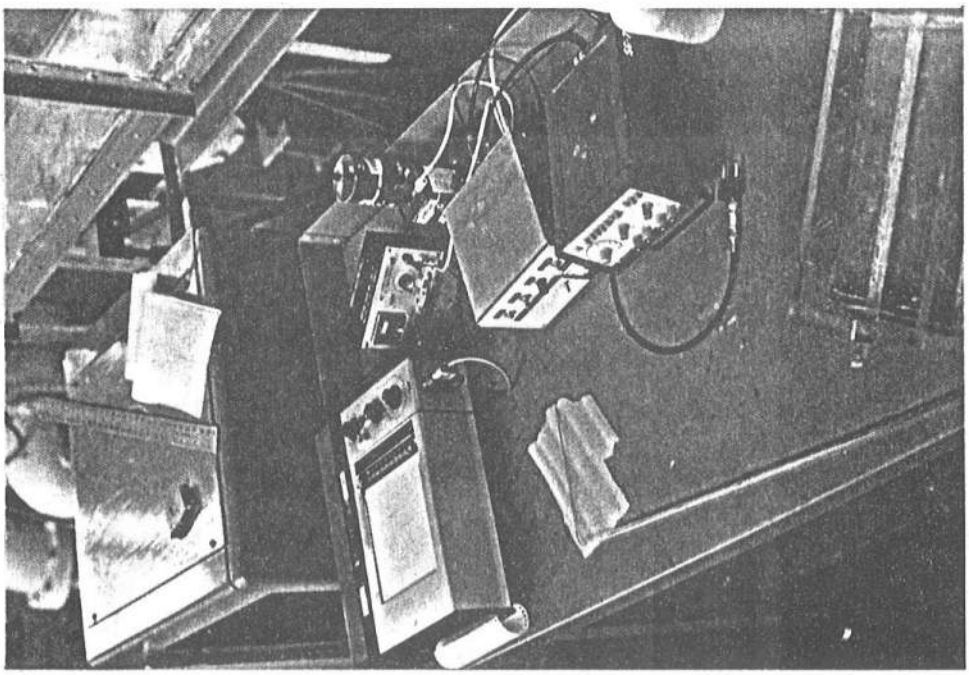

Figure 3-10 Conductivity Probe and Electronics

The electronics for the probe were previously designed by Vadala[17] at the University of Delaware (see Figure 3-10). This system determines the conductivity by balancing an unknown resistance with a known resistance in a Wheatstone Bridge. Since the solution is grounded, no current is lost and the greatest resistance is produced in a small spherical portion of the solution at the probe tip. This resistance plus the probe's resistance are the unknown parts of the Wheatstone Bridge. The actual voltage change is sensed by a differential amplifier and then passed through a D.C. detector. This provides a change in the D.C. voltage for each change in conductivity. The D.C. voltage change is then calibrated with known concentrations of salt solutions. During the experimental runs, the output was recorded on a strip chart recorder.

It was found that the D.C. voltage output was quite sensitive to the condition of the probe tip. This condition was kept consistent by cleansing the probe tip in a 5 percent HCL acid solution prior to the experimental runs. The probe was calibrated immediately before and after each set of runs. Reproducibility was very good.

3.6 The Ambient Velocity Probe

It was necessary to determine accurately the ambient water velocity. Because this velocity was quite small (2 cm/sec), this measurement proved to be somewhat of a problem. Measurement by a

simple means, such as with a pitot tube, was inadequate in this low velocity range. Rather than resorting to the measuring of the velocities of neutrally buoyant chips in the ambient current, it was decided to employ a hot-film probe in conjunction with a Disa constant temperature anemometer. The anemometer used was a type 55D05 Battery-operated CTA. The probe was a type 55R42 Conical Hot-film Probe (see Figures 3-11 and 3-12).

The Disa system relies on the laws governing convective heat transfer. The probe is maintained at some predetermined operating temperature. As fluid flows past the probe, the convective heat flow is increased and consequently more electrical current is supplied to maintain the operating temperature. The electrical current fluctuation is measured and outputted to a digital voltmeter. This output is calibrated in a water flow of known velocities.

Perhaps the most difficult problem with this system is accurately calibrating the probe and electronics. It was decided to calibrate the system by towing the probe on a variable speed carriage, mounted on a tow tank, through stagnant water. This method proved to be quite easy and very accurate. It was only necessary to time the probe through a known distance and record the voltmeter readout. Another advantage of this system was that the tow tank facilities were located adjacent to the flume in which the model jet studies were conducted. In order to switch from the tow tank to the flume, it was

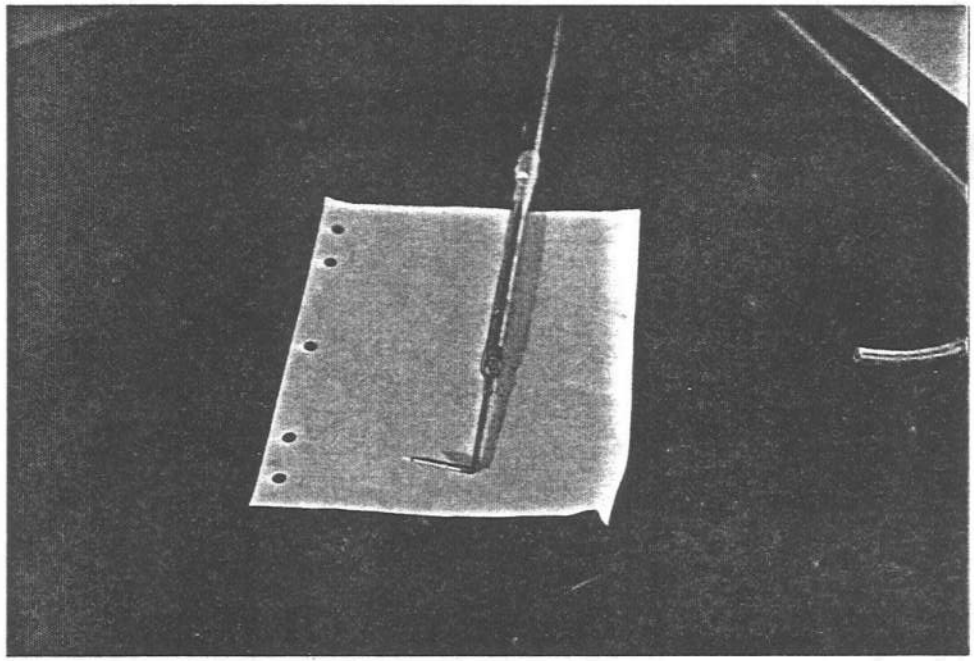

Figure 3-12 Conical Hot-Film Probe

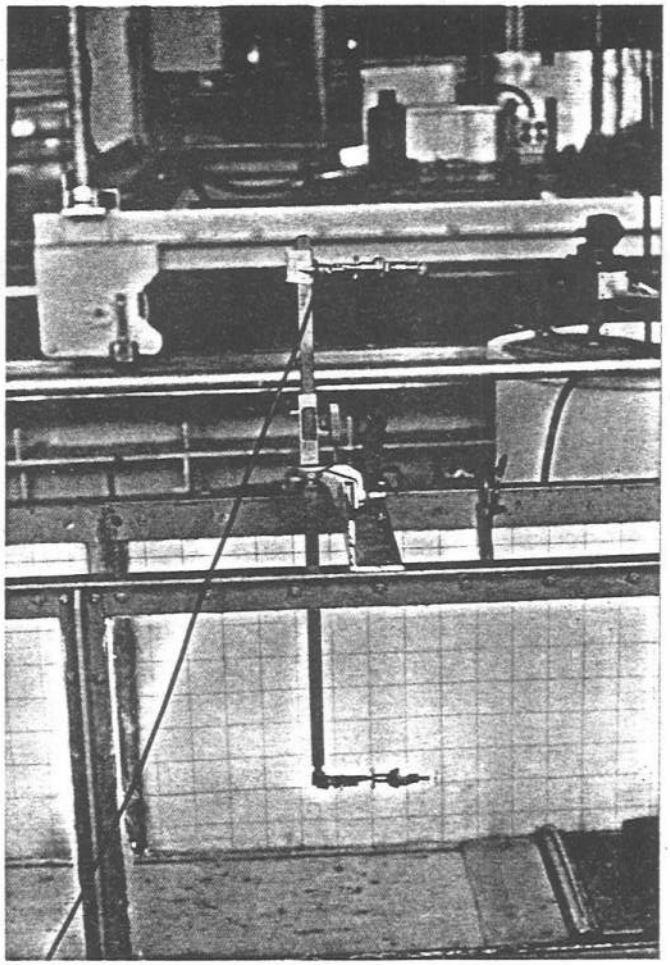

Figure 3-13 Probe Mount and
Poster Card Background

only necessary to move the probe itself, leaving the electronics intact. This provided a quick means of checking calibration at any time during the experiments. The probe's reproducibility proved to be very reliable.

3.7 Ambient Velocity Measurements

Prior to each run, it was necessary to adjust the ambient crosscurrent to the velocity that would achieve the desired k ratio. The Disa probe was mounted on a movable carriage with a vernier depth adjuster (see Figure 3-13). This setup provided an easy way to correlate the verticle distance from the flume bottom with the corresponding velocity measurement. Measurements indicated that the velocity was uniform across the flume width (see Figure 3-14).

A vertical velocity profile at the flume centerline was recorded prior to each run. A typical velocity profile is shown in Figure 3-15. The profile exhibits turbulent characteristics, being essentially uniform except very near the bottom boundary. According to Streeter[18], open channel flow is fully turbulent when the Reynolds' number, R, is greater than 2000, where:

$$R = 4 R_H U_a/\nu \qquad (3\text{-}1)$$

the hydraulic radius, R_H:

$$R_H = \frac{(1.5)(1)}{2(1.5)+1} = .375 \text{ ft } (11.4 \text{ cm}) \qquad (3\text{-}2)$$

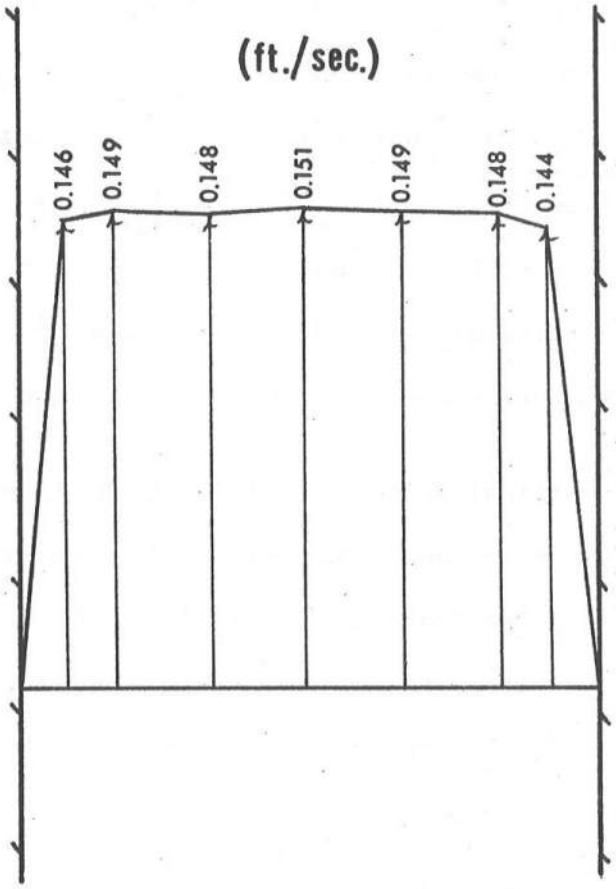

Figure 3-14 Typical Horizontal Profile of the Ambient Velocity at the Mid-Depth of the Flume

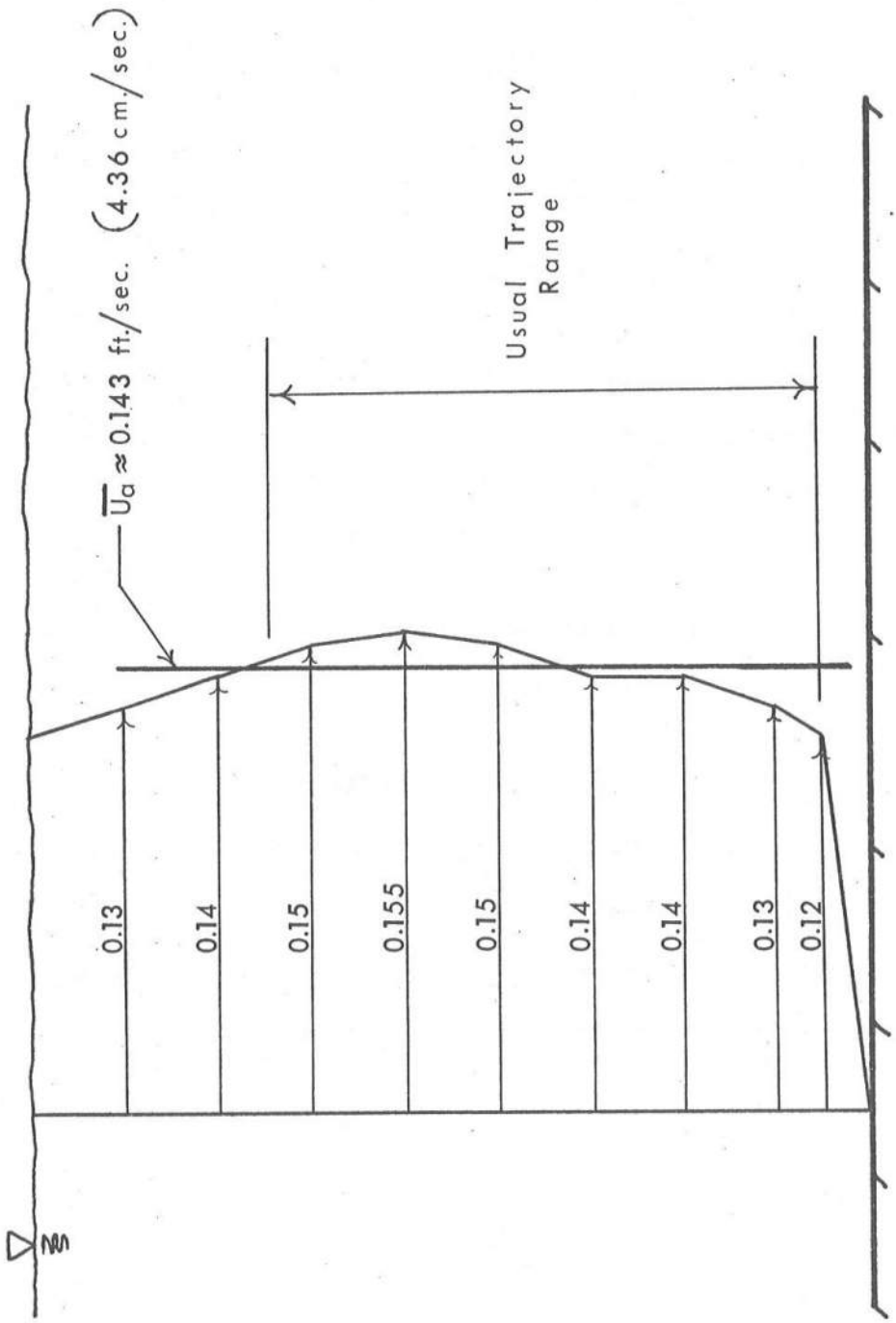

Figure 3-15 Typical Vertical Profile of the Ambient Velocity of the Centerline of the Flume

and the dynamic viscosity of water, ν:

$$\nu = 1.1 \times 10^{-5} \text{ ft}^2/\text{sec} \ (1.02 \times 10^{-2} \text{ cm}^2/\text{sec}) \qquad (3\text{-}3)$$

Substituting (3-2) and (3-3) into (3-1):

$$R = 1.36 \times 10^{5} \ U_a \ (U_a \text{ in ft/sec}) \qquad (3\text{-}4)$$

The slowest ambient velocity used in the experiments had a value of 0.072 ft/sec (2.2 cm/sec); thus, the lowest Reynolds' number was:

$$R = 9800 > 2000 \qquad (3\text{-}5)$$

Therefore, all flowing experiments were conducted in fully turbulent flow.

The vertical velocity profiles were plotted on paper, and the average ambient velocity, $\overline{U}_a$, was determined by eye, keeping in mind what vertical height range the jet trajectory was mostly contained. This prevented the extreme upper and lower point velocities from influencing the average velocity value (see Figure 3-15).

4. Development of an Analytical Model for the Stagnant Case

4.1 Basic Assumptions

The profiles of velocity and density deficiency across the jet are assumed to be both Gaussian and similar at any cross section:

$$u^* = u(s)\, e^{-n^2/b^2} \tag{4-1}$$

$$(\rho-\rho_a)^* = \Delta\rho^* = \Delta\rho(s)\, e^{-n^2/b^2} \tag{4-2}$$

where

u^* = velocity at any point in the jet,

$u(s)=u$ = centerline jet velocity,

ρ^* = density at any point in the jet,

$\Delta\rho(s)=\Delta(\rho)$ = density difference between jet and ambient fluids at the jet centerline,

ρ_a = ambient density (constant)

n = distance perpendicular from the jet centerline,

s = distance along jet centerline,

b = jet characteristic half-width (related to the nominal half-width, W, by $W = \sqrt{2}\, b$), and

λ = spreading coefficient.

Turbulent entrainment is assumed to be proportional to the centerline velocity in the jet (Taylor hypothesis):

$$\frac{dQ}{ds} = 2\alpha u \tag{4-3}$$

where

Q = volume of fluid contained in incremental distance of the jet and

α = entrainment coefficient.

A schematic diagram of the analytical model is shown in Figure 4-1. Initial conditions (subscripted by zero) are those conditions at the end of the zone of flow establishment. The similarity assumptions and hence the model itself are only valid in the zone of fully developed flow.

$$F_r = \frac{U_o}{\sqrt{B \frac{\Delta\rho}{\rho_a} g}}$$

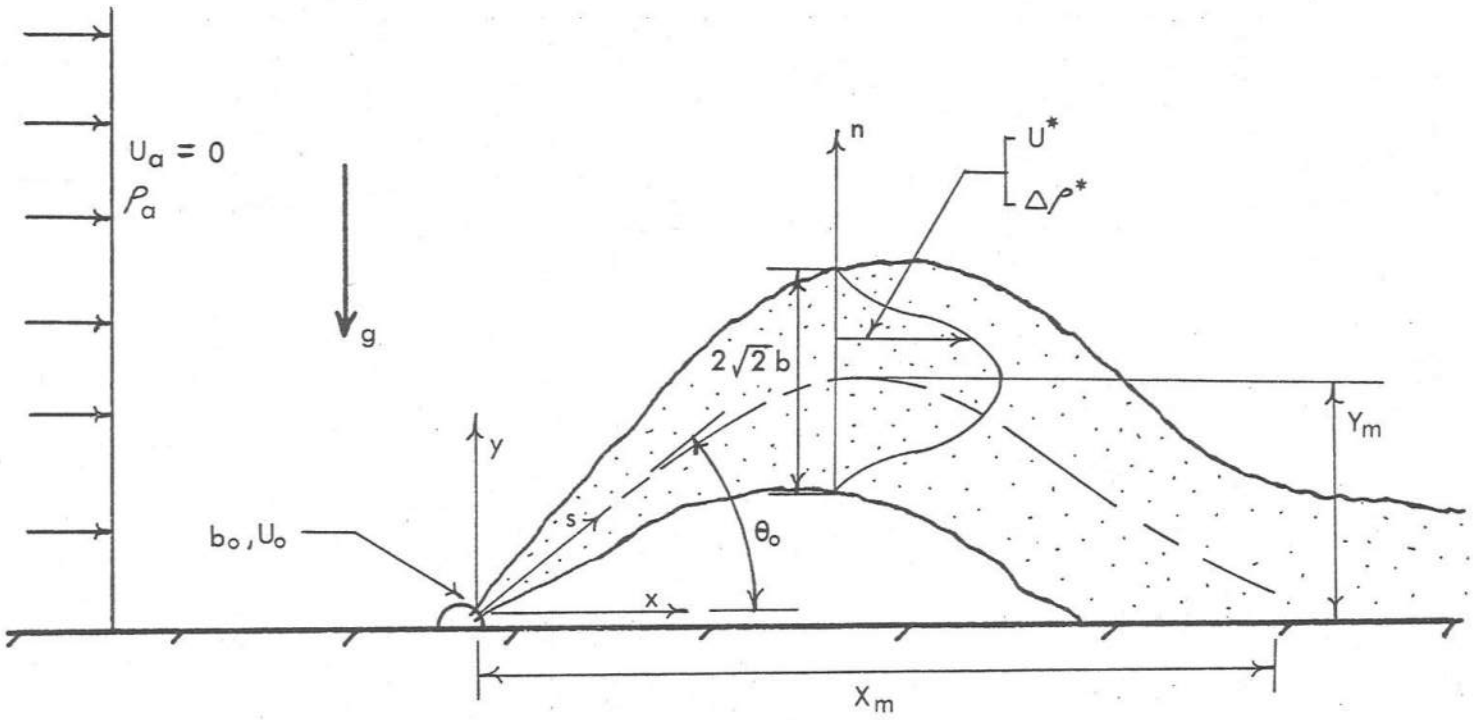

Figure 4-1 Schematic for the Analytical Analysis of a Negatively Buoyant Slot Jet in a Stagnant Environment

4.2 Zone of Flow Establishment

The flow leaves the orifices with essentially uniform velocity and fluid density across the entire width. Due to the lateral mixing action, ambient fluid begins to "eat" away at outside edges of the jet. When this mixing region penetrates to the centerline of the jet, the jet is considered to be fully developed (see Figure 4-2).

According to the study by Albertson et al.[13] on neutrally buoyant jets, the length of the zone of flow establishment, L_e, is a function of the slot width, B:

$$L_e = 5.2B \tag{4-4}$$

The initial characteristic half-width, b_o, is found by applying the momentum relation between the ends of the zone of flow establishment and by assuming that the negative buoyancy force is negligible in such a short region:

$$u_o^2 B = \int_{-\infty}^{\infty} u^{*2}\, dr$$

$$= \sqrt{\frac{\pi}{2}}\, u_o^2 b_o \tag{4-5}$$

Thus:

$$b_o = \sqrt{\frac{2}{\pi}}\, B \tag{4-6}$$

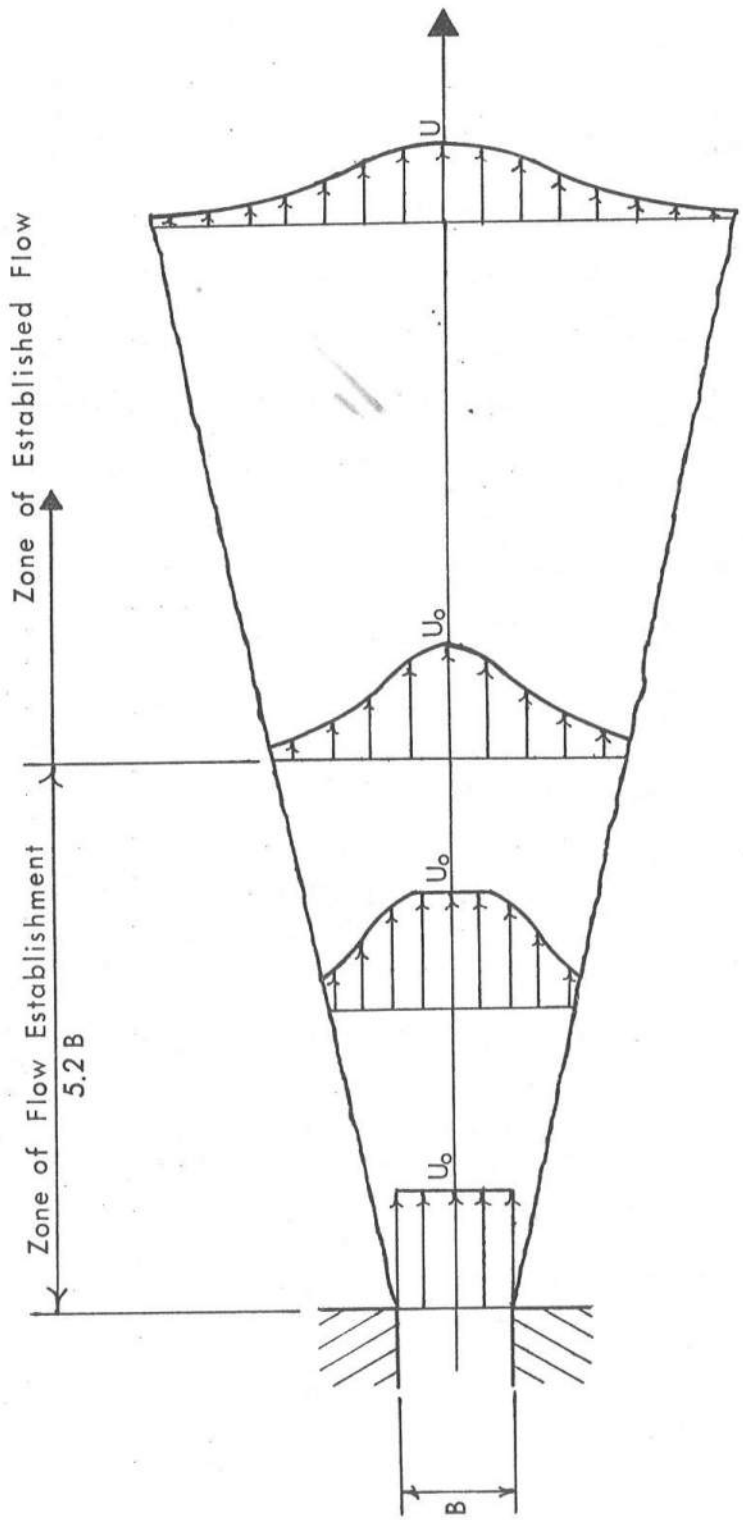

Figure 4-2 Zone of Flow Establishment and Zone of Established Flow

or

$$B = \sqrt{\frac{\pi}{2}}\, b_o \tag{4-6a}$$

4.3 The Model

The analytical model used in this study employs the integral-similarity technique of Morton, Taylor, and Turner[2]. The governing equations developed by Fan and Brooks[16] for positively buoyant plot jets in a stagnant environment are applied to negatively buoyant slot jets under similar conditions. The governing equations are:

Conservation of Mass:

$$\frac{d}{ds}(ub) = 2\alpha u/\sqrt{\pi} \tag{4-7}$$

Conservation of Horizontal Momentum:

$$\frac{d}{ds}\left(\frac{u^2 b \sin\theta}{\sqrt{2}}\right) = 0 \tag{4-8}$$

Conservation of Vertical Momentum:

$$\frac{d}{ds}\left(\frac{u^2 b \sin\theta}{\sqrt{2}}\right) = g\, b\, \frac{\Delta\rho}{\rho_a} \tag{4-9}$$

Conservation of Density Deficiency:

$$\frac{d}{ds}(ub\Delta\rho) = 0 \tag{4-10}$$

Conservation of Tracer Material:

$$\frac{d}{ds}(cub) = 0 \tag{4-11}$$

Geometric Relationships:

$$\frac{dx}{ds} = \cos\theta \tag{4-12}$$

$$\frac{dy}{ds} = \sin\theta \tag{4-13}$$

where

c = centerline concentration of any tracer materials,

x = horizontal coordinate,

y = vertical coordinate,

and all other notations as previously defined.

Equations (4-8), (4-10), and (4-11) may be integrated directly:

$$u^2 b \cos\theta = \text{constant} = u_o^2 b_o \cos\theta_o \tag{4-14}$$

$$ub\Delta\rho = \text{constant} = u_o b_o \Delta\rho_o \tag{4-15}$$

$$cub = \text{constant} = c_o u_o b_o \tag{4-16}$$

respectively. From Equation (4-16), the expression for the centerline dilution, S, is found:

$$S = c_o/c = ub/u_o b_o \tag{4-17}$$

4.4 Solution Technique

Equations (4-7), (4-8), (4-14), and (4-15) are rewritten:

$$d(ub) = (2\alpha u\sqrt{\pi})ds \tag{4-7a}$$

$$d(u^2 b \sin\theta) = \left(\frac{g\ b\ \Delta\rho\ \sqrt{2}}{\rho_a}\right) ds \tag{4-8a}$$

$$u^2 b \cos\theta = u_o^2 b_o \cos\theta_o \tag{4-14}$$

$$ub\Delta\rho = u_o b_o \rho_o \tag{4-15}$$

The solutions to the analytical model may be found by working with the four unknowns, u, b, ρ, and θ, in the last four Equations (4-7a), (4-8a), (4-14), and (4-15). The trajectory centerline coordinate, s, is the independent variable. A step-by-step modified Euler predictor-corrector technique is employed to obtain the solution. The method is as follows:

(1) Start with known values of u, b, $\Delta\rho$, and θ in the right-hand side of Equations (4-7a), (4-8a), (4-14), and (4-15).

(2) Arbitrarily set some value to step size, ds. Solve for d(ub) and $d(u^2b \sin \theta)$ from Equations (4-7a) and (4-8a), respectively. Determine (ub)' and $(u^2b \sin \theta)'$ where: $(ub)' = ub + d(ub)$ and $(u^2b \sin \theta)' = u^2b \sin \theta + d(u^2b \sin \theta)$, where the ( )' term designates the assumed value of the ( ) term at next size along s.

(3) Get $(\Delta\rho)'$ by substituting (ub)' into Equation (4-15).

(4) Get $(\theta)'$ by substituting $(u^2b \sin \theta)'$ into Equation (4-14).

(5) Get (u)' by substituting (ub)' and $(\theta)'$ into Equation (4-14).

(6) Get (b)' by substituting u' into the (ub)' equation.

(7) Average all ( )' values with the known ( ) values and substitute these average values back into the right-hand side of Equations (4-7a) and (4-8a).

(8) Repeat steps 2 to 8 until no appreciable changes occur in the u', b', θ', and Δρ' terms. These last ( )' values become the "new" known values. Now repeat the entire process.

The dilution at each step can be found by substituting the "new" values of u and b into Equation (4-17). It is necessary to use some sort of error control that will reduce the step size, if too large of a change in any of the unknowns occurs at any step interval. The solution scheme is continued until either the limits of boundary conditions or maximum distance are reached. The listing of the computer program used to carry out the solution scheme is presented in Appendix II.

4.5 Application

As previously mentioned, the analytical model is only valid for the zone of established flow. Therefore, to compare it with experimental results, it is necessary to correct for the zone of flow establishment by adding on to the trajectory, in the model, 5.2B. The corrections for the horizontal and vertical components are:

$$\frac{x}{B}\ (\text{corrected}) = \frac{x}{B} + 5.2 \cos\theta \qquad (4\text{-}18)$$

$$\frac{y}{B}\ (\text{corrected}) = \frac{y}{B} + 5.2 \sin\theta \qquad (4\text{-}19)$$

The correction for the centerline dilution may be found by equating the volume of tracer flux across the ends of the zone of flow establishment:

$$u_o B c_o = \int_{-\infty}^{\infty} u_o^* c_o^* \, dr \qquad (4\text{-}20)$$

$$= \sqrt{\frac{\lambda^2 \pi}{1 + \lambda^2}} \, c_o \, u_o \, b_o \qquad (4\text{-}20)$$

where

c_o^* = concentration of tracer material at any point in jet cross section at the end of flow establishment.

Thus:

$$S \text{ (corrected)} = \frac{c_o}{c} \sqrt{\frac{2 \lambda^2}{1 + \lambda^2}} \, \frac{b_o}{B} \qquad (4\text{-}21)$$

Substituting Equation (4-6a) into Equation (4-21):

$$S \text{ (corrected)} = \frac{ub}{u_o b_o} \sqrt{\frac{2 \lambda^2}{1 + \lambda^2}} \qquad (4\text{-}22)$$

5.1 Results and Discussion

5.1 Negatively Buoyant Slot Jets in a Stagnant Environment

5.1.1 General

A total of 32 experimental runs for negatively buoyant slot jets in a stagnant environment were conducted. These runs included four different injection angles, 30°, 45°, 60°, and 90°, and covered a range of densimetric Froude numbers from 10 through 50. All experiments were conducted in a water depth of 60" (40.6 cm). See Table 5-1 for the details, θ_o, Fr, and R (injection angle, densimetric Froude number, and Reynolds' number respectively), of each run. Jet trajectories were recorded on photographs. Dilution ratios at the jet centerline, at the maximum height of rise, Y_m, and at the point of bottom impingement, X_m, were determined.

All jet trajectories were observed to tend to a parabolic shape (except for the 90° jets). The top edge of the jet plume exhibited a clearly defined boundary with the ambient fluid. However, this was not the case with the lower edge of the jet. The portion of ambient fluid beneath the jet trajectory was mixed immediately with jet fluid so as to completely mask any lower boundary (Figure 5-1).

Table 5-1

Details of the Experiments in the Stagnant Environment

Run #	θ°	Fr	R	$(\frac{X}{B}, \frac{Ym}{B})$	$(\frac{Xm}{B}, 0)$	S(X,Ym)	S(Xm,c)	u fps/cps	$\frac{\Delta\rho}{\rho}$	B in./cm.
1	60	31.5	2110	40,50	70,0	3.17	3.70	2.23 68.0	.015	0.125 0.318
2	60	39.9	2190	40,61	72,0	2.76	3.50	2.31 70.4	.010	0.125 0.318
3	60	40.1	2190	32,63	80,0	2.95	3.33	2.31 70.4	.0049	0.125 0.318
4	60	19.9	1890	24,35	56,0	3.10	3.52	2.00 61.0	.030	0.125 0.318
5	60	52.4	2190	48,80	90,0	2.36	3.30	2.31 70.4	.0058	0.125 0.318
6	60	10.4	2060	12,17	24,0	2.09	2.82	1.09 33.2	.0165	0.25 0.035
7	30	29.4	2050	8,2	48,0	1.18	1.58	2.16 65.8	.016	0.125 0.318
8	30	51.3	2160	4,4	48,0	1.52	2.19	2.28 69.5	.0059	0.125 0.318
9	30	37.7	2060	8,2	32,0	1.61	2.03	2.18 66.4	.010	0.125 0.318
10	45	29.2	2020	40,37	88,0	2.76	3.91	2.13 65.0	.016	0.125 0.318
11	45	35.9	2060	64,50	96,0	3.33	4.00	2.18 69.5	.011	0.125 0.318
12	45	50.3	2140	80,64	116,0	2.70	3.21	2.26 68.9	.006	0.125 0.318
13	45	41.3	2060	64,54	110,0	2.72	3.67	2.18 69.5	.0083	0.125 0.318
14	45	20.3	1940	28,31	60,0	3.88	4.22	2.05 62.5	.0305	0.125 0.318
15	45	13.2	2060	12,16	32,0	2.05	2.43	1.09 33.2	.018	0.25 0.035
16	45	20.6	1940	40,29	72,0	3.02	3.88	2.05 62.5	.030	0.125 0.318
17	90	30.8	2050	0,74	44,0	4.00	5.10	2.18 66.4	.0146	0.125 0.318
18	90	37.7	2060	0,90	44,0	2.67	4.36	2.18 69.5	.010	0.125 0.318

(Table 5-1 Continued)

Run #	θ°	Fr	R	$(\frac{X}{B}, \frac{Ym}{B})$	$(\frac{Xm}{B}, 0)$	S(x,Ym)	S(Xm,c)	u fps/cps	$\frac{\Delta\rho}{\rho}$	B in./cm.
19	90	20.6	1940	0,46	40,0	4.36	5.9	2.05 62.5	.0297	0.125 0.318
20	90	10.1	2060	0,22	12,0	2.66	3.74	1.09 33.2	.0173	0.25 0.035
21	90	9.9	2060	0,23	8,0	3.03	3.70	1.09 33.2	.018	0.25 0.035
22	90	29.5	2050	0,62	16,0	3.86	4.72	2.16 65.8	.016	0.125 0.318
23	90	37.5	2060	0,84	16,0	3.27	3.77	2.18 69.5	.010	0.125 0.318
24	90	20.0	1930	0,40	16,0	3.58	5.35	2.04 62.2	.031	0.125 0.318
25	90	19.9	1930	0,39	16,0	3.76	5.53	2.04 62.2	.0313	0.125 0.318
26	60	30.3	2050	40,55	64,0	3.36	4.38	2.16 65.8	.015	0.125 0.318
27	60	38.0	2060	40,64	68,0	3.01	4.00	2.18 69.5	.010	0.125 0.318
28	60	45.4	2060	48,70	72,0	2.95	3.80	2.18 69.5	.0069	0.125 0.318
29	60	20.0	1940	48,32	48,0	3.41	4.10	2.05 62.5	.032	0.125 0.318
30	45	29.7	2050	52,40	96,0	3.70	4.07	2.16 65.8	.0158	0.125 0.318
31	45	38.6	2050	64,48	112,0	3.25	3.90	2.16 65.8	.0093	0.125 0.318
32	45	44.4	2090	72,54	120,0	2.86	3.60	2.21 67.4	.0074	0.125 0.318

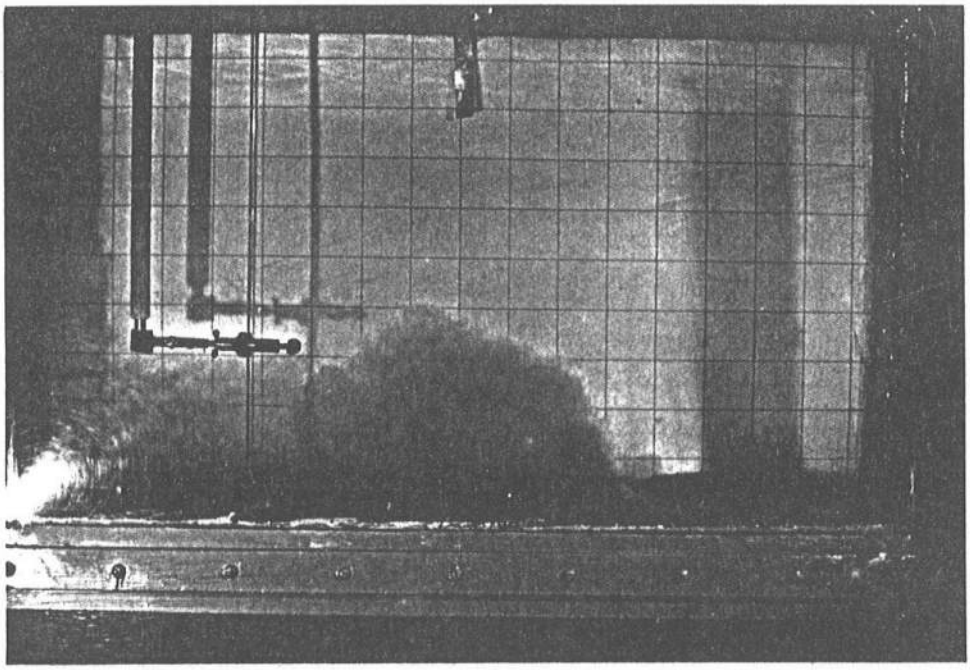

Figure 5-1 Run #14 (θ_o = 45°, Fr = 20.3)

Close observation of this region revealed a reattachment eddy of a flat, elliptical pattern which caused re-entrainment of the jet fluid. The eddy moved in the same direction as the jet in the upper portion of this region and moved back towards the jet orifice in the lower portion (Figure 5-2).

In most cases, the jet fluid tended to split evenly after impinging on the bottom; one half of the fluid volume flowed away from the area in a density current and the other half became caught up in the reattachment eddy. The latter portion of the fluid traveled back towards the jet orifice and was re-entrained into the jet. A result of the reattachment eddy was that uncontaminated ambient fluid could only be entrained in the upper boundary of the jet plume.

5.1.2 Experimental Results

The data are presented in graphs (Figures 5-4 through 5-8) showing the dilutions and trajectories as a function of the densimetric Froude number and injection angle (see Figure 5-3). Figures 5-4 and 5-5 are normalized plots of the two critical points in the centerline trajectory, the maximum height of rise, Ym, and the point of bottom impingement, Xm. The plots indicate the Ym and Xm are very close to being linear function of the densimetric Froude number, similar to findings for round jets. Data for the 30° injection

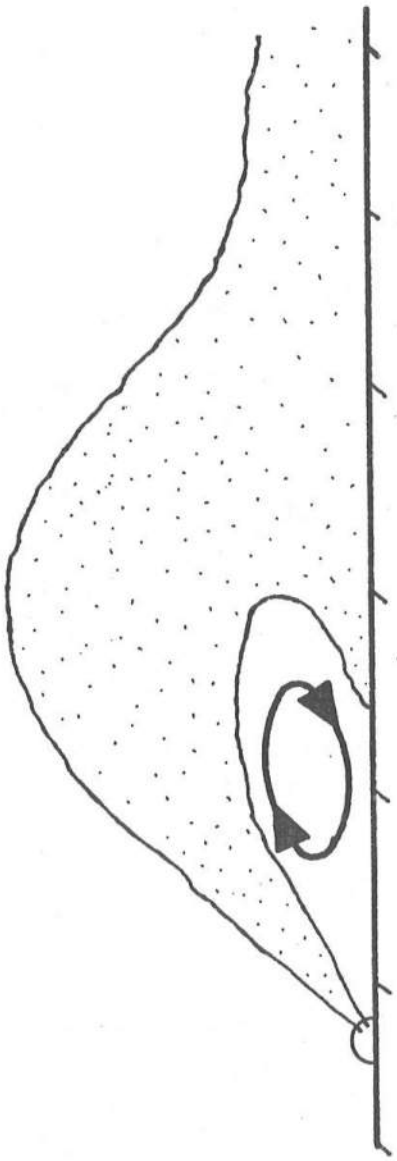

Figure 5-2 Schematic of the Reattachment Eddy

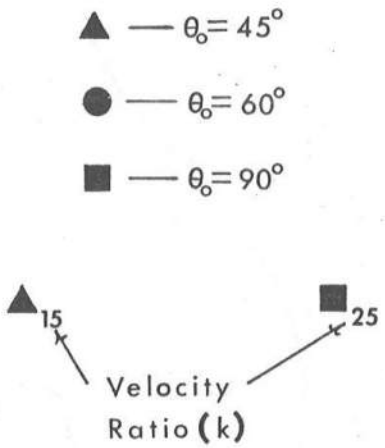

Figure 5-3 Symbols and Notations Used in Figures 5-4 through 5-8 and Figures 5-12 through 5-24

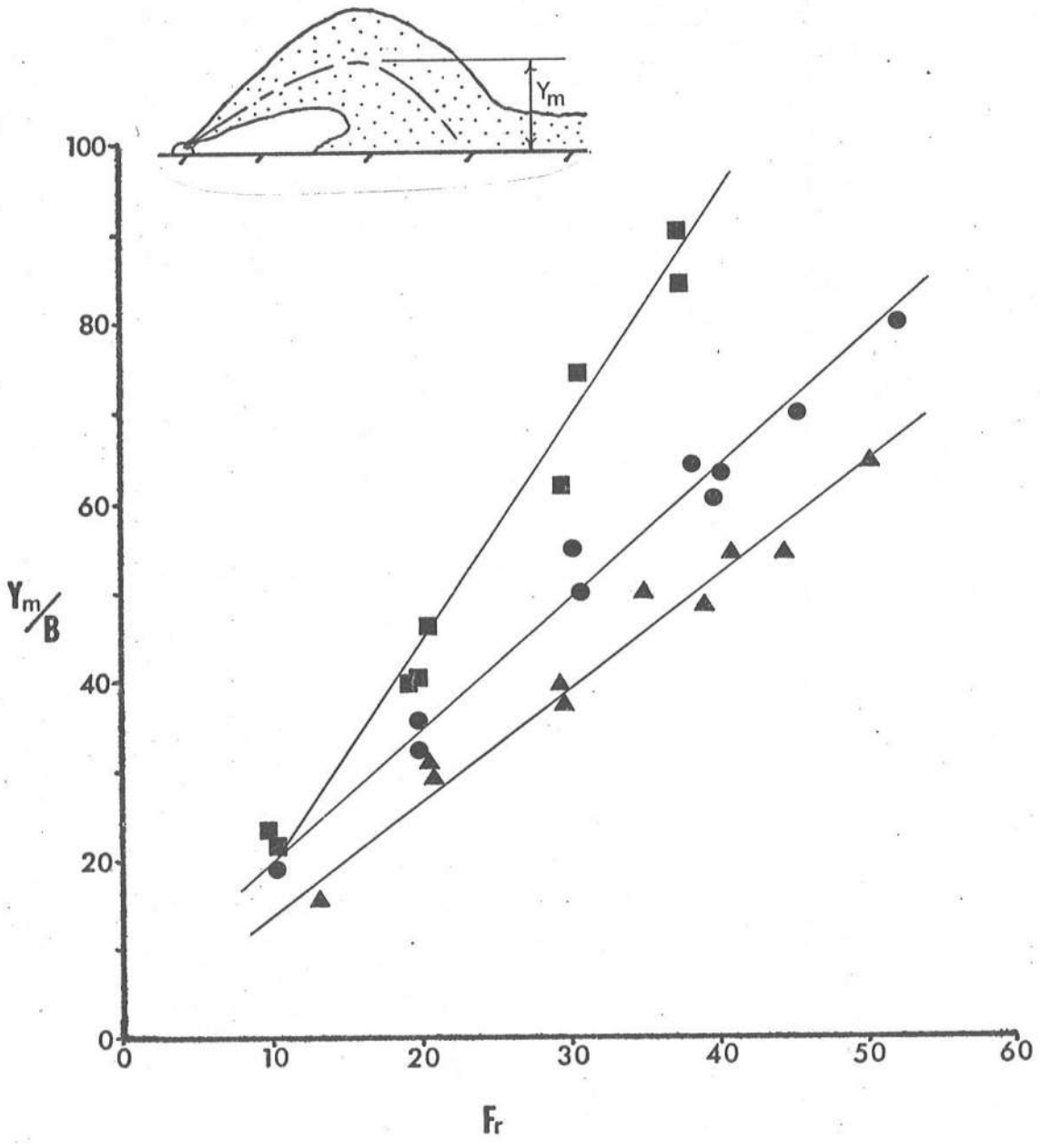

Figure 5-4 Observed Maximum Heights of Rise in a Stagnant Environment

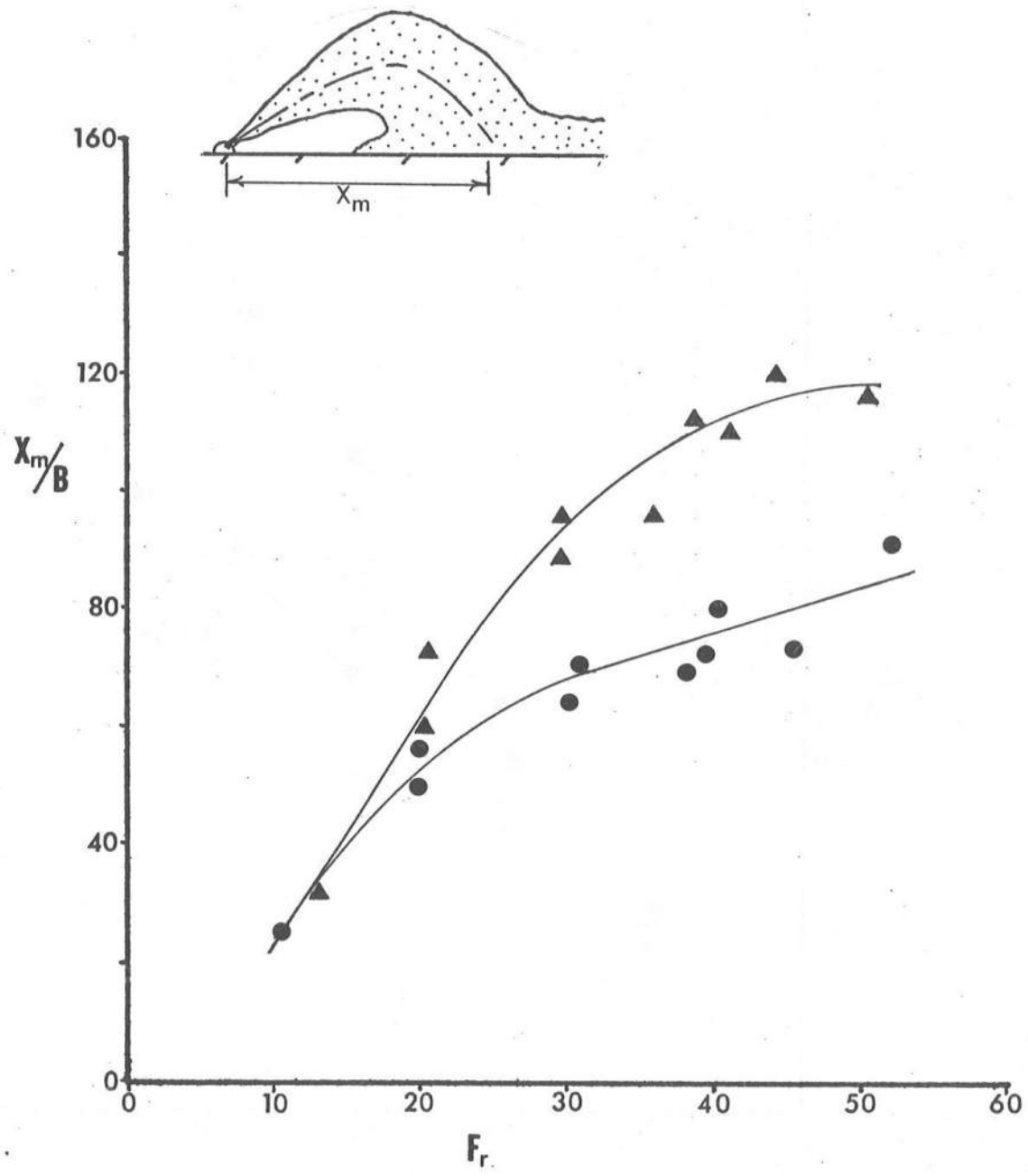

Figure 5-5 Observed Points of Bottom Impingement in a Stagnant Environment

angle cases are not shown because the jet immediately plunged to the bottom; so that there was no discernable path of the centerline trajectory (Figure 5-6).

Figures 5-7 and 5-8 illustrate the downstream dilution ratios of the centerline trajectories at Ym and Xm, respectively. The results are very different from what might be intuitively expected. It would be reasonable to assume that dilution ratios would increase with an increase in the densimetric Froude number, which is indicative of a higher jet velocity, but the experimental data clearly indicate that the dilution ratios decrease with Froude numbers greater than about 20.

The explanation of this phenomenon lies in the existence of the reattachment eddy. At low densimetric Froude numbers, the reattachment eddy is relatively weak and exerts very little influence. This is supported by the observation that, for low Froude number jets, the bulk of the jet fluid flowed away from the area after bottom impingement and was not re-entrained in the jet. Consequently, the dilution ratios did increase as might be expected.

As the densimetric Froude number becomes larger than 20, the effect of the reattachment eddy becomes significant. More of the jet's fluid is sucked into the eddy and re-entrained into the jet. As a result, the dilution ratios decrease.

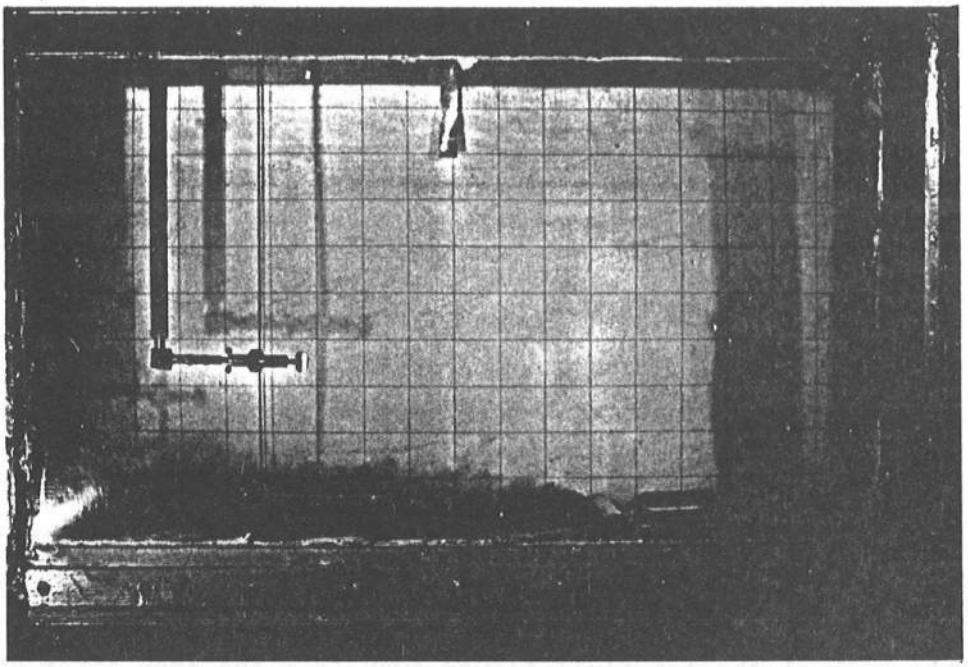

Run #9

$\theta_o = 30°$

Fr = 37.7

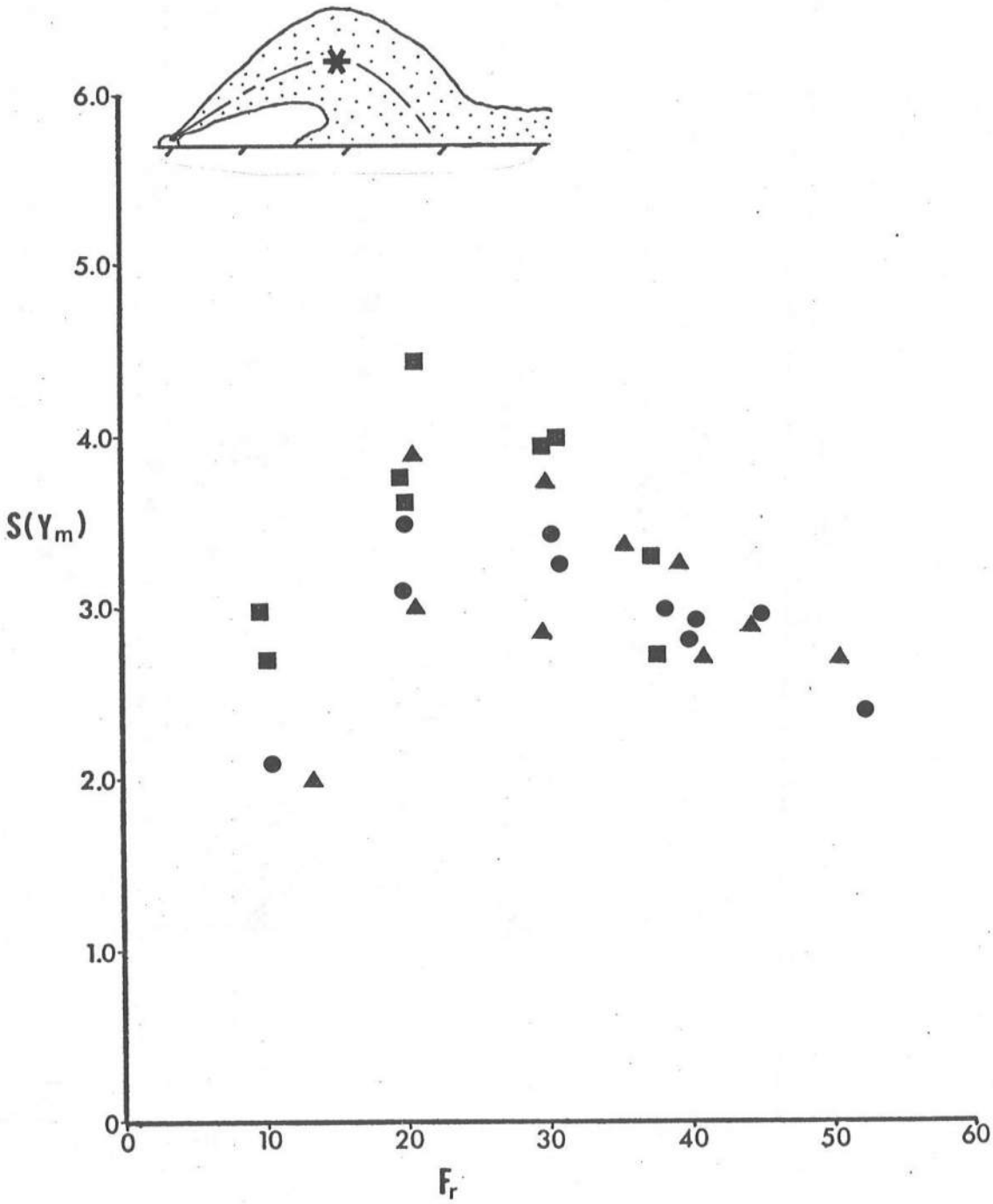

Figure 5-7 Observed Dilutions at the Maximum Height of Rise in a Stagnant Environment

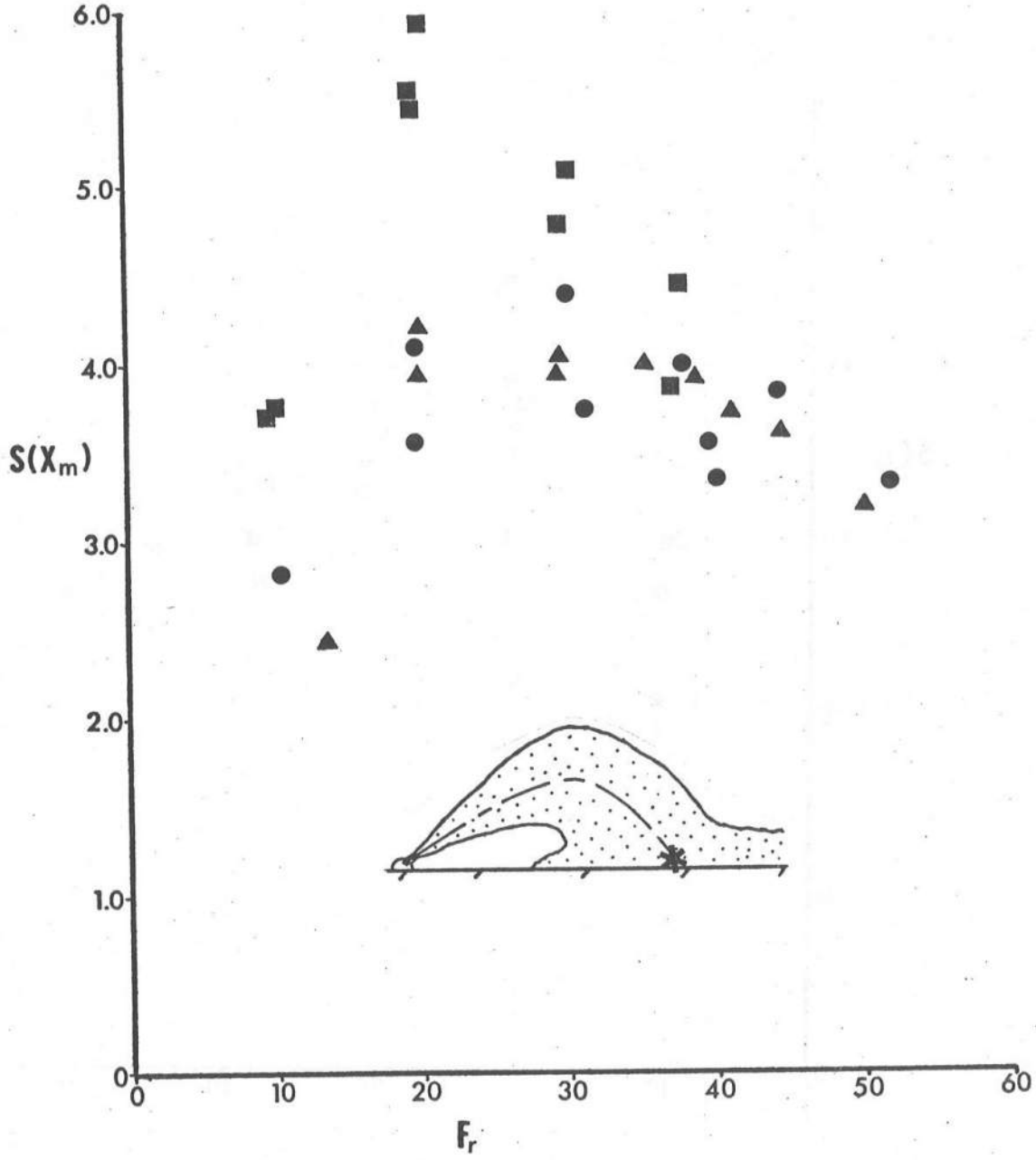

Figure 5-8 Observed Dilutions at the Points of Bottom Impingement in a Stagnant Environment

5.1.3 Analytical Model Predictions

The objective of this part of the study was to apply the conventional integral-similarity technique model of Fan and Brooks (as described in Chapter 4) to the experimental data of negatively buoyant slot jets in a stagnant environment and to ascertain the model's applicability to those cases. Initial conditions, duplicating those of all the experiments, were used for input into the analytical model to generate predicted trajectories and dilutions of each experimental run.

There are two constants used in the analytical model. They are the coefficient of entrainment, α, and the spreading coefficient, λ. The values, $\alpha = 0.16$ and $\lambda = 0.89$, were suggested by Rouse, Humphreys, and Yih[3] in their study of positively buoyant slot jets. Some attempt was made in the present study to investigate the feasibility of changing these constants to gain better predictions of the experimental data. It was reasonable to assume that the coefficient of entrainment could be reduced to compensate artificially for the reduced entrainment (on the top boundary only) that was observed in the experiments. This proved unsuccessful. When α was decreased, a slightly improved prediction for the dilution data was obtained, but at the expense of a much worse prediction of the trajectory data. Similarly, it was found that a better prediction of the maximum height of rise could be obtained if the spreading coefficient, λ, was increased. However, this adjustment yielded a worse prediction of the point of

bottom impingement and the downstream dilution ratios. Therefore, it was concluded that there was no merit in attempting to vary the experimental constants to achieve better comparisons between the analytical model and experiments, since the model did not include the bottom effects explicitly.

Before direct comparison between the model and experiments can be made, it is necessary to correct the model solutions for the zone of flow establishment (as discussed in Chapter 4). Trajectory values are corrected by adding on the proper component of the length of the flow establishment:

$$X \text{ (corrected)} = X + 5.2B \cos \theta_o \qquad (4\text{-}18)$$

$$Y \text{ (corrected)} = Y + 5.2B \sin \theta_o \qquad (4\text{-}19)$$

Because $\lambda \neq 1$, the dilution values must be corrected by the Equation (4-27):

$$S \text{ (corrected)} = \frac{ub}{u_o b_o} \sqrt{\frac{2\lambda^2}{1+\lambda^2}} \qquad (4\text{-}22)$$

(see Fan and Brooks[16], page 70). For $\lambda = 0.89$, the corrected dilution becomes:

$$S \text{ (corrected)} = 9.94 \frac{u_o b_o}{ub} \qquad (5\text{-}1)$$

For a very short distance along the trajectory, s, after the start of the analytical model, the corrected dilution will be computed to be less than unity. This is a physical impossibility. This occurs because when λ is less than 1, the concentration profile is not fully developed at the end of the zone of flow establishment, which is defined by a fully developed velocity profile only. Wherever the corrected dilution is computed to be less than unity, it is assumed that the proper value is unity.

In general, a comparison between model predictions and observed data showed that the computer model overpredicted the trajectories and dilutions. Figures 5-9 through 5-11 (which are corrected for the zone of flow establishment) clearly illustrate this point. Comparison of these figures also reveal that the predictions get worse for jets of higher densimetric Froude numbers. The reattachment eddy, whose effect grows with the Froude number, appears to be the case of the disparity.

The analytical model predictions for the centerline maximum height of rise, Ym, point of bottom impingement, Xm, and the dilutions at these points are presented in Figures 5-12 through 5-15 along with the experimental data for comparison. All plots are corrected for the zone of flow establishment.

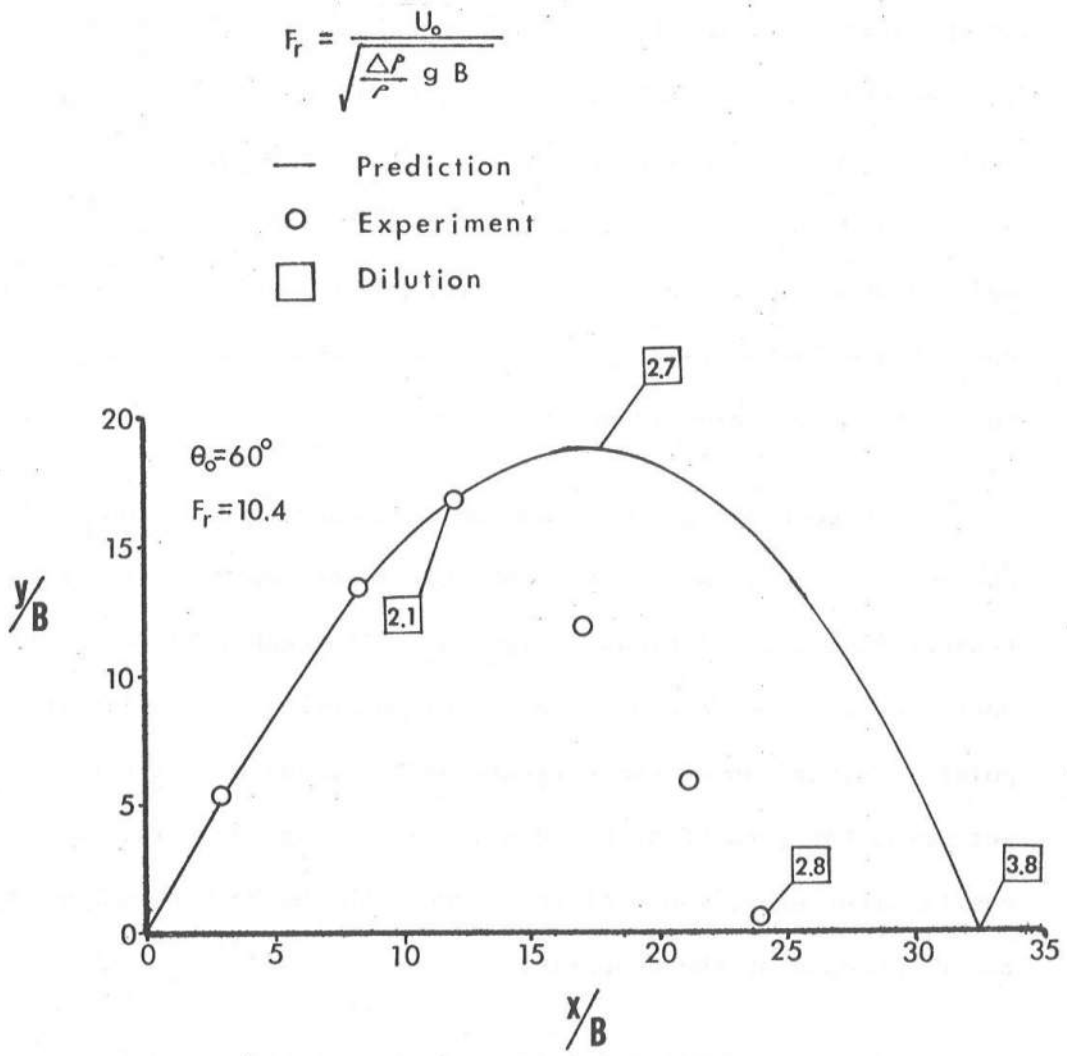

Figure 5-9 Predicted and Observed Trajectories and Dilutions of Experimental Run #6

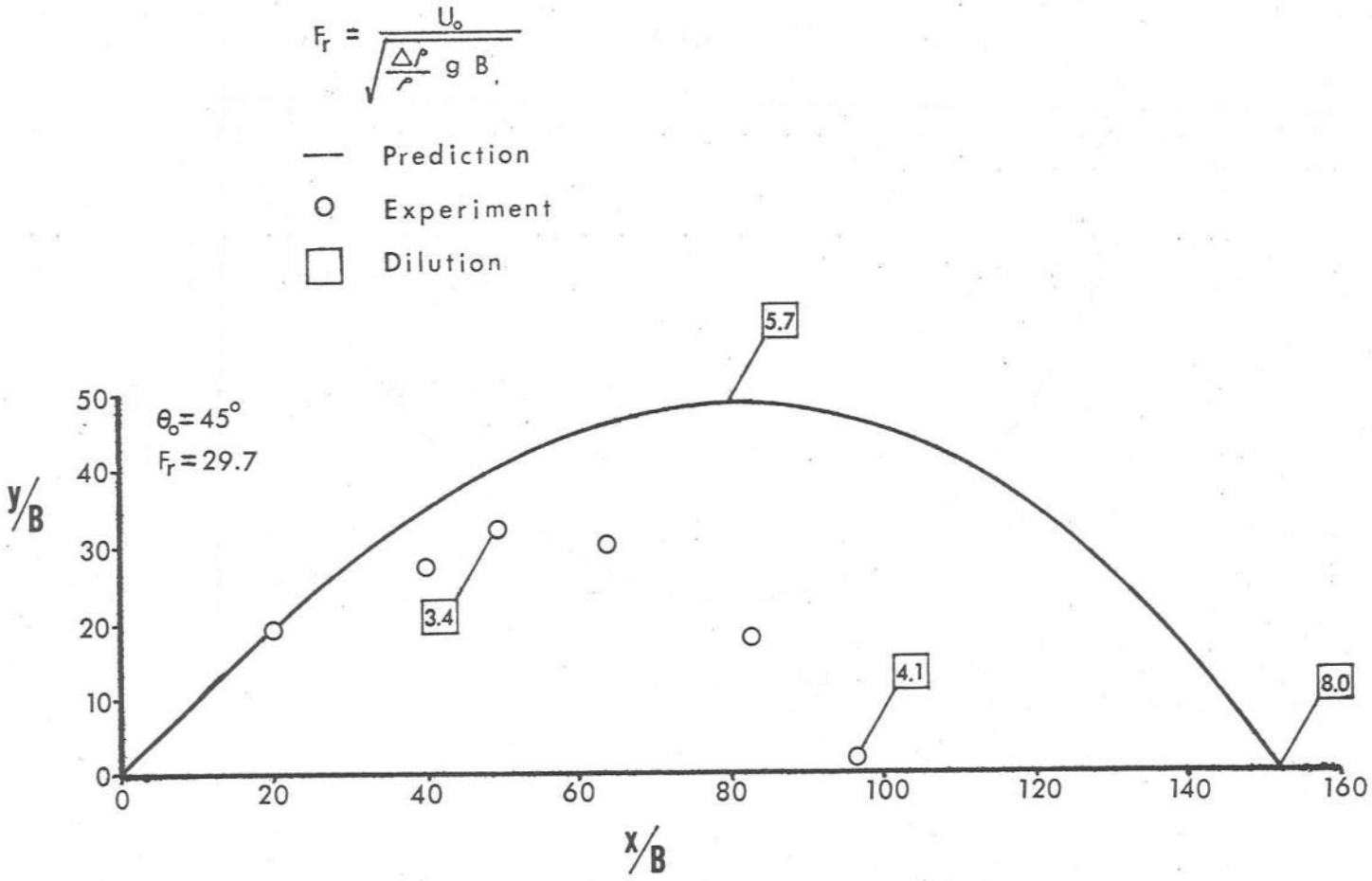

Figure 5-10 Predicted and Observed Trajectories and Dilutions of Experimental Run #30

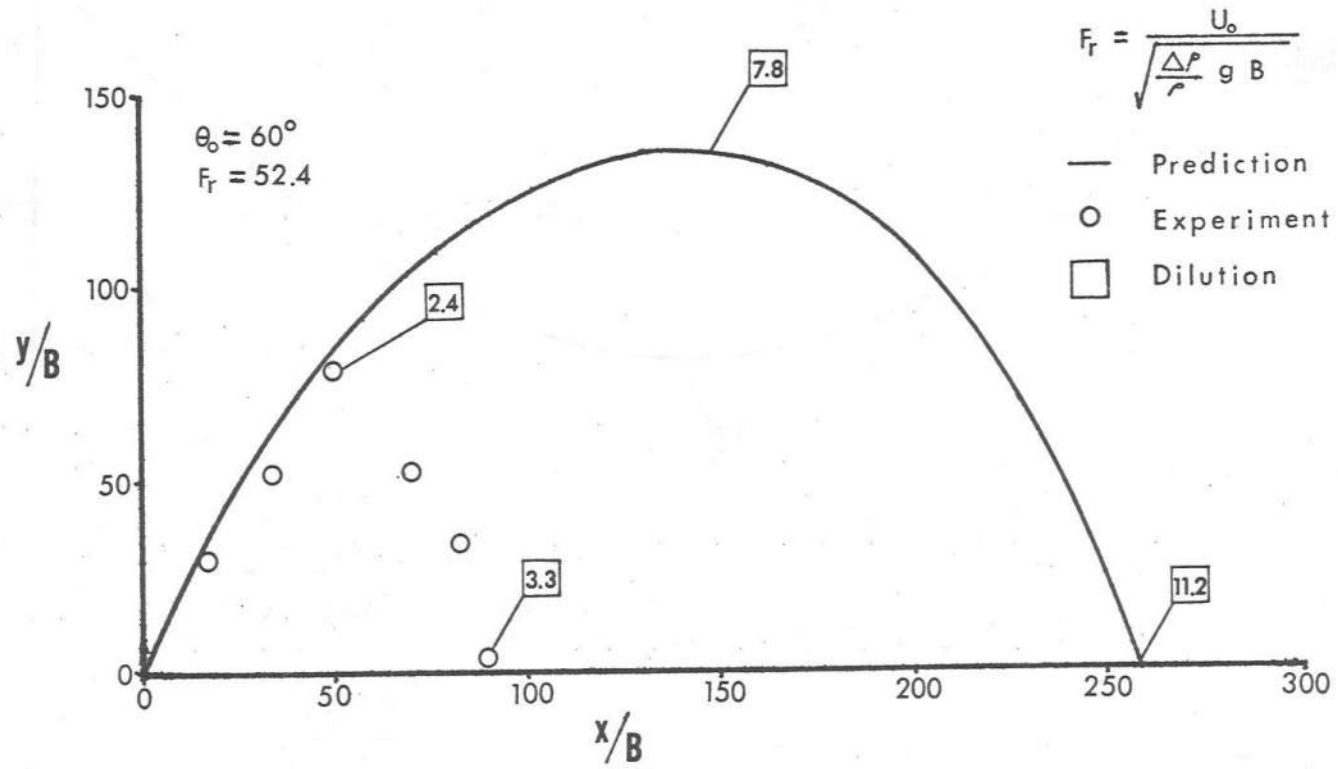

Figure 5-11 Predicted and Observed Trajectories and Dilutions of Experimental Run #5

Figure 5-12 is a plot of the predicted maximum height of rise, Ym, of various injection angles as a function of the densimetric Froude number. Reasonably good prediction occurs in the lower range of Froude numbers, 0 through 20, for the injection angles of 45° and 60°. However, for Froude numbers greater than about 25, the prediction of Ym is poor. The disparity is a result of the reattachment eddy. As previously mentioned, in the range of densimetric Froude numbers of 20 through 50, the reattachment eddy was observed to cause lower jet trajectories. An overprediction of Ym occurs because the analytical model is oblivious to a bottom boundary and any eddy that occurs.

The maximum height of rise for the 30° injection angle in the experiments was hardly perceivable. For these cases, no reasonable comparison between the analytical model and the experiments could be made.

The predicted maximum heights of rise for the 90° cases are not presented. The computer model has difficulty in handling the 90° case and cannot give a predicted Ym. In the experiments of the 90° cases the jet velocity steadily decreases until it reaches zero at the top of the jet plume. Because the analytical model relies on a conservation of mass principle, the ub product (mass flux) must increase along the trajectory (the falling back of fluid is not accounted for). Therefore, as the velocity, u, approaches zero, the jet width,

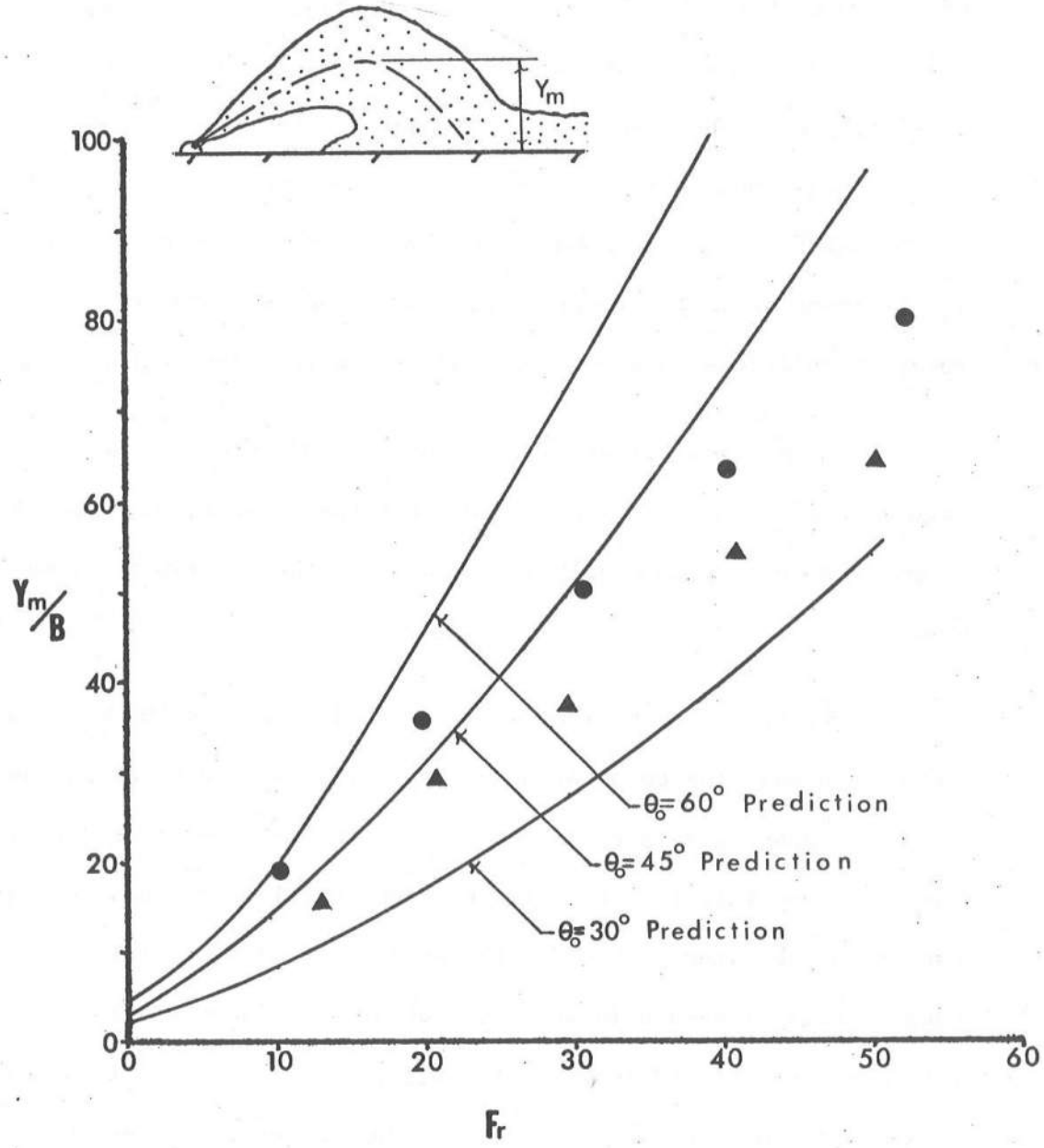

Figure 5-12 Predicted and Observed Maximum Heights of Rise in a Stagnant Environment

b, must become infinitely large to conserve mass. As a result, dilution calculations blow up, i.e., the jet approaches neutral buoyancy. A neutrally buoyant jet feels no gravitational force and, in theory, will never be completely arrested. The analytical model verifies this, because u becomes very small, but never reaches zero.

Figure 5-13 is a plot of the predicted horizontal distance to bottom impingement, Xm, of the jet's centerline trajectory. It is clear that Xm is much over-predicted in the upper densimetric Froude number range (Fr > 20). Again, this is because the analytical model ignores the bottom boundary and hence, the reattachment eddy, which creates a low pressure zone and pulls the trajectory down.

The reattachment eddy severely affects the downstream dilutions and a very poor comparison is realized between the predicted and experimental data. The analytical model assumes that pure ambient fluid is entrained in both the upper and lower edges of the jet plume. As can be seen from the experimental photographs (Figures 5-1, 5-6, and 5-16) this is not an accurate assumption. The reattachment eddy prevents pure ambient fluid from being entrained along the lower boundary. This suggests that dilution ratios of the physical model will be less than those of the analytical model.

Figure 5-14 and 5-15 are plots of the predicted and observed centerline dilutions at Ym and Xm respectively. The predicted

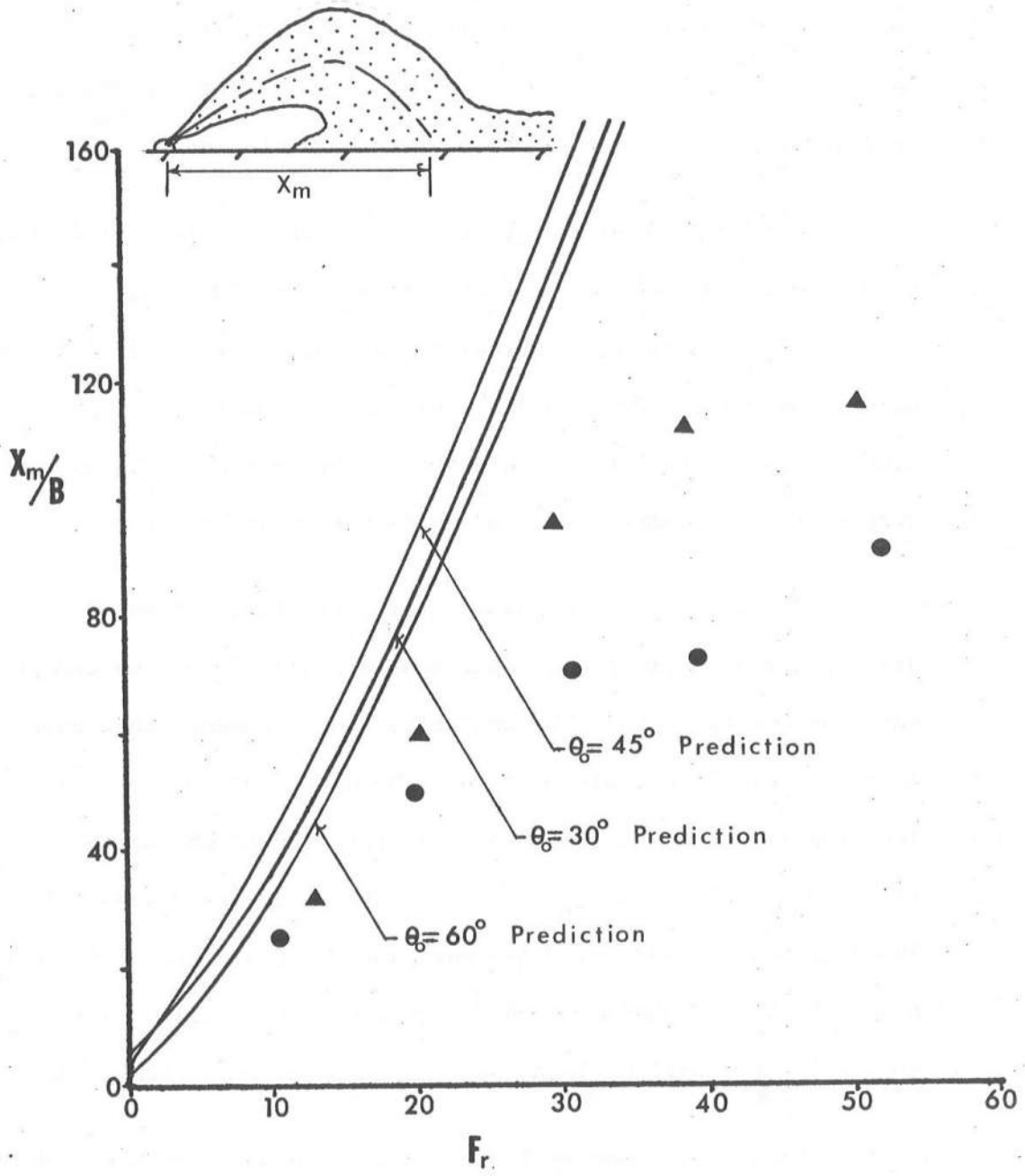

Figure 5-13 Predicted and Observed Points of Bottom Impingement in a Stagnant Environment

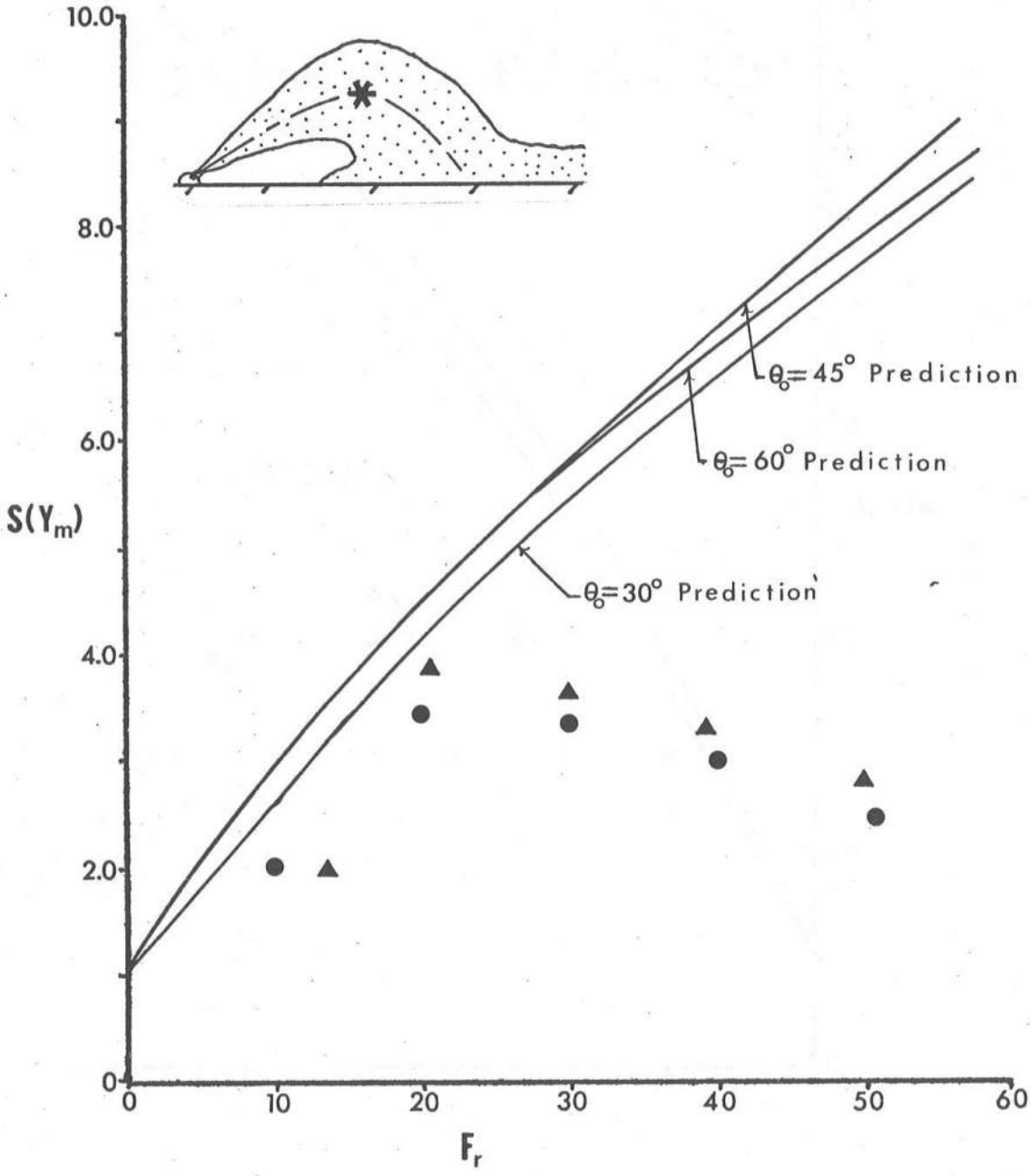

Figure 5-14 Predicted and Observed Dilutions at the Maximum Heights of Rise in a Stagnant Environment

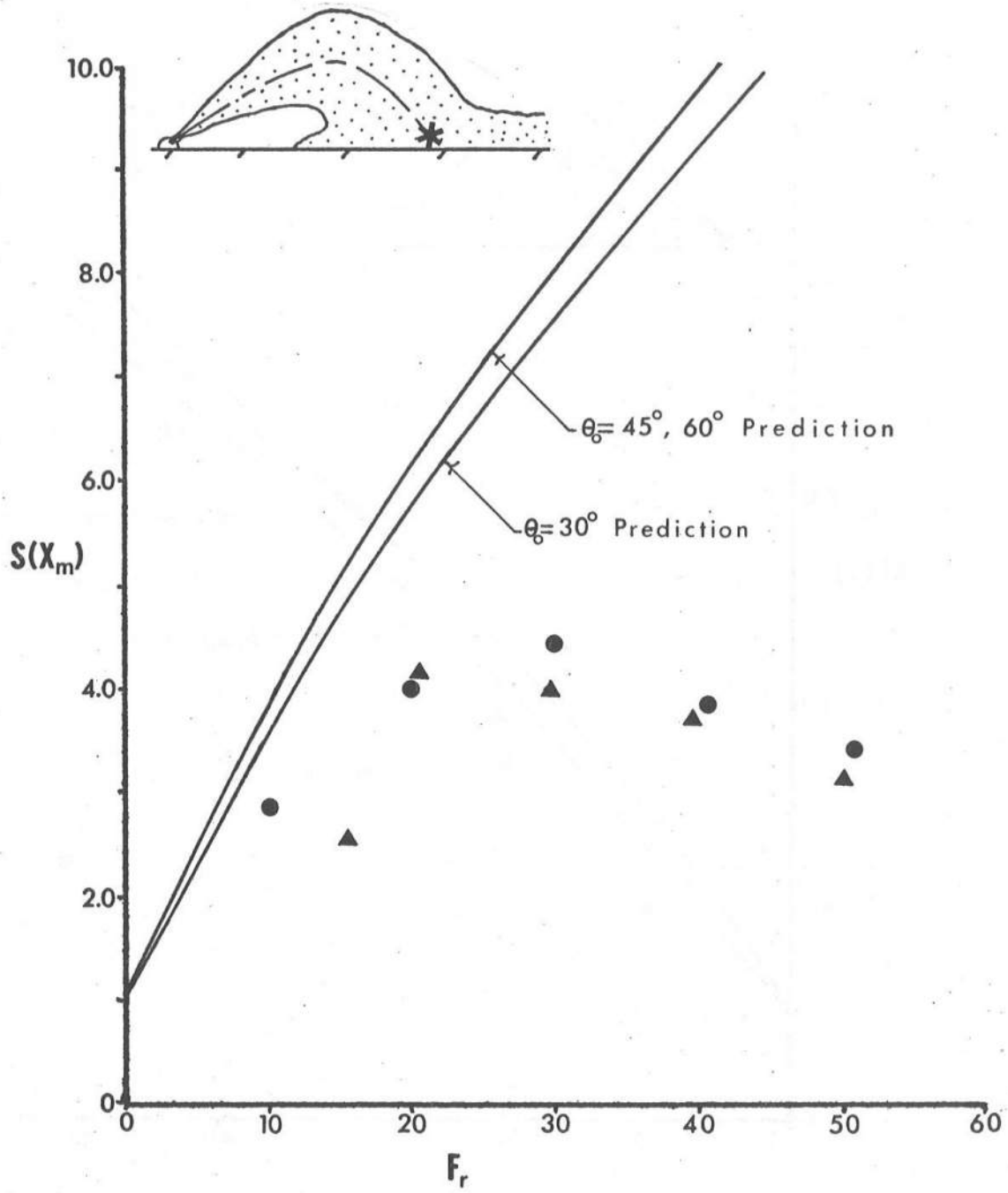

Figure 5-15 Predicted and Observed Dilutions at the Points of Bottom Impingement in a Stagnant Environment

dilution ratios monotonically increase with the densimetric Froude number. Although a fair comparison exists in the very low Froude number range, this "goodness" of fit vanishes for Froude numbers greater than about 20.

5.2 Negatively Buoyant Slot Jets in a Uniformly Flowing Environment

5.2.1 General

A total of 18 experimental runs for negatively buoyant slot jets in a uniformly flowing environment were conducted. These runs included two different injection angles, 45° and 90°, and covered a range of densimetric Froude numbers from 10 through 50. Two different velocity ratios, k = 15 and 25 were employed, where:

$$k = u_o/u_a$$

All experiments were conducted in a water depth of 16" (40.6 cm). See Table 5-2 for the details, θ_o, Fr, R, and k, of each run. Jet trajectories were recorded on photographs. Dilution ratios of the jet centerline at the maximum height of rise, Ym, and point of bottom impingement, Xm, were determined by conductivity experiments.

As with the tests in a stagnant environment, the jets in the flowing environment tended to a parabolic shape, but with a more flattened and stretched out appearance (Figure 5-16). The top edge

Table 5-2

Details of the Experiments in the Uniformly Flowing Environment

Run #	θ_o	Fr	k	R	$(\frac{X}{B},\frac{Ym}{B})$	$(\frac{Xm}{B},0)$	S(X,Ym)	S(Xm,c)	U_a ft/sec/ m/sec	U_o ft/sec/ m/sec	$\frac{\Delta\rho}{\rho}$	B in./cm.
101	45	28.7	14.5	1990	28,10	76,0	2.61	4.18	.145 4.42	2.10 64.0	.016	0.125 0.318
102	45	49.6	15.4	2140	20,12	100,0	1.80	2.77	.147 4.48	2.26 68.9	.006	0.125 0.318
103	45	38.7	15.0	2060	20,10	87,0	2.26	3.53	.145 4.42	2.18 69.5	.0095	0.125 0.318
104	45	10.1	7.7	2060	18,9	30,0	2.68	3.36	.143 4.36	1.09 33.2	.017	0.25 0.635
105	90	9.9	15.0	2060	2,28	16,0	2.59	4.0	.073 2.23	1.09 33.2	.018	0.25 0.635
106	45	9.7	15.1	2060	20,8	36,0	2.69	3.61	.072 2.19	1.09 33.2	.019	0.25 0.635
107	45	20.0	14.1	1940	32,9	68,0	3.47	4.62	.145 4.42	2.05 62.5	.031	0.125 0.318
108	90	28.2	14.7	1990	80,58	190,0	3.84	4.88	.143 4.36	2.10 64.0	.016	0.125 0.318
109	90	43.5	15.9	2060	56,80	304,0	3.33	4.70	.138 4.21	2.18 69.5	.0075	0.125 0.318
110	90	30.2	24.0	2050	32,68	132,0	4.21	5.50	.090 2.74	2.16 65.8	.015	0.125 0.318
111	90	39.3	24.0	2050	76,91	204,0	3.92	5.42	.090 2.74	2.16 65.8	.009	0.125 0.318
112	90	10.1	27.0	2050	0,26	20,0	3.13	4.75	.040 1.22	1.08 32.9	.017	0.25 0.635

(Table 5-2 Continued on Next Page)

(Table 5-2 Continued)

Run #	θ_o	Fr	k	R	$(\frac{X}{B},\frac{Ym}{B})$	$(\frac{Xm}{B},0)$	S(X,Ym)	S(Xm,c)	U_a ft/sec/ cm/sec	U_a ft/sec/ cm/sec	$\frac{\Delta\rho}{\rho}$	B in./cm.
113	45	30.0	27.7	2050	40,24	112,0	2.75	4.68	.078 2.38	2.16 65.8	.015	0.125 0.318
114	45	45.0	24.7	1990	40,27	156,0	2.40	4.40	.085 2.59	2.10 64.0	.006	0.125 0.318
115	45	10.0	24.0	2050	18,15	40,0	2.16	3.79	.045 1.37	1.08 32.9	.017	0.25 0.635
116	45	30.6	14.8	2050	25,11	81,0	3.04	4.31	.146 4.45	2.16 65.8	.0148	0.125 0.318
117	90	21.2	14.1	1940	40,43	116,0	3.92	4.95	.145 4.42	2.05 62.5	.0279	0.125 0.318
118	90	19.6	25.9	1940	20,49	80,0	4.35	5.05	.079 2.41	2.05 62.5	.0326	0.125 0.318

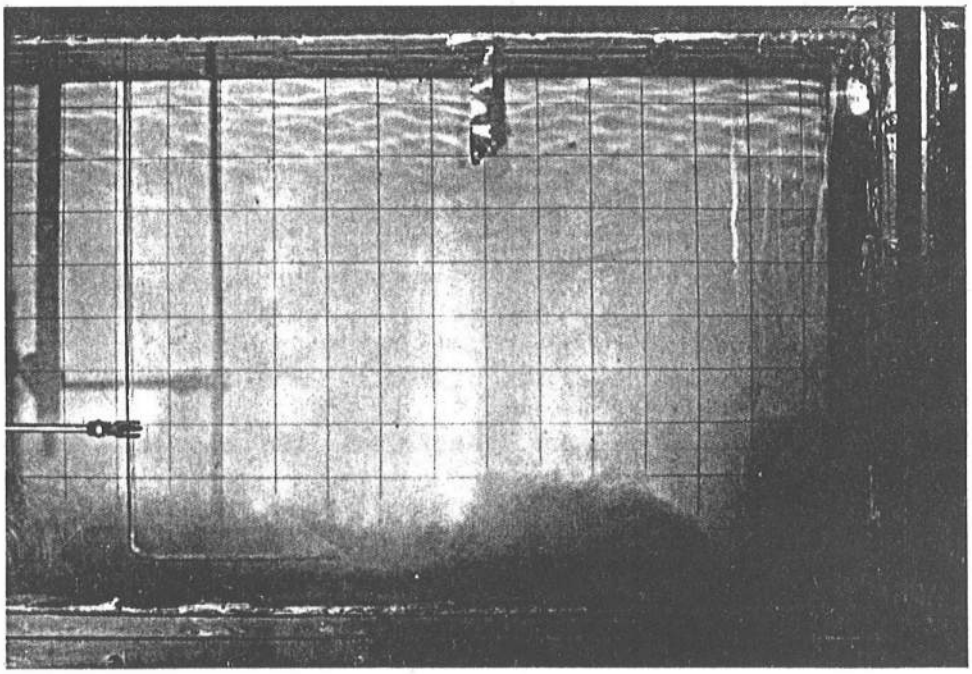

Run #107

$\theta_o = 45°$

Fr = 20.0

K = 14.1

of the jet exhibited a clear, sharp boundary, while the lower edge was hidden in the reattachment eddy. After bottom impingement, a large portion of the jet fluid was entrained into the eddy and recirculated back into the jet. Pure ambient fluid was entrained only on the top edge of the jet plume.

5.2.2 Experimental Results

Data for negatively buoyant slot jets in a uniformly flowing environment are presented in graphs, similar to those for stagnant case results, in Figures 5-17 through 5-24. Results of both flowing cases (k = 15 and 25) are shown in comparison with the stagnant environment cases (where the velocity ratio is equal to infinity). The maximum heights of rise, Ym, of the 45° and 90° cases, are presented in Figure 5-17 and 5-18, respectively. Of the two injection angles, the one of 45° appears to be the more sensitive to the cross-flow. In the higher ambient velocity runs (k = 15), the 45° jet is almost completely wiped out, exhibiting very little trajectory rise at all (see Figure 5-16). This seems to be correct intuitively. If the ambient crosscurrent were to be considerably increased ($k \to 0$), it would be logical to expect no rise at all and for the jet trajectory to lay along the bottom.

This trend is slightly evident in the 90° jet cases. Close examination of Figure 5-18 reveals that, for the flowing environment data, the slower crosscurrent (k = 25) consistently shows greater Ym

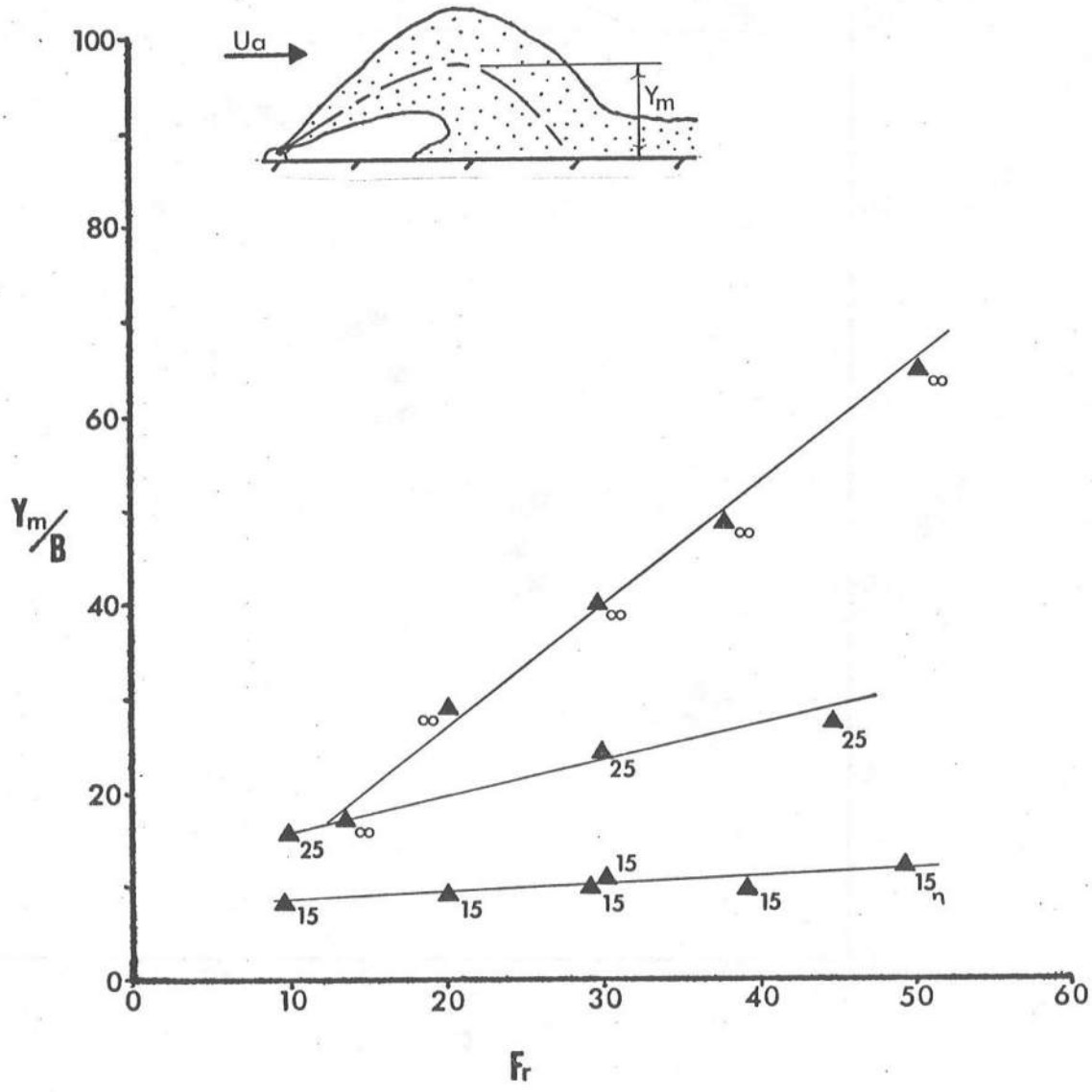

Figure 5-17 Observed Maximum Heights of Rise in a Uniformly Flowing Environment (45° Jets)

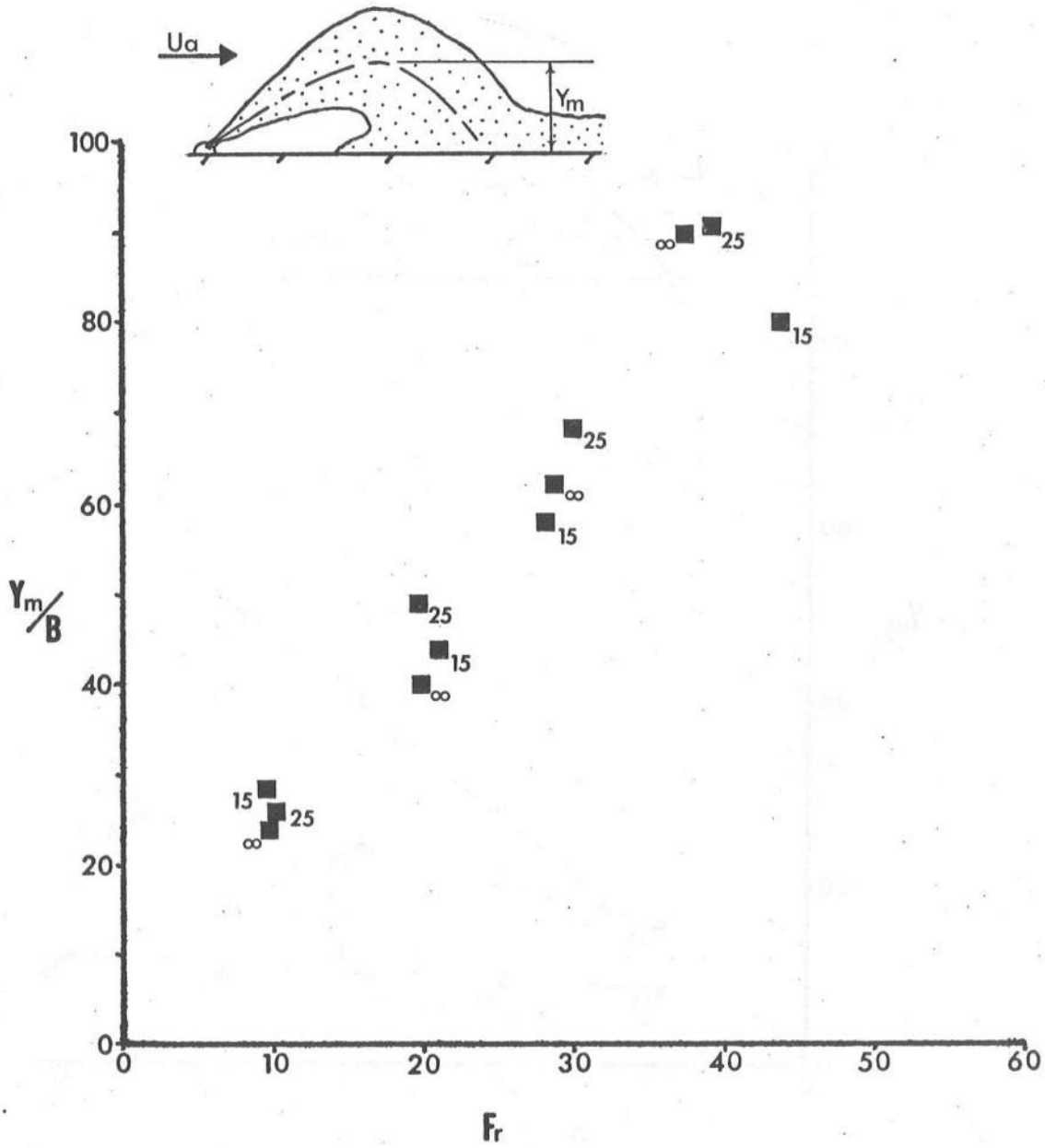

Figure 5-18 Observed Maximum Heights of Rise in a Uniformly Flowing Environment (90° Jets)

values than those in the faster crosscurrent (k = 15), except at Fr = 10. Assuming that this exception is due to experimental error, then it appears that increasing the crosscurrent decreases the maximum height of rise for the 90° jet, as observed in the 45° jet cases. The reason for the inconsistency for the 90° stagnant data is that in the stagnant cases, the jet never reaches a steady state equilibrium, but tends to oscillate about some mean height. This phenomenon was noted by Turner[4] in vertically directed, heavy round jets. This oscillation action makes it impossible to determine accurately the maximum height of rise of a 90° jet in a stagnant environment.

The effects of the crosscurrent on the horizontal distance of bottom impingement, Xm, are presented in Figures 5-19 and 5-20. In Figure 5-19, the 45° case, it is clear that in the weaker crosscurrent (k = 25), Xm increases, but in the stronger crosscurrent (k = 15), Xm decreases (in the higher densimetric Froude number range). This effect is not seen in the 90° case, where for either velocity ratio, Xm is increased. However, a trend similar to the one in the 45° case probably would have been observed if the tests had covered a lower range velocity ratios (i.e., a faster ambient current); it is reasonable to assume that a very fast ambient current would also wipe out the 90° jet's trajectory and decrease Xm.

The crosscurrent effect on the centerline dilution is presented in Figures 5-21 through 5-24. All of the plots reveal that

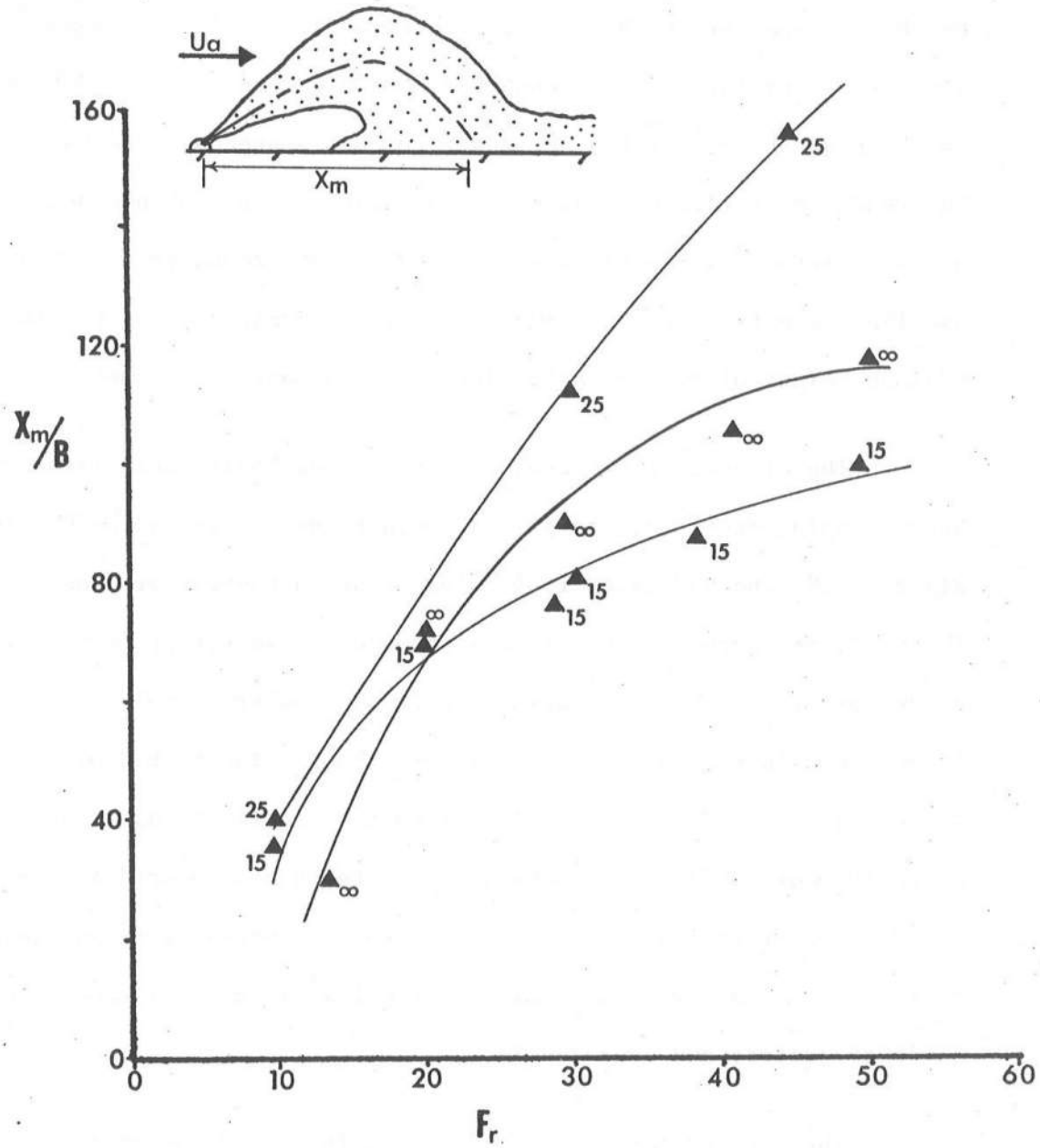

Figure 5-19 Observed Points of Bottom Impingement in a Uniformly Flowing Environment (45° Jet)

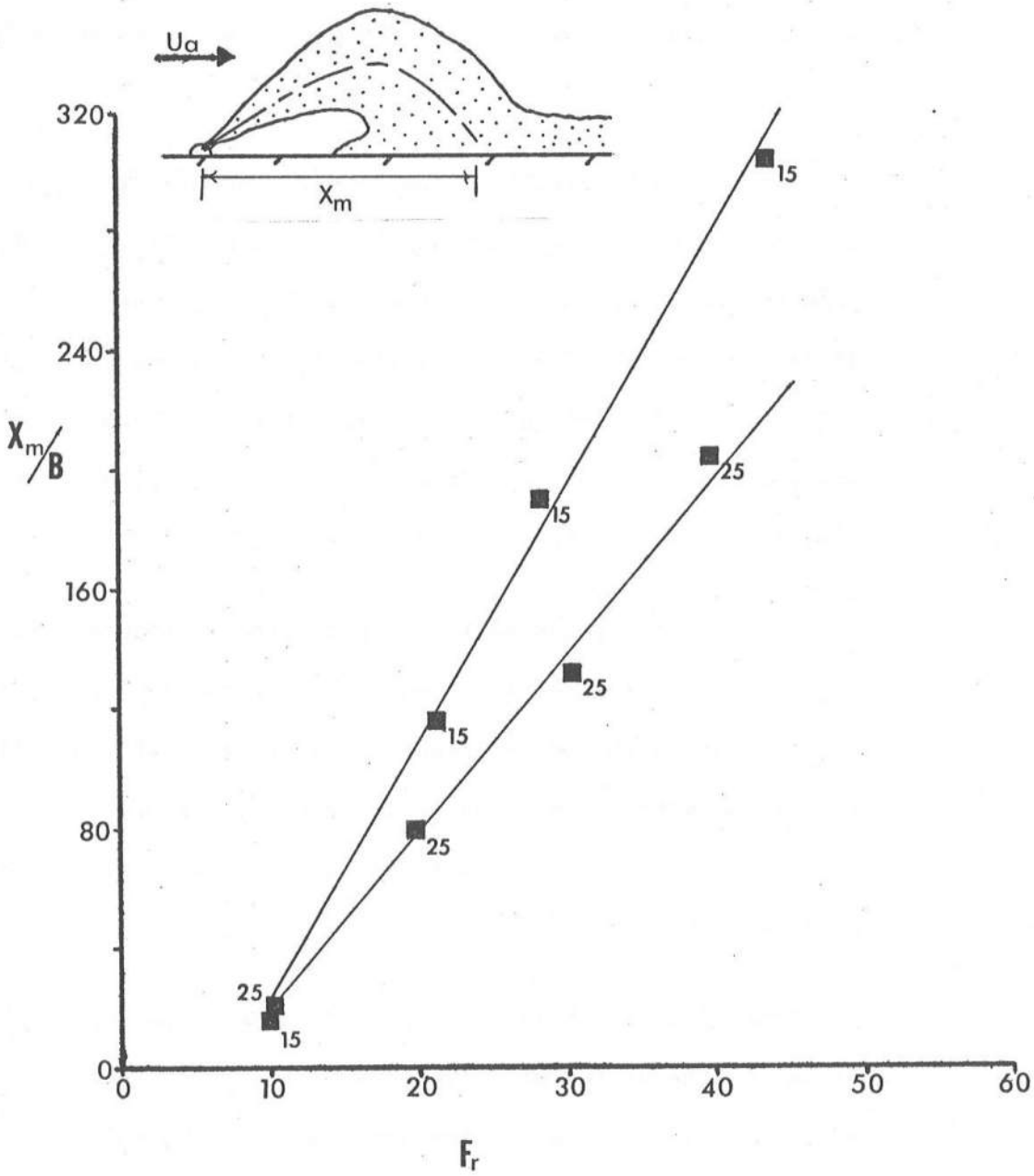

Figure 5-20 Observed Points of Bottom Impingement in a Uniformly Flowing Environment (90° Jet)

the dilution ratios follow the same trend that was observed in the stagnant cases (the dilution ratios decrease with densimetric Froude numbers greater than about 20 to 25). This indicates that the effect of the reattachment eddy is also an important factor in the flowing environment.

There are subtle differences between the dilutions observed in the stagnant and flowing environments. Those differences can be explained by examining the crosscurrent's effect on the jet trajectory. The dilution ratio is a function of the distance along the trajectory of the jet plume. Therefore, if the trajectory has been shortened or lengthened, then a corresponding decrease or increase in the dilution ratios would be anticipated.

The dilution ratios at Ym are presented in Figure 5-21 and 5-22. In Figure 5-21, the dilutions at Ym for the 45° jets, it can be seen that in the upper Froude number range (>10) the dilution ratios decrease with an increase in the ambient current velocity, which corresponds with the decrease in Ym for an increase in the ambient crosscurrent (Figure 5-17).

Similarly, this relationship holds when comparing the dilution data at Ym for the different crossflows of the 90° jets (Figures 5-18 and 5-20). Again there is the inconsistency for the 90° stagnant case as previously discussed.

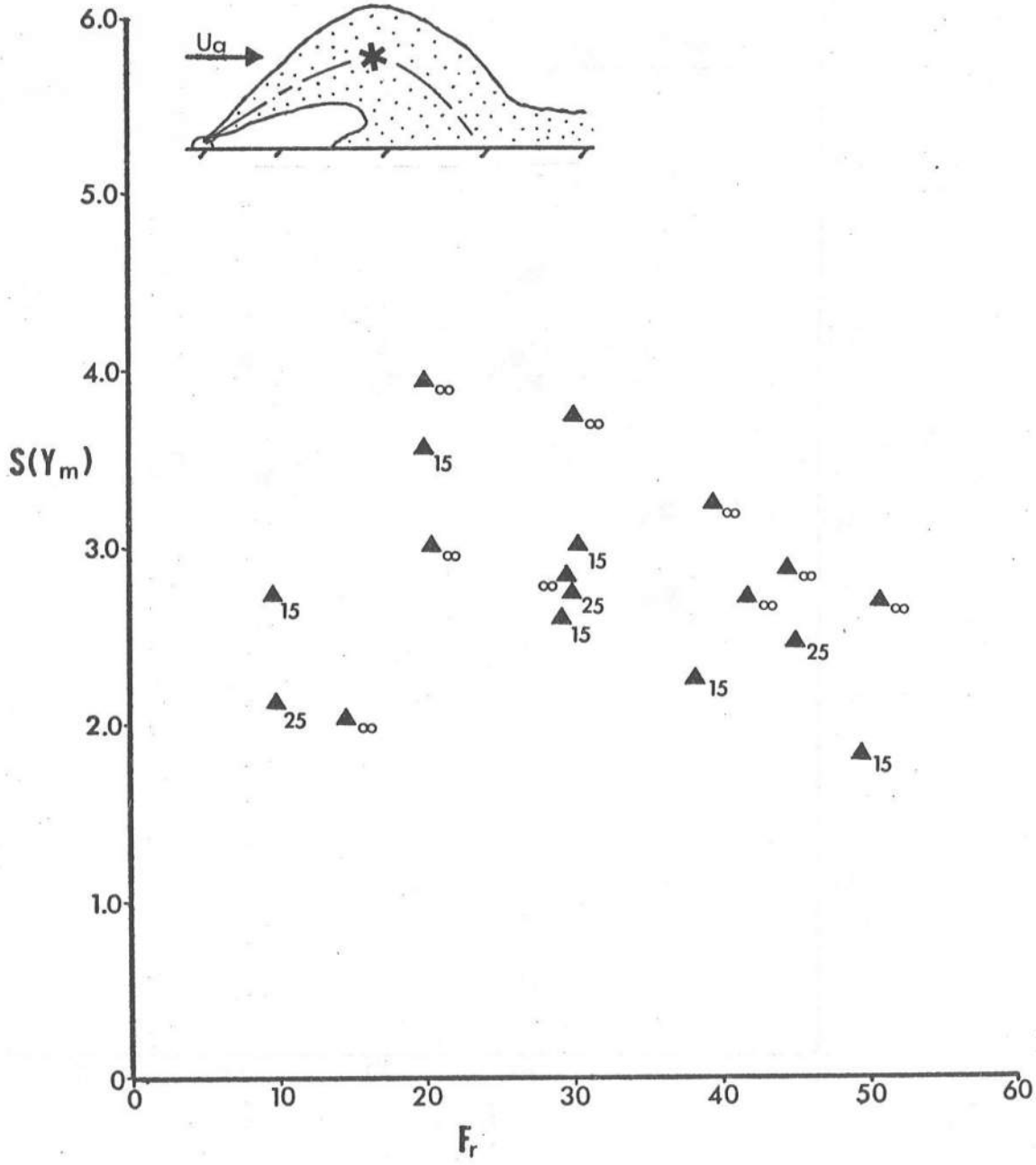

Figure 5-21 Observed Dilutions at the Maximum Height of Rise in a Uniformly Flowing Environment (45° Jets)

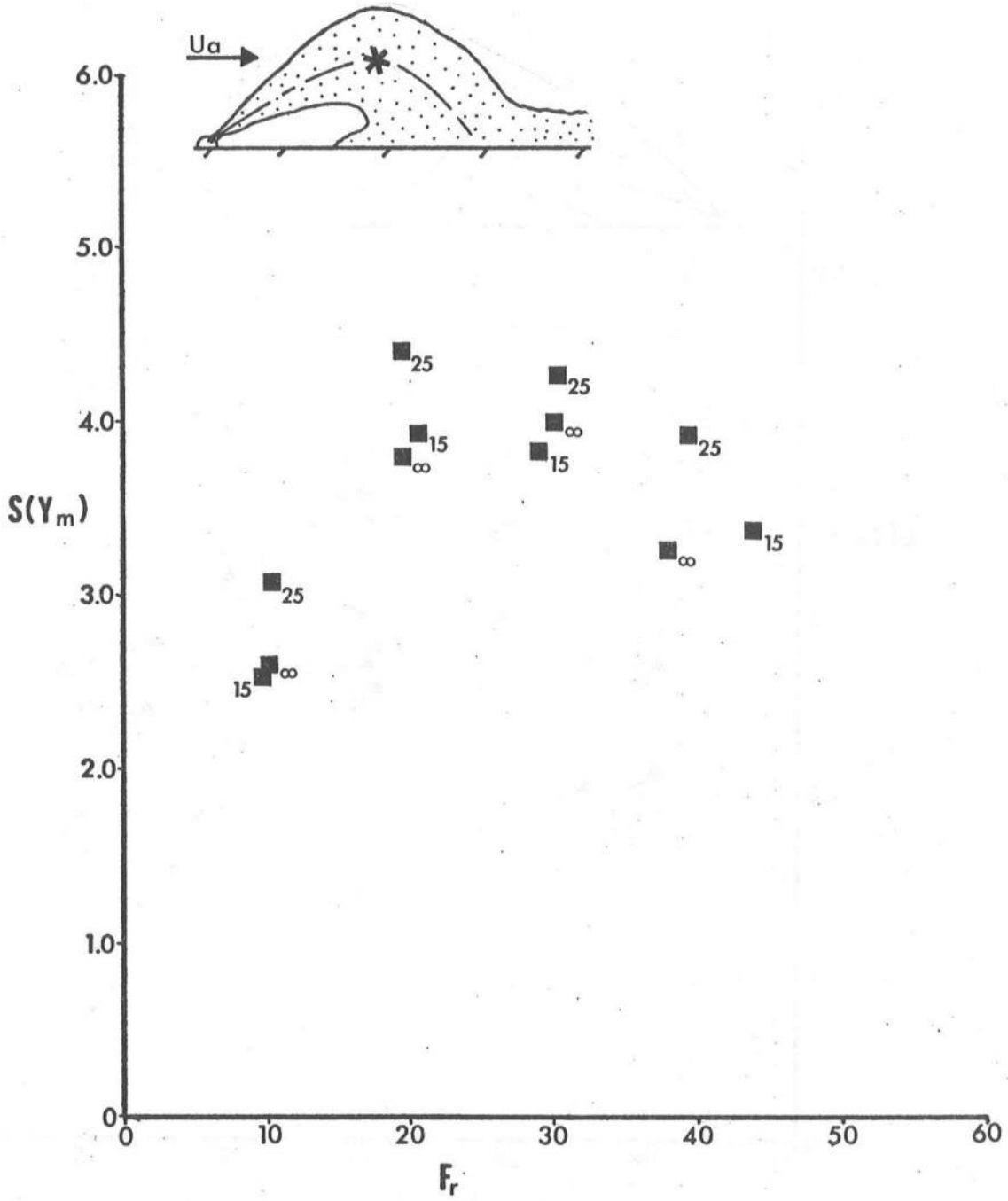

Figure 5-22 Observed Dilutions at the Maximum Heights of Rise in a Uniformly Flowing Environment (90° Jets)

The dilution ratios at Xm are plotted in Figure 5-23 and 5-24. If Figures 5-19 and 5-23 (the plots of Xm and the dilution at Xm, respectively, for the 45° jets) are compared, then corresponding trends can be found. Figure 5-19 indicates that in the upper densimetric Froude number range (>35), the slower crosscurrent (k = 25) increases Xm while the faster current (k = 15) decreases Xm; correspondingly, there is an increase in dilution for the slow current and a decrease in the 90° cases (Figures 5-20 and 5-24). In the upper Froude number range (>35), the ambient crosscurrent has increased Xm and, consequently, the dilutions tend to be slightly greater than those in the stagnant environment.

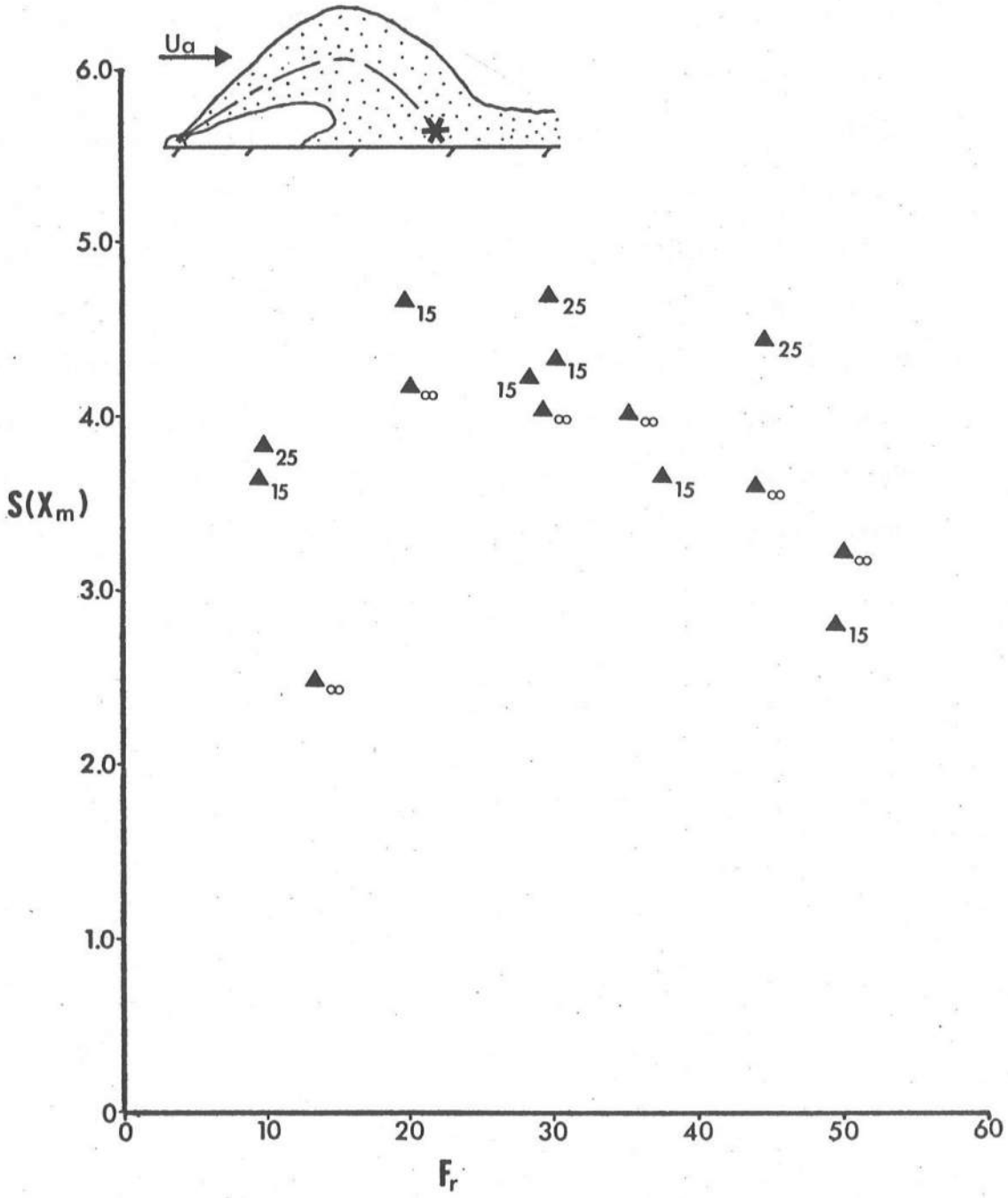

Figure 5-23 Observed Dilutions at the Points of Bottom Impingement in a Uniformly Flowing Environment (45° Jets)

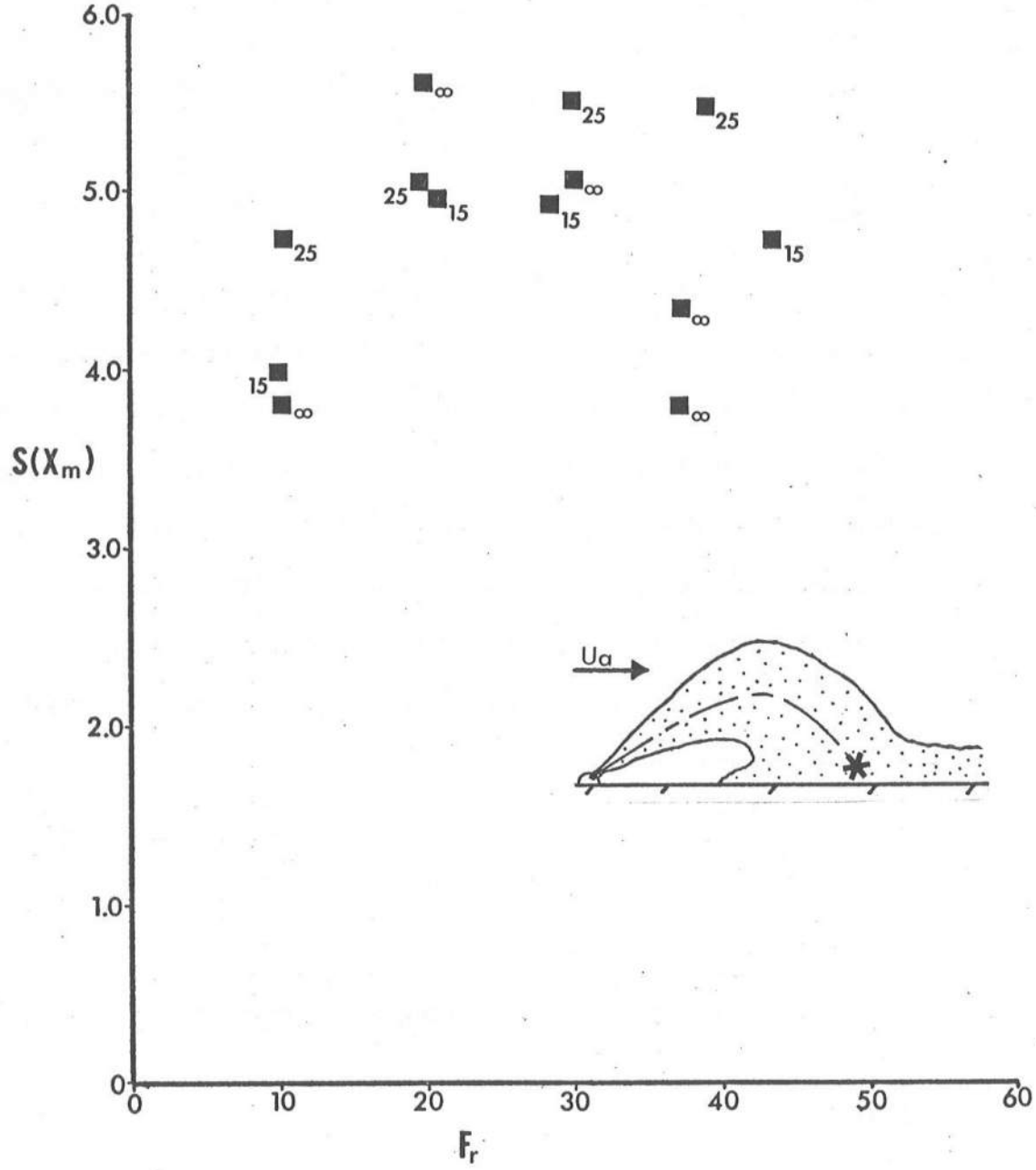

Figure 5-24 Observed Dilutions at the Points of Bottom Impingement in a Uniformly Flowing Environment (90° Jets)

6. Example Calculation and Comparison with Round Jet Behavior

6.1 "Equivalent Slot-Jet" Theory

To illustrate the differences in behavior between round, negatively buoyant jets and slot, negatively buoyant jets, the following example is presented. As "equivalent slot-jet" will be computed from a given round jet diffuser system and used to compare their differences in behavior. Cederwall[19] defines an "equivalent slot-jet" as one which has the same volume and momentum fluxes per unit length as a given series of round jets. Given a diffuser with port spacing, ℓ, port diameter, D, and discharge velocity, u_r, the "equivalent slot jet" is computed by:

$$\text{vol flux/unit length} \quad \frac{u_r \cdot D \pi}{\ell 4} = u_s B \tag{6-1}$$

$$\text{momentum flux/unit length} \quad \frac{u_r^2 \pi D^2}{\ell 4} = u_s^2 B \tag{6-2}$$

Which requires:

$$u_r = u_s \tag{6-3}$$

Thus:

$$B = \frac{D^2 \pi}{4\ell} \tag{6-4}$$

and

$$Fr_s = Fr_r \left(\frac{4\ell}{D\pi}\right)^{1/2} \tag{6-5}$$

where

u_s = discharge velocity for the "equivalent slot jet,"

Fr_s = densimetric Froude number for the "equivalent slot jet,"

Fr_r = densimetric Froude number for the round jet,

$$= \frac{u_r}{\sqrt{\frac{\Delta\rho}{\rho_a} g D}}$$

and all other notations as previously defined.

6.2 Example Problem

The following are the given conditions for the round jet:

discharge velocity u_r = 8.03 ft/sec (2.45 m/sec)

port diameter D = 2" (5.08 cm)

port spacing ℓ = 0.5' (15.2 cm)

discharge angle θ = 45°

fluid density difference $\Delta\rho/\rho$ = -0.03

ambient velocity u_a = 0.39 ft/sec (11.9 cm/sec)

The round jet densimetric Froude number is computed:

$$Fr_r = \frac{8.03}{\sqrt{(0.03)(32.2)\ 2/12}} = 20.0 \qquad (6\text{-}6)$$

and the velocity ratio:

$$k = u_r/u_a = 8.03/0.39 = 20.6 \qquad (6\text{-}7)$$

The "equivalent slot-jet" values:

$$u_s = u_r = 8.03 \text{ ft/sec} \qquad (6\text{-}8)$$

and the velocity ratio remains unchanged:

$$= u_s/u_a = u_r/u_a = 20.6 \qquad (6\text{-}10)$$

For the given conditions, the solution for the round jet is the experimental data for Run #24 of the experiments by Anderson[10] on negatively buoyant round jets (using the modified Abraham model). Run #24 yields the following information:

$$Ym/D = 15 \rightarrow Ym = (2/12)15 = 2.5'(.76\ m)$$

$$Xm/D > 100 \rightarrow Xm(2/12)100 > 16.7'(5.09\ m)^{*}$$

$$S(x,Ym) = 15$$

$$S(Xm,0) > 40^{*}$$

*Anderson's graph terminated shortly before the bottom was reached. (This solution has ignored any adjacent port interference effects.)

The corresponding information for the "equivalent slot-jet" may be found by interpolating between the velocity ratios, k = 25 and k = 15, for a 45° jet with a densimetric Froude number of 39.1. From Figures 5-18, 5-20, and 5-22:

$$Ym/B = 19 \rightarrow Ym = (19)\left(\frac{.52}{12}\right) = 0.82'(25\ cm)$$

$$Xm/B = 118 \rightarrow Xm = 180\left(\frac{.52}{12}\right) = 5.1'(1.56\ m)$$

$$S(x,Ym) = 2.5$$

$$S(Xm,0) = 4.1$$

Comparing both solutions:

	Round Jet Solution	Slot Jet Solution
Ym	2.5' (.76 m)	0.82' (.25 cm)
Xm	>16.7' (5.09 m)	5.1' (1.56 m)
S(x,Ym)	15	2.5
S(Xm,0)	>40	4.1

The differences are very significant. The most critical difference would probably be at the predicted point of bottom impingement. If this diffuser were designed on the basis of single port, round jet data, then a dilution in excess of 40° would be predicted when the jet fluid impinges on the bottom. But, according to the slot jet data, a dilution of less than 5 would be predicted. The correct dilution would depend on the degree of adjacent port interference. The interference reduces the surface area available for entrainment and creates a slot-type discharge which is subjected to the reattachment eddy phenomenon which reduces entrainment all the more. The "strength" of the reattachment eddy will clearly be diminished as the penetration of flow between the adjacent round jets increases. Thus, the ability of the eddy to cause reentrainment and reduced dilution would be inhibited. Also, the finite length of an actual diffuser would act to weaken the eddy as entrainment flow at the ends of and along the axis of the diffuser would tend to lessen eddy effect. However, the slot jet data provide a lower bound on the situation which might exist in the center portions of a longer diffuser with closely spaced ports.

7. Conclusions

An investigation of the behavior of submerged, negatively buoyant slot jets in stagnant and uniformly flowing environments has been conducted. Through experiments, centerline trajectories and centerline dilutions (at the maximum height of rise and point of bottom impingement) were determined. The analytical model of Fan and Brooks[16], using the integral-similarity technique, previously developed for positively buoyant slot jets was applied to negatively buoyant slot jets in a stagnant environment.

It was found that the presence of the bottom boundary severely affected the jet behavior in the experiments. A reattachment eddy was created between the jet and the bottom of the test flume. The eddy acted both to pull the jet downward due to the pressure gradient established and to drastically reduce fluid entrainment. The "wall-effect" became stronger with an increase in the densimetric Froude number of the jet.

The analytical model, which ignores the presence of the bottom boundary, was found to be ineffective for predicting the jet's behavior. Dilutions and trajectories were greatly overpredicted,

especially in the higher Froude number range. The "wall-effect" could not be adequately accounted for by modifying the experimental constants in the computer model.

The effect of the reattachment eddy: to "pull" the discharge toward the bottom and result in shortened trajectories and limited dilution, was evident (for the range of velocity ratios of this study) in the flowing environment as well. The existence of a crosscurrent did not necessarily result in greatly enhanced mixing.

The results of this study apply strictly to the case of a slot discharge located at the bottom of the receiving water and extending completely across the receiving water (strict two-dimensionality). It has been shown that the reattachment eddy downstream of the discharge has a pronounced effect on the jet behavior. Because the existence and strength of that eddy depend on the physical situation studied, caution is necessary in the extrapolation of the results found to different physical discharge situations.

A slot discharge on the bottom of and extending across a river or stream clearly resembles the case studied. However, a slot discharge elevated some distance above the bottom would permit entrainment flow to the lower side of the slot and weaken or possibly eliminate the reattachment eddy. In such a case, it is expected that the integral similarity model predictions would more readily reflect the jet behavior than the experimental results. Likewise, a slot discharge of finite length, not extending across the receiving water body, could induce flow inward along the axis of the slot for entrainment and mitigate the strength of the eddy. The merging of adjacent round jets of a multi-port diffuser to form a slot jet may also constitute a different physical

situation. Although an "equivalent" slot discharge is easily calculated, the flow between the initial round jets would probably result in a weaker reattachment eddy than would be formed had the initial discharge geometry been a slot.

All of the physical situations mentioned before provide for the possibility that the reattachment eddy be weakened and hence that the dilution be increased over that predicted by the experimental data reported for this study. The sensitivity of the results to these factors and the degree to which dilution predictions can be increased remains to be studied. The results for the two-dimensional case reported here do, however, provide something of a "worst-case" or lower-bound on the mixing to be realized from a slot or slot-like discharge of a negatively buoyant effluent.

8. References

(1) Morton, B. R., "Forced Plumes," Journal of Fluid Mechanics, 5, 151-163, 1954.

(2) Morton, B. R., Taylor, G. I., and Turner, J. S., "Turbulent Gravitational Convection from Maintained and Instantaneous Sources," Proc. Roy. Soc. London, A234, 1-23, 1956.

(3) Rouse, H., Yih, C. S., and Humphreys, H. W., "Gravitational Convection from a Boundary Source," Tellus, 4, 201-210, 1952.

(4) Turner, J. S., "Jets and Plumes with Negative or Reversing Buoyancy," Journal of Fluid Mechanics, 26, Part 4, 779-792, 1966.

(5) Abraham, G., "Jets with Negative Buoyancy in Homogeneous Fluid," Journal of Hydraulic Research, 5, 4, 235-248, 1967.

(6) Zeitoun, M. A., et al., "Conceptual Designs of Outfall Systems for Desalting Plants," Department of Interior Research and Development Progress Report No. 550, May, 1970.

(7) Fox, D. G., "The Forced Plume in a Stratified Fluid," NCAR Manuscript 68-197, National Center for Atmospheric Research, 51 pp., April, 1969.

(8) Holly, F. M. and Grace, J. L., "Model Study of a Dense Fluid in a Flowing Fluid," Preprint No. 1587, presented at the American Society of Civil Engineers National Water Resources Engineering Meeting, Atlanta, Georgia, January, 1972.

(9) Pincince, A. B. and List, E. J., "Disposal of Brine into an Estuary," Journal of Water Pollution Control Federation, 45, 11, 2335, 1973.

(10) Anderson, J. L., et al., "Negatively Buoyant Jets in a Cross Flow," EPA-660/2-73-012, Environmental Protection Technology Series, Environmental Protection Agency, 1973.

(11) Fan, L. N., "Turbulent Buoyant Jets into Stratified or Flowing Ambient Fluids," Technical Report No. KH-R-15, W. M. Keck Laboratory of Hydraulics and Water Resources, California Institute of Technology, Pasadena, California, June, 1967.

(12) Abraham, G., "The Flow of Round Jets Issuing Vertically into Ambient Fluid Flowing in a Horizontal Direction," Proceedings of the Fifth International Water Pollution Research Conference, San Francisco, pp. III 15/1 - III 15/7, July-August, 1970)

(13) Albertson, M. L., Dai, Y. B., Jensen, R. A., and Rause, H., "Diffusion of Submerged Jets," Transactions, American Society of Civil Engineers, 115, 639-697, 1950.

(14) Richards, J. M., "Experiments of the Motion of Isolated Cylindrical Thermals through Unstratified Surroundings," International Journal of Air and Water Pollution, 7, 17-34, 1963.

(15) Penã, J. M. and Jain, S. C., "Numerical Analysis of Warm, Turbulent Sinking Jets Discharged into Quiescent Water of Low Temperature," Iowa Institute of Hydraulic Research Report No. 154, University of Iowa, February, 1974.

(16) Fan, L. N. and Brooks, N. H., "Numerical Solutions of Turbulent Buoyant Jet Problems," W. M. Keck Laboratory, California Institute of Technology, Report No. KH-R-18, 1969.

(17) Vadala, P. D., "A Probe to Measure Density," University of Delaware, Civil Engineering Department, unpublished.

(18) Streeter, V. L., Fluid Mechanics, p. 542, McGraw-Hill Book Company, New York, 1966.

(19) Cederwall, K., "Buoyant Slot Jets into Stagnant or Flowing Environments," Technical Report No. KH-R-25, W. M. Keck Laboratory of Hydraulics and Water Resources, California Institute of Technology, Pasadena, California, April, 1971.

9. Notations Used in this Study

α = entrainment coefficient

β = slot width

b = characteristic jet half width

c = centerline concentration of any tracer material

c^* = concentration of any tracer material at any point in the jet

F_r = densimetric jet Froude number

k = velocity ratio

λ = spreading coefficient

Le = length of zone of flow establishment

n = distance perpendicular from jet centerline

Q = volume of fluid in incremental length of jet

ρ_a = ambient density

ρ^* = density at any point in jet

$\Delta\rho(s)$ = $\Delta(\rho)$ = density difference between jet and ambient fluids at centerline

u_a = ambient density

u^* = velocity at any point in jet

u(s) = u = centerline jet velocity

W = nominal width of jet

X = horizontal coordinate

Xm = horizontal distance to bottom impingement of centerline

y = vertical coordinate

Ym = maximum height of use of centerline

$(\ )_o$ = initial condition of ( )

Appendix I

Discussion of the paper by Jain and Penã,

"Turbulent Jets With Reversible Buoyancy,"
Proceedings, American Society of Civil
Engineers, Vol. 101, HY9, 1221-1223, 1975.
(submitted to Jour. Hydr. Div., ASCE)

TURBULENT JETS WITH REVERSIBLE BUOYANCY[a]

Discussion by John D. Ditmars,[3] A.M. ASCE and
David M. Shahrabani[4]

The analysis of turbulent jets with reversible buoyancy due to the temperature-density relationship of water near the freezing point represents another useful application of the integral-similarity approach. The conservation of heat flux, rather than buoyancy flux, is appropriate for this case.

Similar analyses for positively buoyant jets have been verified with experimental data, and appropriate values of the entrainment coefficient, α, and spreading coefficient, λ, have been determined. However, trajectory and dilution data for negatively buoyant and reversing buoyancy jets are sparse. Such data are necessary as the assumption of velocity and density similarity becomes open to question when the trajectory of a sinking jet reverses direction with a relatively small radius of curvature. Zeitoun, et al. (A) had reasonable success verifying models which were based on the integral-similarity technique for negatively buoyant round jets into stagnant environments. The similarity question becomes particularly important in the case of a jet with reversing buoyancy, when, as pointed out by the authors, the buoyancy may vary across a section of the jet from positive at the center to negative at the edges.

The writers have been studying the characteristics of negatively buoyant slot jets discharged into stagnant environments of uniform density (B). Although that case is not identical to the authors' case of jets with net negative buoyancy, it has many of the same features. While our jets maintain a

---

[a]September, 1975, by Subhash C. Jain, Jose M. Peña (Proc. Paper 11586).

[3]Asst. Prof. of Civ. Engrg., Univ. of Delaware, Newark, Delaware (presently on leave of absence at Argonne National Laboratory, Argonne, Illinois).

[4]Graduate Student, Dept. of Civ. Engrg., Univ. of Delaware, Newark, Delaware.

constant buoyancy flux, those with reversing buoyancy do not, but instead have a constant heat flux. Otherwise, we attempted to model negatively buoyant slot jets using the integral-similarity approach employed by the authors. We have measured the trajectories and dilution characteristics of negatively buoyant discharges from slots located on the bottom of a long tank. Experiments for stagnant environments have been performed for slot jets discharged at angles of 30°, 45°, 60° and 90° from the horizontal and discharge densimetric Froude numbers ranging from 10 to 50.

Example comparisons of our predictions (corrected for the zone of flow establishment) of negatively buoyant slot jet trajectories and centerline dilutions with experimental data are shown in Figures A(A) and A(B). The predictions are made using the integral-similarity approach with $\alpha = 0.16$ and $\lambda = 0.89$, as have been used for positively buoyant slot jets (5). Sensitivity studies indicated that these values are as reasonable as other values, which while improving the fit of trajectory predictions, resulted in greater deviations of dilution predictions from the experimental data. The analytical predictions tend to over-estimate the trajectory coordinates and the centerline dilutions. This disparity appears to increase for a given discharge angle as the discharge densimetric Froude number increases. Similar results were found for the other experimental cases considered.

The disagreement between model predictions and experimental data appears to be due to the presence of the bottom boundary. Although the analysis used by us and the authors has been verified for positively buoyant slot jets rising from near-bottom discharges, the situation is physically different when the bottom is near the discharge slot of a sinking jet. The recirculation eddy formed between the sinking slot jet and the bottom (see Figure B) acts both to pull the jet downward due to the pressure gradient established and to

enhance re-entrainment. Thus, the trajectories and dilutions realized are lower than predicted. This "wall effect" cannot be accounted for adequately by modifying the α and λ values.

Our experiences with model predictions and experiments for sinking slot jets cause us to urge caution in the application of the authors' model results for slot jets discharged near a bottom boundary. Although we are unable to provide definitive guidelines as to when bottom effects are negligible, it would appear that such slot discharges should be well removed from the bottom boundary for the authors' solutions to be applicable. Unfortunately, most discharges with negative or reversing buoyancy of slot or merging round jet geometries are from structures located near the bottom. This is particularly true of structures for thermal discharges which rise during seasons other than winter and which would be located as near the bottom as possible to take advantage of the increased depth for rising jet dilution. The authors' solutions for sinking jets are likely to predict a bottom impact location farther from the discharge slot than actually would occur and to over-estimate the dilution at that point. Measurements of sinking jet trajectories and dilution for slot geometries are needed to determine the range of geometric and jet parameters for which the authors' model is valid.

Appendix - References

A. Zeitoun, M. A., et al., "Conceptual Designs of Outfall Systems for Desalting Plants," Dept. of Interior Research and Development Progress Rept. No. 550, May, 1970.

B. Shahrabani, D. M., "Negatively Buoyant Slot Jets in Stagnant and Flowing Environments," M.C.E. Thesis, Dept. of Civil Engrg., Univ. of Delaware, Newark, Delaware (in preparation).

Appendix II

Listing of the Analytical Model

B6700/B7700 F O R T R A N C O M P I L A T I O N

```
      DIMENSION AU(15),AB(15),AFDDIF(15),ATHET(15)
  100 READ(5,1)ALPHA,SCHMDT,GRAV

    1 FORMAT(3F10.5)
      READ(5,2)SLOT,ROA,ROO,THETO,UO,DEL
    2 FORMAT(6F10.6)
      DILO=1.0
      PI=3.141592654
      FDDIFO=(ROA-ROO)
C   SET ERROR RESTRICTION
      E=0.1
C   SET STABLIZING VALUE
      BET=0.0
C   SP IS THE S COORD. WHERE LAST PRINT OUT HAS OCCURRED
      SP=0
C   DSS IS MAX STEP SIZE
      DSS=0.2
C   DSP IS PRINT OUT STEP
      DSP=2.0
C   BO IS THE INITIAL CHARACTERISTIC HALF WIDTH
      BO=(SLOT)*((2/PI)**.5)
      C1=UO**2+BO*COS(THETO*PI/180)
      C2=UO*BO*FDDIFO
      WRITE(6,3)ALPHA,SCHMDT,GRAV,SLOT,FDDIFO,UO,THETO

    3 FORMAT(5X,"ALPHA =",F10.5,3X,"SCHMIDT NO. =",F10.5,3X,"GRAV. ="
     1F10.5,3X,"SLOT WIDTH =",F10.5/5X,"DEN. DIF. =",F10.5,3X,
     1"JET VEL. =",F10.5,3X,"THETA =",F10.5)
C   SET CALCULATION LIMITS
      XLIM=60.0
      YLIM=50.0
      ULIM=0.0
C   THE DENSIMETRIC FROUDE NO.,F, AND REYNOLDS NO.,R
      F=UO/SQRT(ABS(GRAV*SLOT*FDDIFO/ROA))
      R=UO*SLOT/((1.1E-05)*(2.54*12)**2)
      WRITE(6,4)F,R
    4 FORMAT(5X,12HFROUDE NO. =,F10.5,3X,14HREYNOLDS NO. =,F10.5///)
      WRITE(6,5)
    5 FORMAT(9X,"X",9X,"Y",9X,"S",9X,"B",8X,"VEL.",3X,"DEN. DIF.",3X,
     1"THETA",4X,"DILUT.")
      U=UO
      B=BO
      THET=THETO
      S=0.0
      X=0.0
      Y=0.0
      FDDIF=FDDIFO
      WRITE(6,8)X,Y,S,SLOT,U,FDDIF,THET,DILO
  200 THET=THET*PI/180
      SP=SP+DSP
C   THE NEXT TWO STATEMENTS ALWAYS ALLOW COORD. S TO LAND ON A PRINT COOR D.
  151 DS=SP-S
      IF(DS.GT.DSS) GO TO 180
  181 AU(1)=U
      AB(1)=B
      ATHET(1)=THET
      AFDDIF(1)=FDDIF
      BU=U
      BB=B
```

```
      BFDDIF=FDDIF
  152 DO 153 I=1,8
      UUBS=U**2*B*SIN(THET)+((GRAV*SCHMDT*BB*BFDDIF*2**.5)/ROA)*DS
      UB=U*B+(2*ALPHA*BU/(PI**.5))*DS
      AFDDIF(I+1)=C2/UB
      ATHET(I+1)=ATAN2(UUBS,C1)
      AU(I+1)=C1/(COS(ATHET(I+1))*UB)
      AB(I+1)=UB/AU(I+1)
      BU=0.5*(U+(BET*AU(I))+(1.0-BET)*AU(I+1))
      BB=0.5*(B+(BET*AB(I))+(1.0-BET)*AB(I+1))
      BFDDIF=0.5*(FDDIF+(BET*AFDDIF(I))+(1.0-BET)*AFDDIF(I+1))
  153 CONTINUE
      IF(ABS((AU(I)-U)/U).GT.E) GO TO 154
      IF(ABS((AB(I)-B)/B).GT.E) GO TO 154
      IF(ABS((AFDDIF(I)-FDDIF)/FDDIF).GT.E) GO TO 154
      U=AU(I)
      B=AB(I)
      FDDIF=AFDDIF(I)
      THET=ATHET(I)
      DX=DS*COS(THET)
      X=X+DX
      DY=DS*SIN(THET)
      Y=DY+Y
      S=S+DS
      IF(X.GT.XLIM)GO TO 6
      IF(Y.GE.YLIM) GO TO 10
      IF(U.LE.ULIM) GO TO 13
      IF(S.GE.SP) GO TO 155
      GO TO 151
  154 DS=DS/2
      GO TO 152
  180 DS=DSS
      GO TO 181
  155 WID=B*(2**1.5)
      DIL=U*B/(UO*BO)
      THET=THET*180/PI
      WRITE(6,8)X,Y,S,WID,U,FDDIF,THET,DIL
    8 FORMAT(3X,8F10.5)
      GO TO 200
    6 WRITE(6,7)
    7 FORMAT(//25X,"300 SLOT WIDTHS HAS BEEN REACHED"/////)
      GO TO 100
   10 WRITE(6,9)
    9 FORMAT(//25X,"THE BOTTOM HAS BEEN REACHED"/////)
      GO TO 100
   13 WRITE(6,14)
   14 FORMAT(//25X,"THE JET HAS BEEN ARRESTED"/////)
      GO TO 100
      CALL EXIT
      END
```

Appendix III

Photographs of Various Experimental Runs

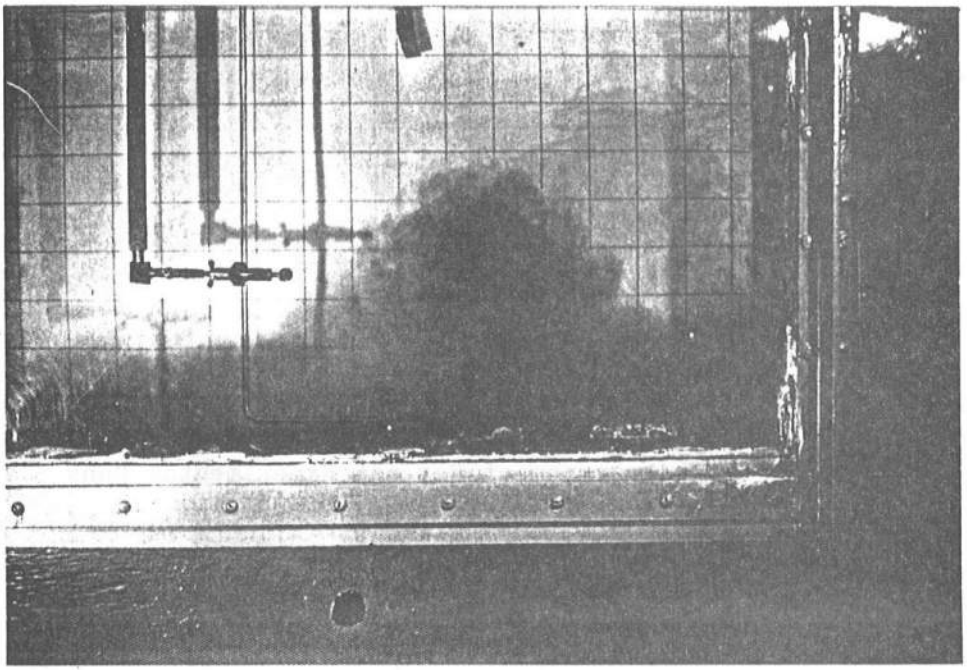

Run #21

Θ_o = 90°

Fr = 9.9

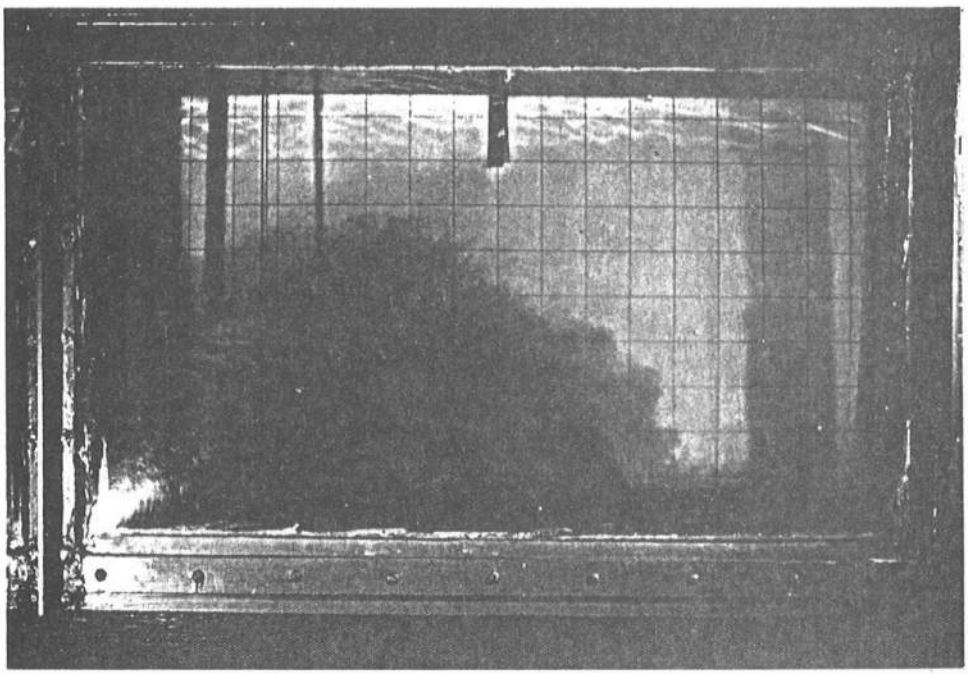

Run #13

Θ_o = 45°

Fr = 41.3

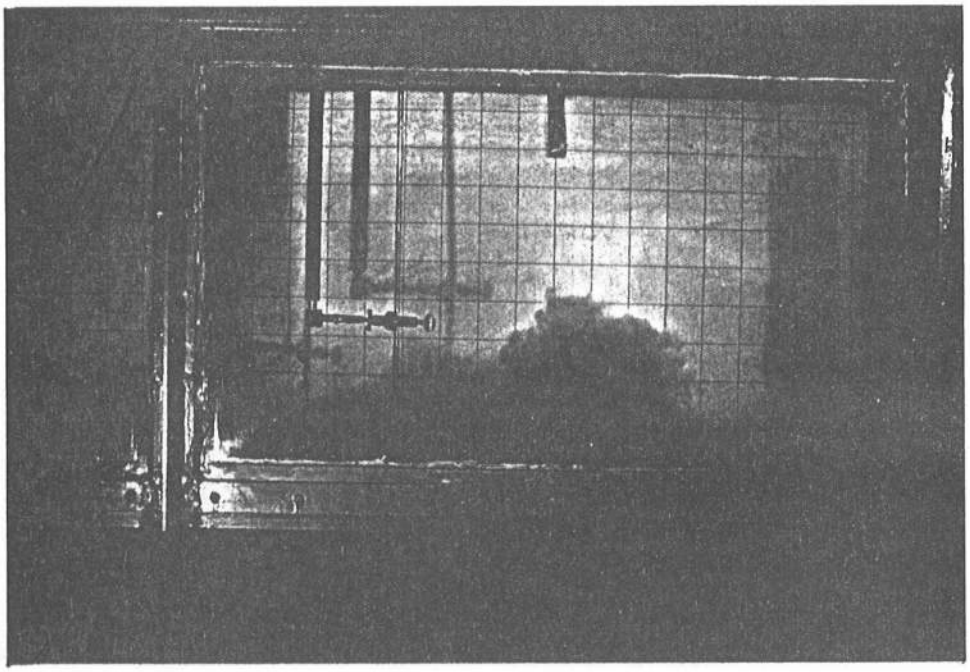

Run #4

θ_o = 60°

Fr = 19.9

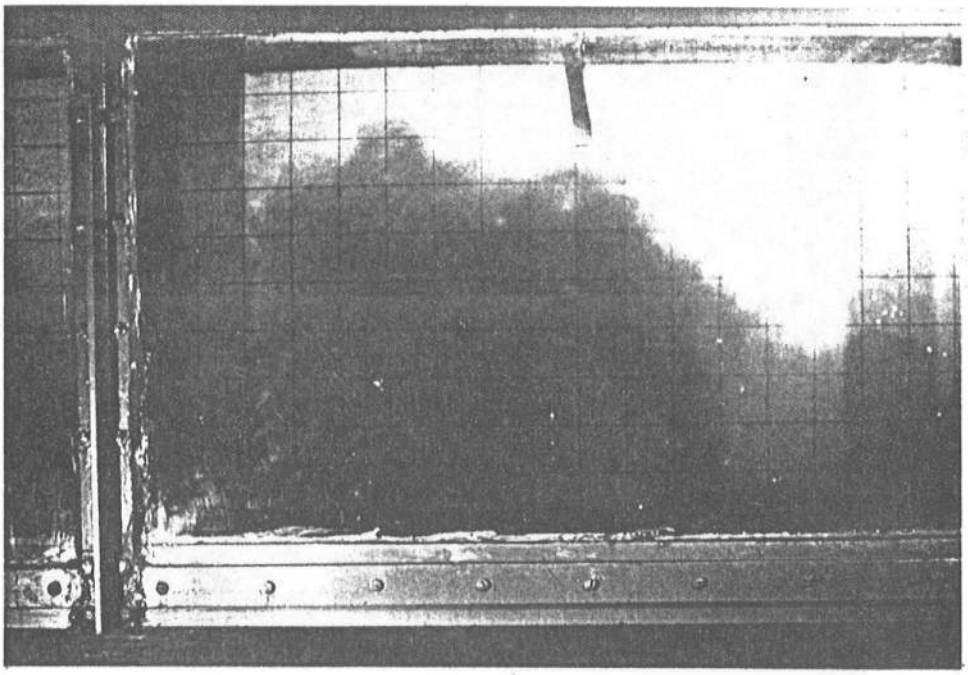

Run #5

θ_o = 60°

Fr = 52.4

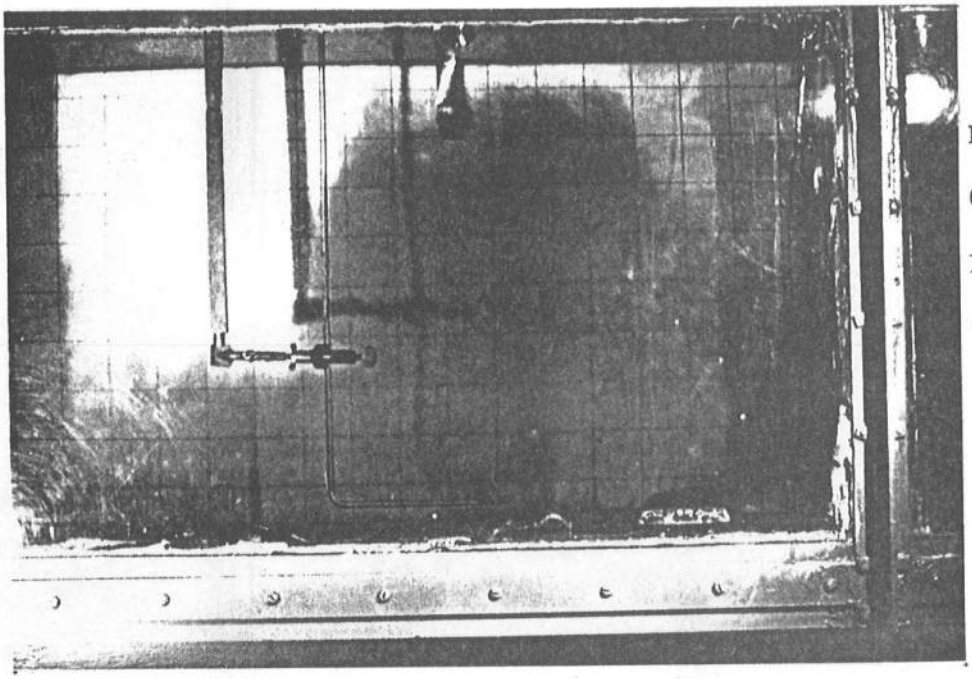

Run #23

θ_o = 90°

Fr = 37.5

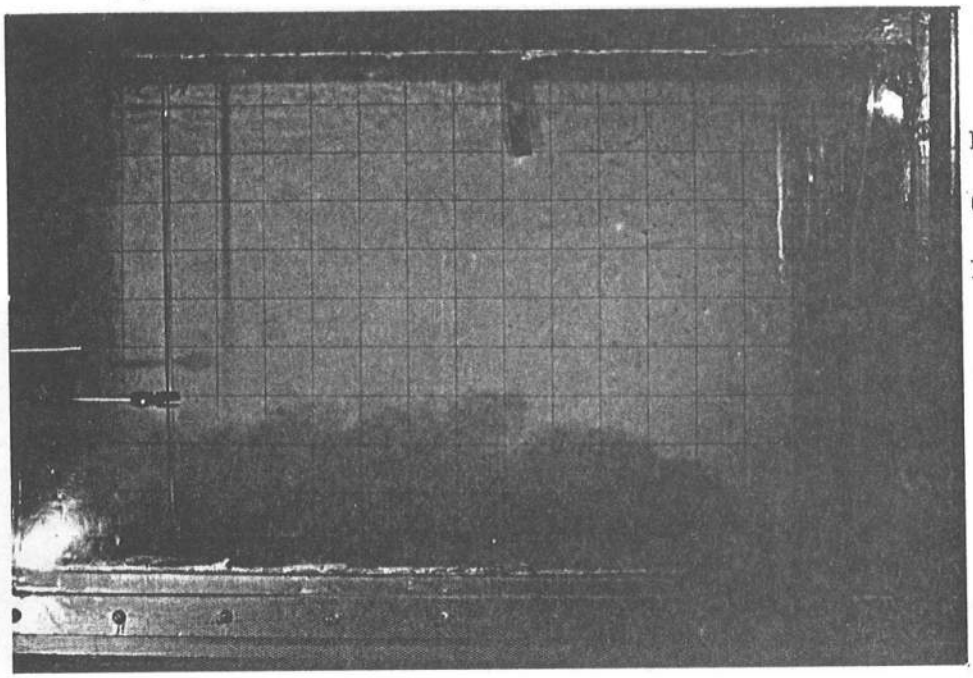

Run #102

θ_o = 45°

Fr = 49.6

k = 15.4

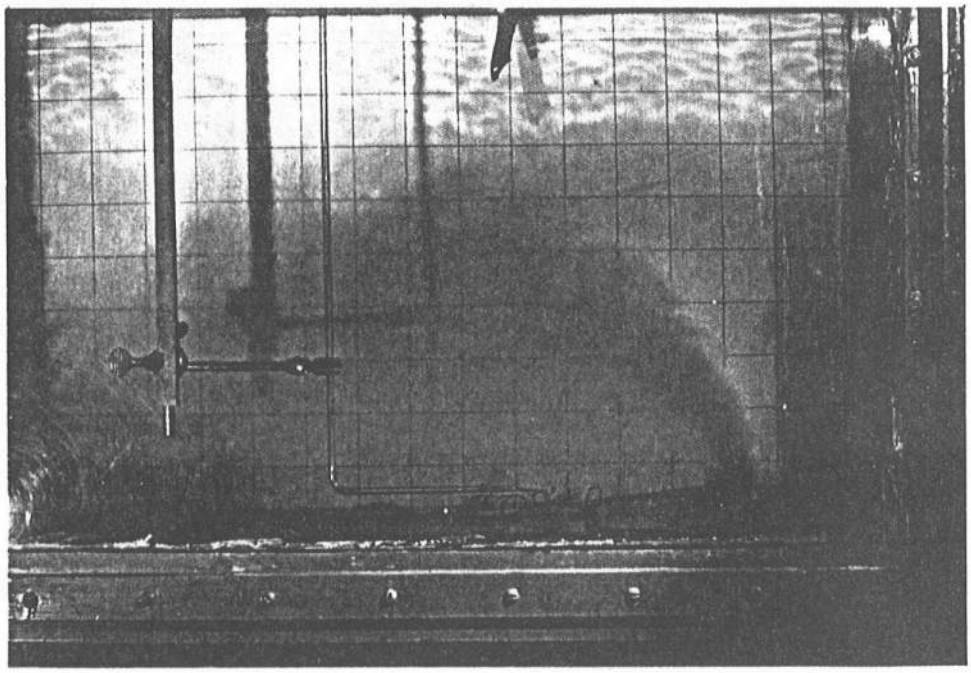

Run #108

$\theta_o = 90°$

Fr = 28.2

k = 14.7

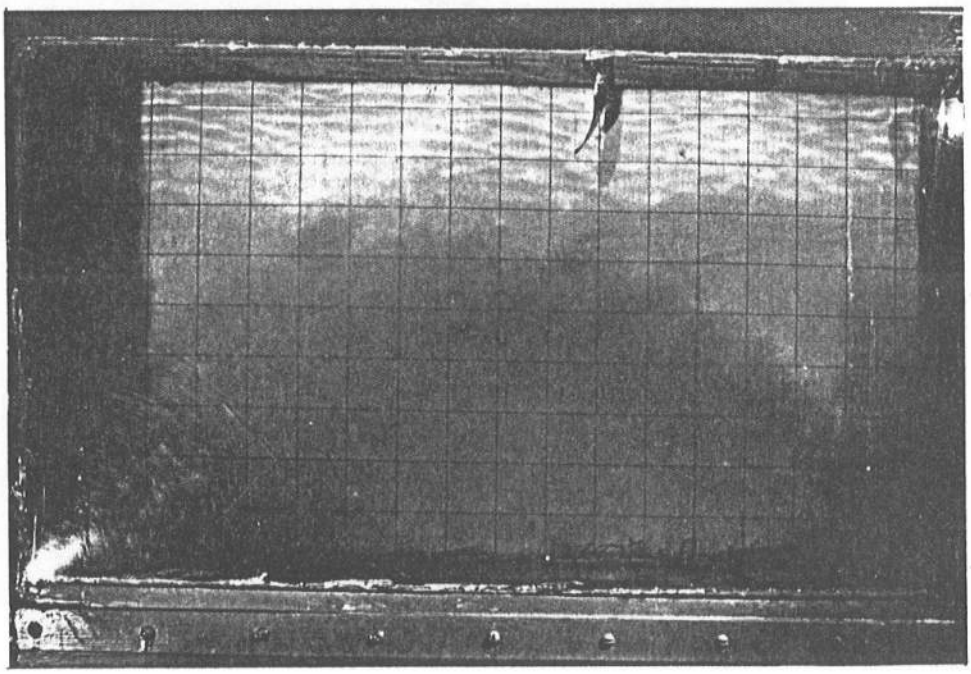

Run #109

$\theta_o = 90°$

Fr = 43.5

k = 15.9

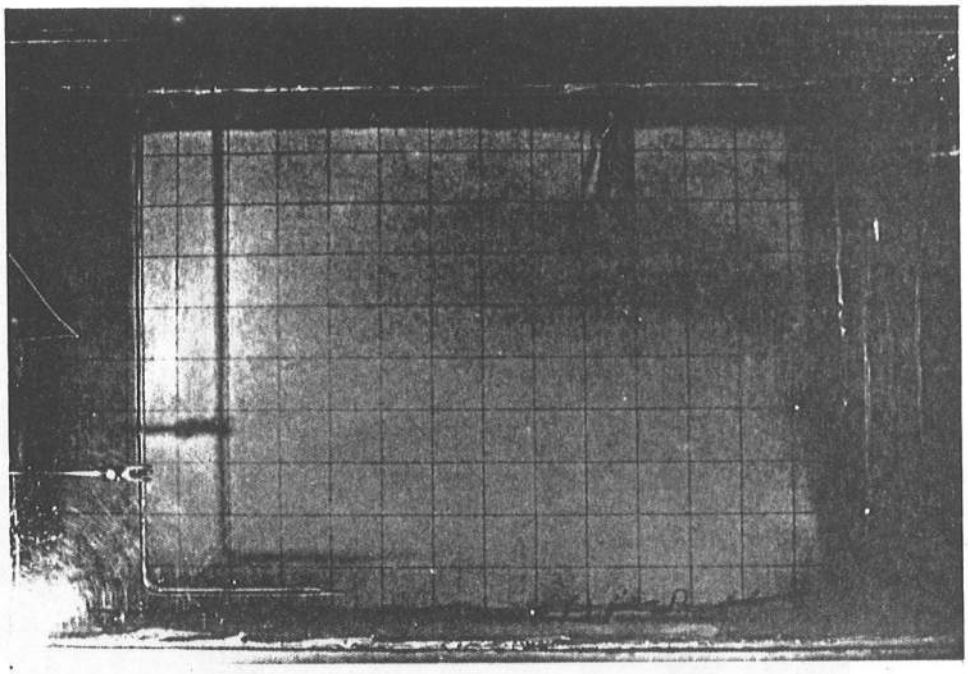

Run #111

θ_o = 90°

Fr = 39.3

k = 24.0

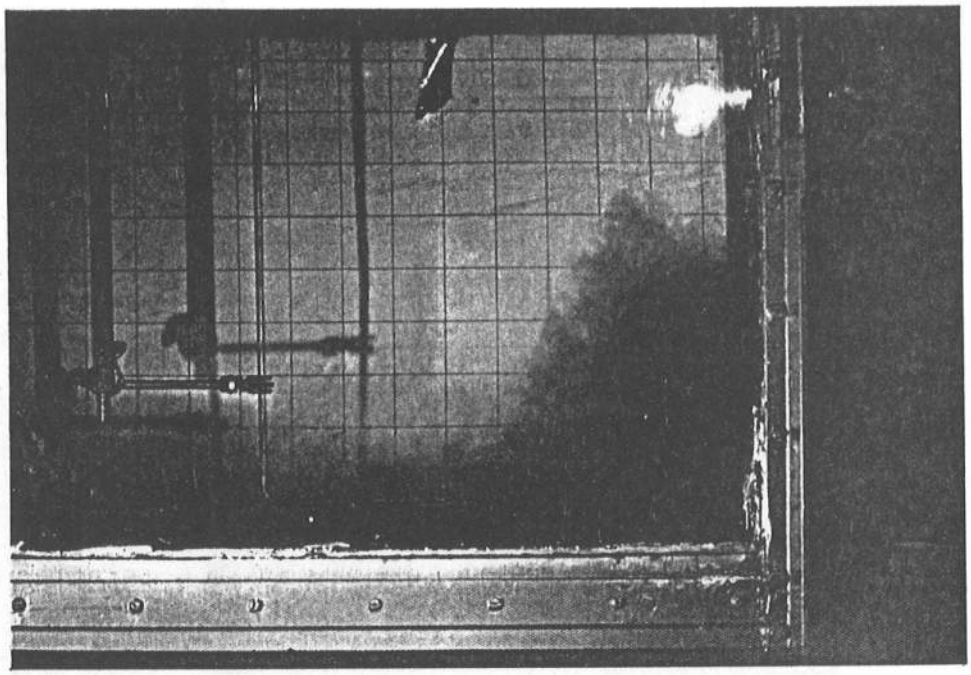

Run #112

θ_o = 90°

Fr = 10.1

k = 27.0

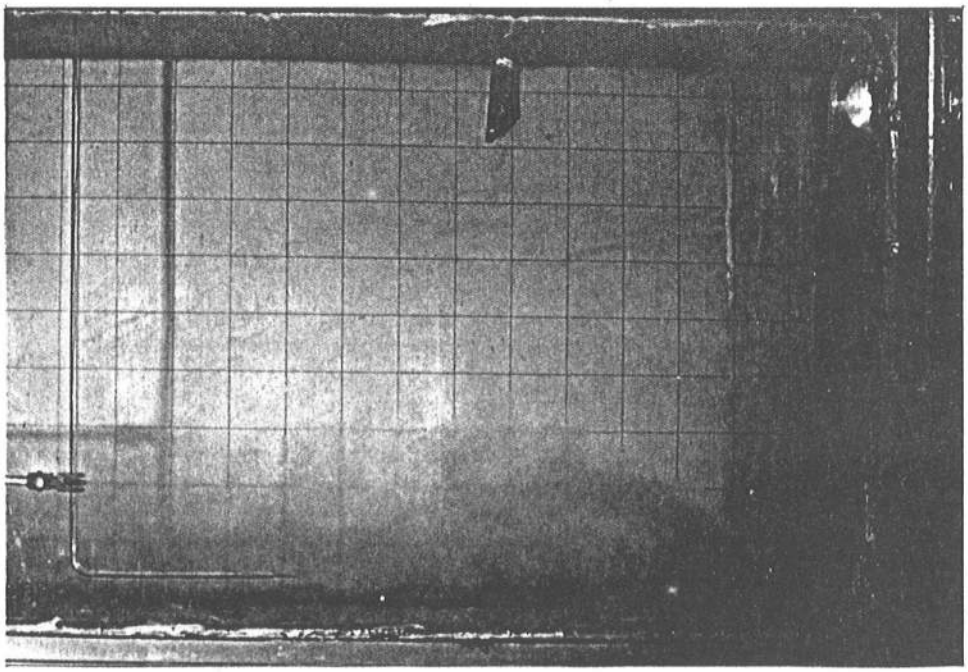

Run #113

θ_o = 45°

Fr = 20.0

k = 27.7

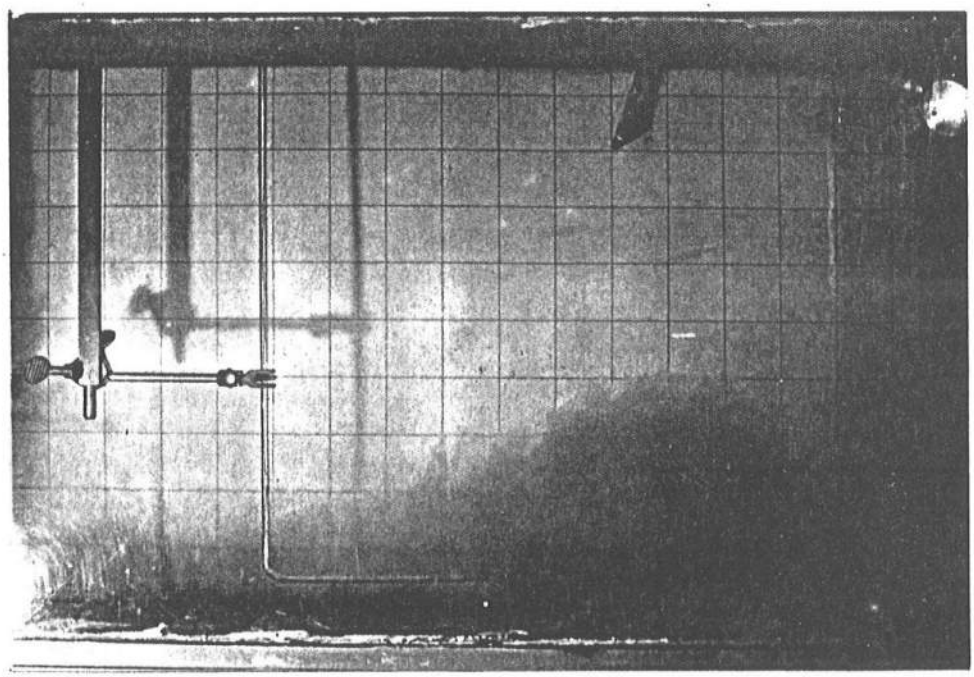

Run #115

θ_o = 45°

Fr = 10.0

k = 24.0

Appendix IV

Calibration Curves

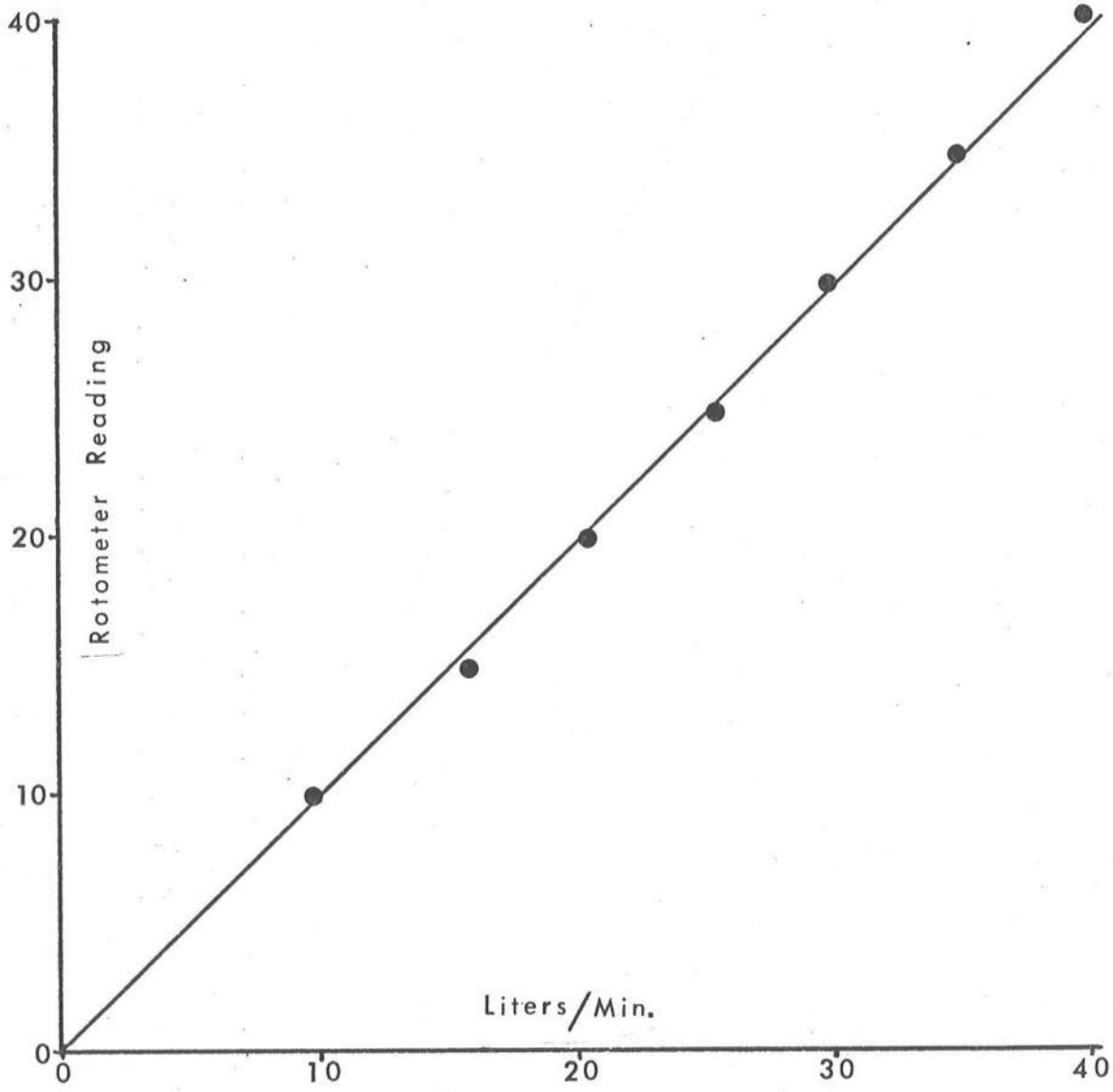

Figure IV-1 Calibration Curve for the Brook's "Full-View" Rotometer

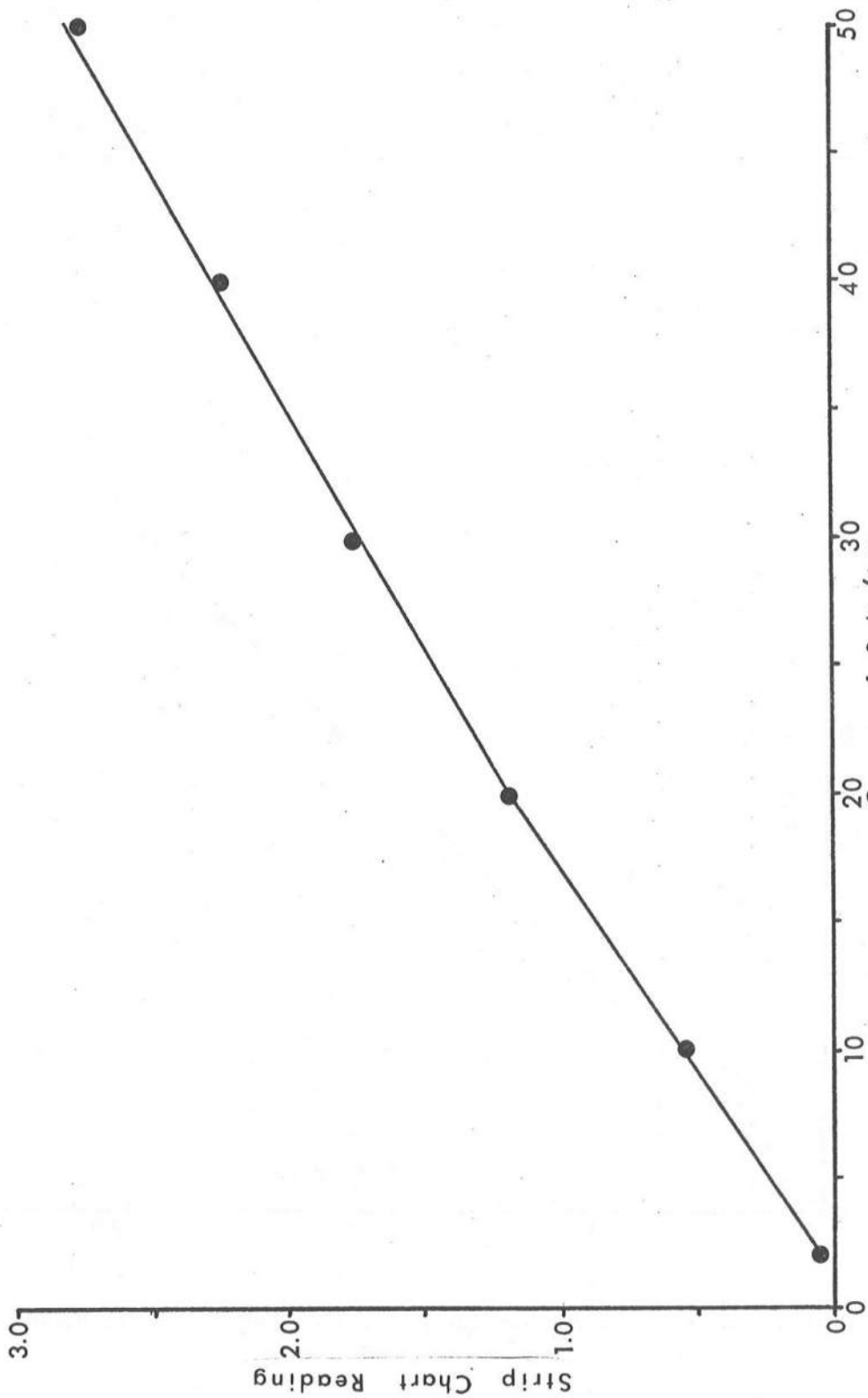

Figure IV-2 Calibration Curve for the Electrical Conductivity Probe

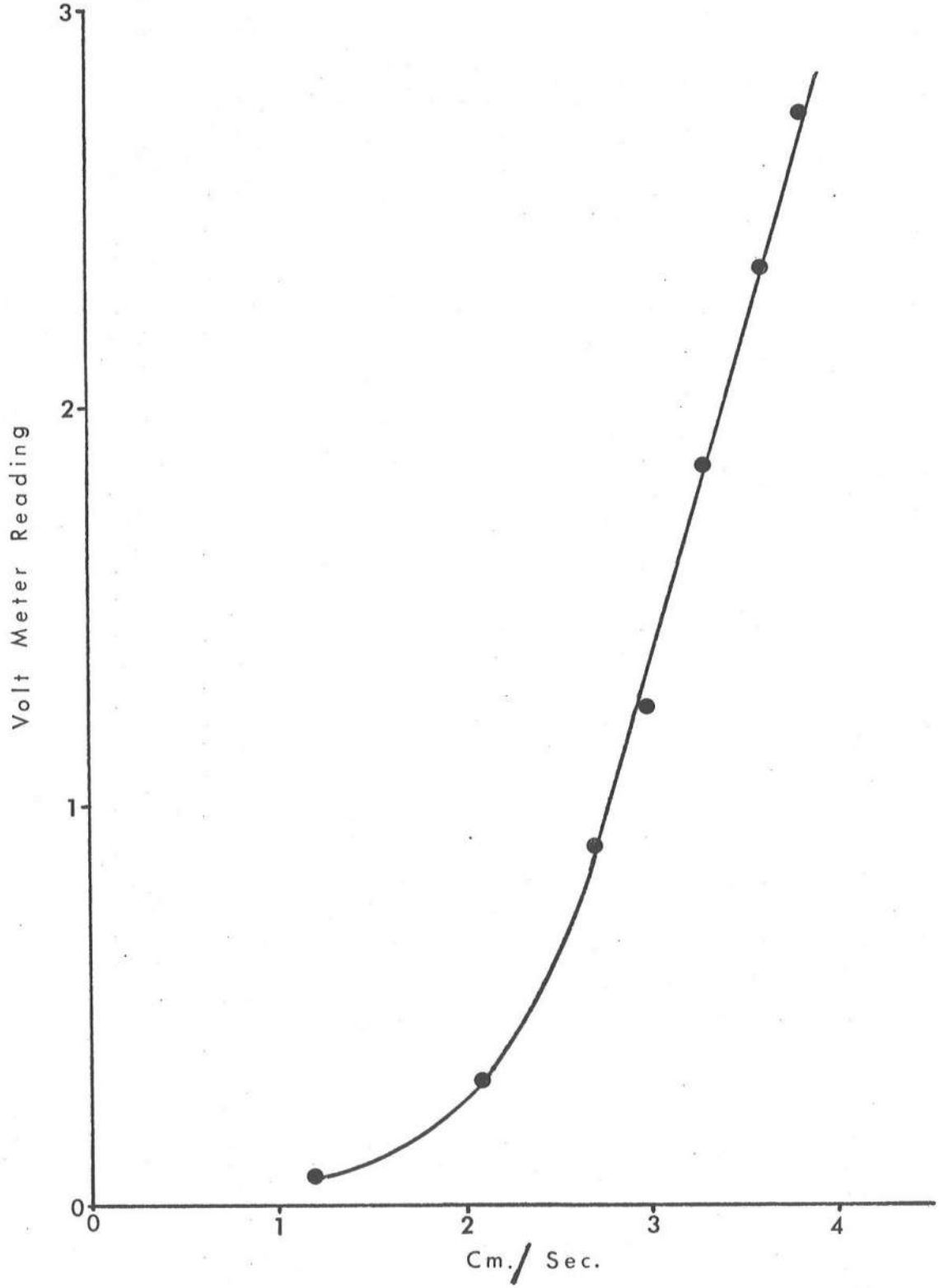

Figure IV-3 Calibration Curve for the Disa Type 55R42 Conical Hot-Film Probe